

https://dspace.org/

The study of measurement and determination of water retention characteristics of coal ash

Mathoho, Gundo

2021
https://hdl.handle.net/10539/31904

Downloaded from a DSpace repository. https://dspace.org/



THE STUDY OF MEASUREMENT AND DETERMINATION OF WATER RETENTION CHARACTERISTICS OF COAL ASH

by

Gundo Mathoho

Submitted in partial fulfillment of the requirements for the degree

Master of Science in Chemical Engineering (50/50),

in the

Faculty of Engineering and Built Environment

(School of Chemical and Metallurgical Engineering)

at the

University of the Witwatersrand, Johannesburg

Supervisor: Dr L.S. Mokhahlane

January 2021

DECLARATION

I, Gundo Mathoho, hereby declare that the present research report, submitted to the School of Chemical and Metallurgical Engineering in the Faculty of Engineering and Built Environment at the University of the Witwatersrand, in fulfillment of the degree of The Master of Science in Chemical Engineering, is my own work. It has not previously been submitted by me to any other institution of higher education. In addition, I declare that all sources cited have been acknowledged by means of a list of references.

I furthermore cede copyright of the research report and its contents in favour of the University of the Witwatersrand.

Gundo Mathoho



14 January 2021

ACKNOWLEDGEMENTS

This research emanated from Eskom's Sustainability Division, their support throughout the project is worth mentioning. This study has become a great journey of success with the selfless efforts and contributions of countless men and women. I hereby like to express my sincere gratitude to all who have motivated and helped me in the completion of this research:

- My Family (Dad, Brothers, Sister, Wife, and Children) including my late Mother, thank you for the gift of life, continue to rest in peace. Your love remains our 'glue' for eternity.
- Eskom's Applied Chemistry and Microbiology staff and colleagues, thank you for all your guidance. I appreciate your support and believing in me and ensuring coordination of this research is achieved.
- My supervisors, Sehai Mokhahlane, I have tried to emulate you to date, your dedication and knowledge is inspiring. Thank you for being with me throughout this journey.

TABLE OF CONTENTS

ABSTRACT

CHAPTER 1 : INTRODUCTION 9

1.1 BACKGROUND AND PROBLEM STATEMENT 9
1.2 AIM OF STUDY 10
1.2.1 Specific objectives 10
1.2.2 Research questions 10
1.2.3 Study approach and thesis outline 11
1.3 CHAPTER ONE SUMMARY 11

CHAPTER 2 : LITERATURE REVIEW 12

2.1 FORMATION OF COAL COMBUSTION RESIDUES 12
2.1.1 Fly ash generation and deposition 15
2.1.2 Coal combustion residue deposition 16
2.1.2.1 Dry ashing 17
2.1.2.2 Wet ashing 17
2.2 FLY ASH PROPERTIES 18
2.2.1 Physical and mineralogy of fly ash 18
2.2.1.1 Mineralogy 19
2.2.2 Chemical and classification of fly ash 20
2.3 ENVIRONMENTAL REGULATIONS: WASTE DISPOSAL 21
2.4 UNCONSOLIDATED MATERIAL UNSATURATED ZONE AND WATER RETENTION 23
2.4.1 Porosity and soil water content 24
2.4.2 Water Flow in Unsaturated Unconsolidated earth material 25
2.4.2.1 Mechanical energy concept 26
2.4.2.2 Liquid in motion: Darcy equation 27
2.5 COAL ASH WATER RETENTION CHARACTERISTICS 27
2.5.1 Soil water characteristics curve hysteresis 29
2.5.2 Soil water characteristics curve hysteresis 30
2.6 SOIL WATER SUCTION MEASUREMENT TECHNIQUES 30
2.7 CHAPTER TWO SUMMARY 31

CHAPTER 3 : SITE DESCRIPTION 32

3.1 MATIMBA ASHING PRACTICES 33
3.2 TOPOGRAPHY AND DRAINAGE 34
3.3 GEOLOGICAL AND HYDROGEOLOGICAL SETTING 35
3.3.1 Regional Geological Conditions 35
3.3.2 Local geological Conditions 36
3.3.3 Local Geohydrological Conditions 37
3.4 HYDROLOGY AND CLIMATIC CONDITIONS 38
3.5 CHAPTER THREE SUMMARY 39

CHAPTER 4 : METHODOLOGY 40

4.1 SAMPLING 40

4.2 PARTICLE SIZE AND DISTRIBUTION 41
4.2.1 Sieving and hydrometer analysis 42
4.3 MINERALOGICAL ANALYSIS: QUANTITATIVE EVALUATION OF MINERALS BY SCANNING ELECTRON MICROSCOPY (QEM SCAN) 44
4.3.1 Sample preparation procedure 45
4.4 ELEMENTAL COMPOSITION: XRF 46
4.5 LEACH TEST: CHARACTERIZATION LEACHING TEST PROCEDURE (TCLP) 46
4.6 HYPROP WIND/SCHINDLER METHOD: EVAPORATION METHOD 48
4.6.1 Sampling and sample saturation 49
4.6.2 Degassing the device using syringes 49
4.6.3 Filling the sensor unit 49
4.6.4 Assembling the sensor unit and the ash sample 50
4.6.4.1 Determination of soil water retention characteristics and hydraulic conductivity 50
4.7 CHAPTER FOUR SUMMARY 54

CHAPTER 5 : RESULTS 55

5.1 MINERALOGICAL AND ELEMENTAL COMPOSITION COMPOSITION 55
5.2 LEACH TEST RESULTS: TOXICITY CHARACTERIZATION LEACH TEST PROCEDURE (TCLP) 57
5.2.1 Leach test results compared with drinking standard 59
5.2.2 Major elements 60
5.2.3 Trace elements 62
5.3 PARTICLE SIZE AND DISTRIBUTION ANALYSIS 64
5.3.1 Particle size and texture analysis 64
5.3.2 Atterberg limits 65
5.4 RETENTION ANALYSIS RESULTS 66
5.4.1 Model selection and parameter estimation 68
5.4.2 Soil water characteristics curve by Brooks-Corey 71
5.4.3 Ash dump water retention 76
5.4.3.1 Matimba liquid retention potential 77
5.5 CHAPTER FIVE SUMMARY 85

CHAPTER 6 : CONCLUSIONS AND RECOMMENDATIONS 86

6.1 CONCLUSIONS: 86
6.2 RECOMMENDATIONS: 87

LIST OF FIGURES

Figure 2.1: Fly ash treatment in the dry ash disposal process (Roberts, 2008).....14

Figure 2.2: Fly ash treatment in the dry ash disposal process (Roberts, 2008).....16

Figure 2.3: Matimba power station dry ash dump (Photograph: 2018).....17

Figure 2.4: A typical scanning electron microscope image of fly ash (Terzano *et al*., 2005) 18

Figure 2.5: Cross-sectional view of the unsaturated zone underlain by the saturated zone (McCauley *et al*., 2005) 24

Figure 2.6: Microscopic view through a porous media illustrating the three phases conditions present in the unsaturated zone 26

Figure 2.7: A typical SWCC and its main components for a silty soil sample after (Fredlund and Xing, 1994) 28

Figure 2.8: A SWCCs for sandy, silty and clayey soils after (Fredlund and Xing, 1994)29

Figure 2.9: Soil-water contents of various soil textures at field capacity and wilting point stages (source: Pardossi et al. 2009) 30

Figure 3.1: Matimba Power station and the Ash disposal site locality map.....32

Figure 3.2: Schematic overview of Matimba ash management practices.....33

Figure 3.3: Topography sections 35

Figure 3.4: Geological setting of Matimba power station and ash disposal Area.....36

Figure 3.5: Site conceptual model showing distinct aquifer systems (GHT, 2011).....37

Figure 3.6: Groundwater contour map and flow direction.....38

Figure 3.7: Lephalale Town's Annual Mean, Maximum and Minimum Temperature..39

Figure 4.1: Two different size rotary splitters used for sampling (size reduction).....40

Figure 4.2: Schematic illustration of Hydrometer (left) and sieving (right) configurations 42

Figure 4.3: Sieve stack configuration (a) and hydrometer measurements setup (b).....44

Figure 4.4: Summarized TCLP (EPA, 1992) steps by Liu *et al,* (2019) 47

Figure 4.5: Schematic cross-section trough HYPROP evaporation method device (Schindler et al., 2010) 48

Figure 4.6: HYPROP-FIT sample page showing visualization and editing of measured data (from Peters and Durner, 2015) 52

Figure 4.7: HYPROPs sample preparation, setup and measurement 53

Figure 5.1: Matimba power station dry ash dump 55

Figure 5.2: Matimba ash TCLP major elements results of using Fluid #1 and 2 57

Figure 5.3: Tutuka ash TCLP major elements results of using Fluid #1 and 2 58

Figure 5.4: Matimba ash TCLP trace elements results when using Fluid #1 and 2 58

Figure 5.5: Tutuka ash TCLP trace elements results when using Fluid #1 and 2 58

Figure 5.6: Matimba power station dry ash dump 64

Figure 5.7: Matimba power station dry ash dump 65

Figure 5.8: Van-der Merwe chart for clay swelling potential.....66

Figure 5.9: Matimba coal ash sample A, B, and C retention measurement.....67

Figure 5.10: Matimba coal ash (Sample A) Brook-Corey fitting uncertainty.....70

Figure 5.11: Matimba coal ash (Sample A: Silt-loam) Brook-Corey fitting results 72

Figure 5.12: Matimba coal ash (Sample A: Silt-loam) Fredulad-Xing fitting results 73

Figure 5.13: Matimba coal ash (Sample A: Silt-loam) Kasogi fitting results.....74

Figure 5.14: Matimba coal ash (Sample A: Silt-loam) Van-Genuchten(m=n-1/n) fitting results 75

Figure 5.15: A typical simplified water balance of a dry ash dump.....76

Figure 5.16: Matimba ash disposal active ashing portion (2018) (in green).....78

Figure 5.17: Hyprop determined mean-field capacity values compared to mean literature value.....79

Figure 5.19: Hyprop-Fit estimated field capacity values at different pressures for different Matimba ash samples.....80

Figure 5.19: Evaporation monthly mean, minimum and maximum of stations A4E003 and A4E007 83

Figure 5.20: Station Stockport yearly and mean rainfall 83

LIST OF TABLES

Table 2.1: African countries recoverable coal reserves (EIA, 2005) 12

Table 2.2: 2015/14 FY Estimated ash volumes per power station after Sigh and Reynolds-Clausen (2015) 15

Table 2.3: Common minerals in coal and their thermal transformation (in fly ash), After (Mattigod, 1983) 20

Table 2.4: Chemical constituents in South African fly ash (Kruger, 2003) 21

Table 2.5: Waste Disposal Facility Classification System (DEA, 2013). 22

Table 2.6: Summary of common water suction techniques (Pan *et al.*, 2013). 30

Table 3.1: Local lithography after Snyman (1998) 37

Table 4.1: Soil particle size classification according to the South African system (MacVicar, 1977) 41

Table 4.2: Summary of the polishing process 45

Table 5.1: Matimba and Tutuka chemical constituents 56

Table 5.2: Chemical analysis compared to the SANS 241 drinking standard 60

Table 5.3: TCLP results of Al, Ca, and SO_4, including their mole equivalent 61

Table 5.4: Model selection statistical summary 69

Table 5.5: Correlation matrix of estimated retention parameters 70

Table 5.6: Model estimated field capacity values for different samples 78

Table 5.7: Comparison of Tutuka and Matimba field capacity values 81

Table 5.8: Stations A4E003 and A4E007 monthly mean evaporation data 82

Table 5.9: Matimba ash dump liquid retention calculations 84

ABSTRACT

Eskom produces million tons of ash from burning coal for power generation. The majority of the generated coal ash generated ends up in designated dry ash dumps. This study assessed various physical and geochemical properties of coal ash to estimate the water retention of a dry coal ash dump. Also, coal ash geochemical properties were studied to ascertain its leachability and identify possible mineralogical phases responsible for water retention.

It is a national priority to improve water conservation, quality, and water usages to avoid water demand exceeding currently limited available supplies. South Africa is a water-scarce country. Groundwater resources play a vital role in ensuring sustainable water security for the country in both rural and urban areas. Groundwater pollution from the dry ash disposal facilities also referred to as ash dumps remains a threat to the precious water resource. Generally, the leachate associated with heavy metal toxins and other inorganic contaminants is of concern and may cause detrimental health effects as well as environmental damage. Pollution of groundwater pollution may occur from the ash dumps particularly when the field capacity is exceeded. This study through construction and assessment of various water characteristic curves estimated the field capacity of an ash dump.

Sieving together with the hydrometer analysis were conducted to determine the coal ash particle sizes and distribution. The texture of Matimba coal ash is silt-loam and can be generally characterised as fines. Fine-grained materials generally exhibit better water retention properties than coarse-grained materials due to the high surface area available for possible ADForption of water molecules. However, the results also indicate ash with an insignificant amount of clay particles(<0.002 mm) but rather dominated by silt-sized particles (0.05-0.002 mm). QEMSCAN, a scanning electron microscope was used to analyse the bulk mineral composition of the coal ash samples. The mineralogical composition of coal ash characteristically resembles the composition of the original parent coal, which is generally dominated by the high proportion of aluminosilicate, quartz, and glass cenospheres. The mineralogical analysis on both samples yielded appreciable quantities of clay mineral, with Kaolinite as the dominant mineral phase. TCLP tests were conducted to determine the leachability of the ash. Trace elements are chemical elements present in ash in small amounts, but still at lower levels pose

a threat to the environment and human health. The detected trace elements from TLCP results in an increasing concentration order are Manganese>Chromium>Copper. HYPROP-FIT software was used to access and analyse the ash retention experimental data recorded and acquired using HYPROP-View software. The tested ash material suggests a high moisture retention capacity at low suction, with a progressive decrease in retention apparent with increasing negative head pressures. The study found the Brooks-Corey model as a suitable representative of the Hyprop measured data, confirmed by AICc and RMSE analysis. The Brooks-Corey estimated retention function parameters within +/- 1% error. A mean value of 35.3% for the three samples was determined as the water retention or field capacity value for Matimba Coal ash.

After considering site-specific conditions like rainfall and evaporation rate within Matimba ash disposal facility, the active ashing portion can hold about 7.96 megalitres per day of liquid through its capillary storage. If the ash dump is operated in excess of this value, the chances of groundwater pollution are high. It is essential to treat this value as an overestimate, and be used to aid in terms of realistically determining dust suppression or irrigation volumes, for overall effective water management at a dry coal ash dump.

CHAPTER 1: INTRODUCTION

1.1 BACKGROUND AND PROBLEM STATEMENT

Electricity generation in South Africa is mainly from coal combustion. Coal is pulverised prior to being fed into boilers for the steam generation that turns the turbines, as a result, coal combustion residuals (CCRs) of varying particle sizes are generated. Some of the CCRs include fly ash, bottom ash, and boiler slag including scrubber materials such as synthetic gypsum. Coarser ash particles are known as bottom ash drop and get collected in the hoppers at the bottom of the boiler. Fine particles are trapped and get separated from the flue gas stream by electrostatic precipitators or fabric filter bags systems.

Eskom employs two ash disposal systems depending on the water to ash ratio, being wet and dry ashing system (Eskom, 2016). Slurry of ash and water is transported using dedicated pipelines for disposal in designated ponded areas during wet ashing (Eskom, 2016). In the dry ashing system, a composite of dry fly and bottom ash is preconditioned with water during the transportation process to avoid the formation of airborne ash dust. The composite ash is transported using the conveyer belt system to the ash disposal area. The airborne mobility nature of the composite ash dust not only results in environmental impacts through air pollution but has impact on the operation (Eskom, 2010). Ash dust if not managed properly creates a cloud cover, making it unbearable, unsafe to operate and may potentially cause damage to the equipment and human health.

Ash dust suppression at Eskom sites is mainly carried out using irrigation sprinklers and sprays. More often, water used for dust suppression is water originating from different processes in the power generation cycle. For instance, sources of water for ash dump dust suppression in Tutuka power station are process water from regeneration effluent from the demineralised plant, ion exchange resin clarifier sludge, cooling water blowdown, and, at times, mine water is utilized.

South Africa is a water-scarce country, receiving only about half of the global rainfall (450 mm/annum). It is a national priority to improve water conservation, quality, and water usages as to avoid water demand exceeding the currently available supply. Co-disposal of ash and process water is an important part of the water management systems at coal-fired power stations, even though it is not an ideal practice. An excess amount of process water at power

stations may lead to misrepresenting the desired water balance, which is critical for maintaining various plant processes in a coal-fired power station environment. Dry ash dumping is then used as a salt sink with intention of safely disposing of and allow maximum evaporation to occur with excess water stored within the ash matrix. Groundwater and soil contamination constitute the majority of reported environmental incidents associated with dry ash disposal (Carlson and Adriano, 1993; EIP, 2019). Leachate generation is promoted and amplified through excess water supplied into the ash dump. exceeding the liquid limit storage of ash, ensuing the leachate migrating into the groundwater systems overlain by the ash dump facilities. Typically, the leachate is associated with heavy metal toxins and other inorganic contaminants, and insufficient levels may cause detrimental health effect as well as environmental damage (Carlson and Adriano, 1993)

1.2 AIM OF STUDY

The study aims to determine the total moisture-holding limit of an ash dump from a coal-fired power station.

1.2.1 Specific objectives

The SWCC tests will be relying on CCRs from an existing coal-fired power station. One sizeable sample will be homogenously divided into single homogenous samples for each different test conducted.

Soil texture and structure can potentially influence water infiltration, permeability, and water holding capacity of soil. The study, through various laboratory tests, will:

- Determine the CCRs particle sizes and distribution.
- Determine the CCRs' dominant mineralogical phases.
- Construct various soil-water characteristic curves (SWCC) of CCRs through the water draining path for various coal ash samples.

1.2.2 Research questions

The following research questions are answered as part of this study:

- What is the total water retention of Matimba coal-fired power station dry ash disposal facility?

- What are the physical and geochemical properties responsible for retaining water in ash?

1.2.3 Study approach and thesis outline

The outline of the thesis is structured around specific objectives. A brief description of each chapter is given below:

- **Chapter 1** provides the background to the study and thus introduces the aim of the study with its objectives. This forms the foundation of this research and gives the outline of the rest of the chapters.
- **Chapter 2** is a literature review of the study. Providing a quick brief on various topics related to the coal and generation of coal ash as well as disposal. Coal ash chemical and physical properties are discussed. An unsaturated flow zone is briefly explained as well as the hydraulic properties in this zone.
- **Chapter 3** provides the sampling practices, experimental methodology, and analytical techniques employed in this study.
- **Chapter 4** presents the results of the study. All generated geochemical and engineering results are presented and discussed. Unsaturated flow parameters, in particular, the hydraulic conductivity are then estimated.
- **Chapter 5** provides the conclusion of the study. Recommendations are also provided based on the findings of the study.
- **Appendices** This section presents supplementary data and information relevant to the study and specific to Chapter 4, which may not have been captured in the main research report.

1.3 CHAPTER ONE SUMMARY

Eskom generates a million tonnes of coal combustion residuals. Loosely termed ash. This by-product poses an environmental risk to the environment, in particular groundwater. It is usually when the holding capacity, also known as the field capacity of ash is exceeded that groundwater is impacted by the leachate generated. Understanding the ash water characteristic will go a long way in refining the ash dump water balance and reduce leachate generation which will go a long way in averting water resource pollution.

CHAPTER 2: LITERATURE REVIEW

2.1 FORMATION OF COAL COMBUSTION RESIDUES

Coal is the leading fuel produced and consumed in South Africa, mainly for electricity production. South Africa has the largest coal (anthracite and bituminous) reserves in Africa, with estimated economically recoverable reserves of 53 378 billion tonnes (Table 1) (EIA, 2005). Approximately 96% of the reserves are bituminous coal which is mainly used for steam generation (Eberhard, 2011). The anthracite coal rank amounts to 2%, is mainly utilized by the metallurgical industries and reserved for international markets. Export coal grade requires at least 15% of ash content post washing with a heating value of about 26 MJ/Kg (Eberhard, 2011).

Table 2.1: African countries recoverable coal reserves (EIA, 2005)

Country	Coal Reserves (billion tonnes)
South Africa	53 378
Zimbabwe	553
Mozambique	234
Swaziland	229
Tanzania	220
Botswana	44
Zambia	11

Electricity generation

A simplified schematic layout of typical pulverized coal combustion (PCC) power station is shown in Figure 2.1. Coal for electricity generation is either transported via conveyor belts from adjacent mines or by trucks to the power station. Coal is pulverized in the pulverizer prior to being fed into the furnace. The pulverized coal is crushed into a powder with a particle diameter of approximately 50 μm (Osman et al., 2014). At this stage, the coal exhibits consistency similar to cake flour. The pulverized coal is then transported by hot air into the boiler, where combustion produces heat. Water contained in tubes, typically in a coiled configuration surrounding the boiler is heated. The water in the heat exchanger tubes is turned into superheated steam at high pressure (Osman et al., 2014). The steam is used to drive the turbine. Similarly to a bicycle dynamo generator, the turbine shaft is linked to a generator rotor, which generates electricity through electromagnetic phenomena. The most commonly used

turbine arrangement is the tandem compound system, which has all turbine cylinders (high, intermediate, and low pressure) mounted inline, driving a single alternator. Most modern power generation units rely on reheating of steam before entering the intermediate pressure turbine (IEA, 2017). The electricity flows through transmission lines and transformers to reach the end-users at required voltages. The steam used is then cooled and condensed in cooling towers or through the Induced Draft (ID) fan, and recycled to the boilers for reheating. Combustion residues are produced inside the boiler furnace. The gases are filtered either using the bag of filters or electrostatic precipitators as they exit the boiler. This is done to remove all possible emissions, however, depending on the flue gas composition trapping system, gases like sulphur dioxide, carbon dioxide, and nitrogen oxides escape to the environment due to extreme finer particulates. If the gas mixture contains substantial sulphurous and nitrogenous emissions, particularly (Sulphur Oxides) SO_X and Nitrogen Oxygen (NO_X) compounds, then desulphurisation and denitrification processes may be installed to trap these compounds (Osman et al., 2014). The typical composition of flue gases is approximately 12–12.8% CO_2, 6.2% H_2O, 4.4% O_2, 50 ppm CO, 420 ppm NO_x, 420 ppm SO_2 and 76 - 77% N_2. The flue gas is typically emitted at pressures ranging from 100 kPa to 170 kPa and temperatures of 363.15 - 412.15 K (Osman et al., 2014). Other combustion residues include fly ash, bottom ash, and boiler slag are produced in large quantities and require dedicated disposal areas for long-term storage, where the residue material is kept isolated from interacting with the environment. Bottom ash and boiler slag are deposited at the base of the boiler. The bottom ash is typically dark grey, granular, porous predominately comprised of sand particles (0.05-2mm) (Ramme et al., 1998). Boiler slag is coarse, hard, and black having a glassy texture. Bottom ash forms as a result of particle agglomeration after softening or melting and collect in the hoppers at the base of the furnace (Ramme et al., 1998). Boiler slag is formed from a wet-bottom furnace when non-combustible mineral melts and rapidly cooled when in contact it the quenching water in the ash hopper furnace. Due to the rapid cooling of the molten ash, it fractures, crystalizes, and forms pellets-like particles with glassy texture, angular, coarse black grains (Ramme et al., 2014).

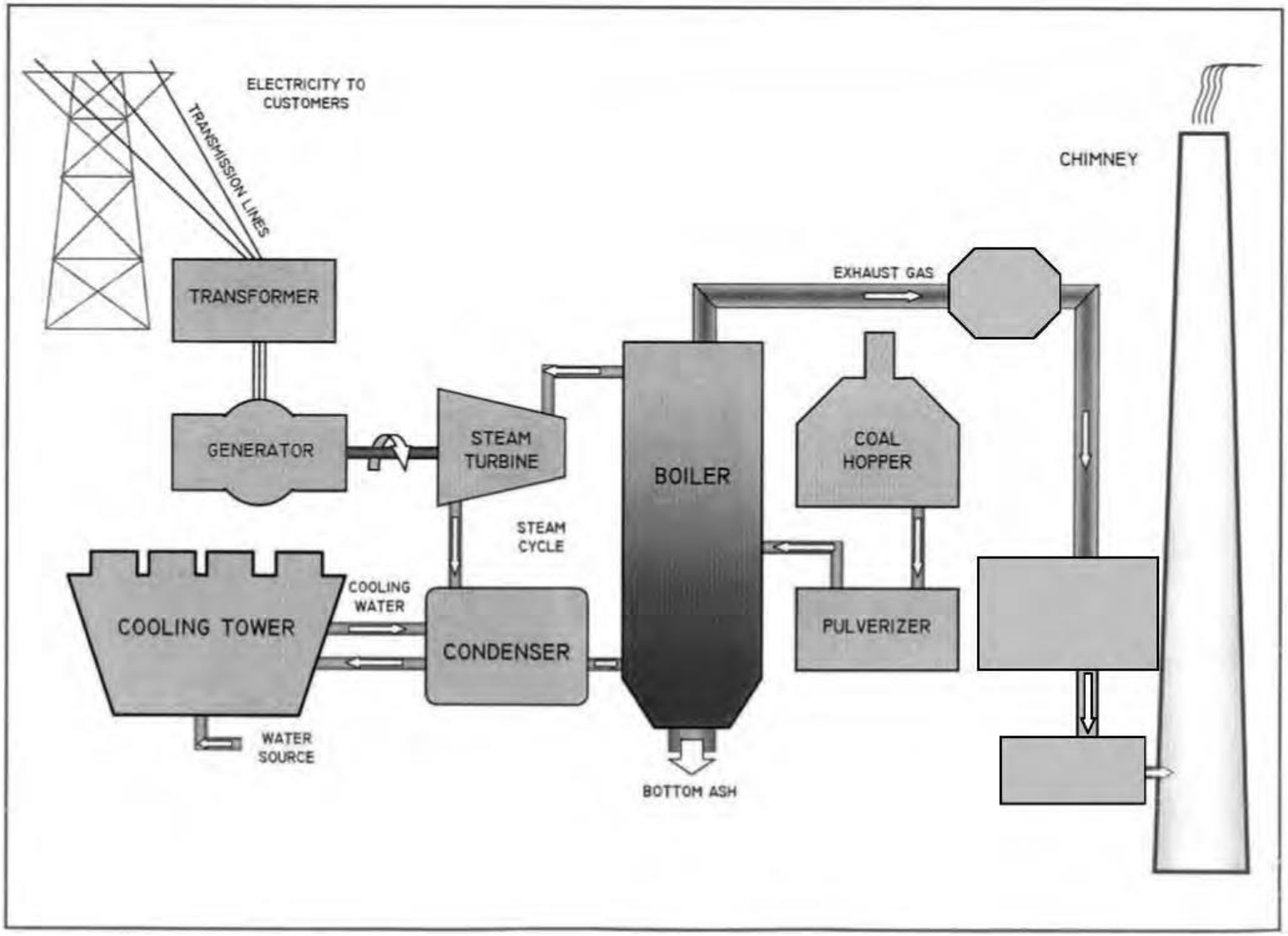


Figure 2.1: Fly ash treatment in the dry ash disposal process (Roberts, 2008)

2.1.1 Fly ash generation and deposition

According to Sigh and Reynolds-Clausen (2015), in the 2015/14 financial year (FY) Eskom produced 33.3 million tons of ash from burning at least 119.2 million tons of coal. Approximately 7% of the total generated ash is utilised, mainly by the construction industry for bricks and cement manufacturing (Sigh and Reynolds-Clausen, 2015). Table 2.2 provides volumes of ash produced and sold from thirteen Eskom power stations during the 2015/14 FY. Of the total ash disposed in designated landfills or ponds at Eskom power stations, 85% is fly ash and only 15% is bottom ash. It is for this reason that from herein, the emphasis will be given to the fly ash component of all generated coal combustion residues.

Table 2.2: 2015/14 FY Estimated ash volumes per power station after Sigh and Reynolds-Clausen (2015)

Power station	Total ash produced (Mt)	Saleable Ash (Mt)	Sold ash (Mt)
Arnot	1.65	0.40	0.00
Camden	1.07	0.00	0.00
Duvha	2.51	0.20	0.00
Grootvlei	1.00	0.00	0.00
Hendrina	1.82	0.20	0.00
Kendal	4.91	3.00	0.54
Komati	0.32	0.00	0.00
Kriel	2.30	1.00	0.31
Lethabo	6.48	1.30	1.23
Majuba	3.43	1.00	0.04
Matimba	4.75	2.00	0.01
Matla	3.04	0.40	0.40
Tutuka	2.93	0.00	0.00

Fly ash treatment

Fly ash, a fine residue composed mainly of spherical micron-sized particles is collected from the flue gas stream in the electrostatic precipitators and transported to bunkers through chain conveyors and bucket elevators as illustrated in Figure 2.2. For easy conveyance of fly ash to a dedicated disposal area, 15% moisture is added from the conditioner sludge before being transported by the open conveyor belt system (Roberts, 2008).

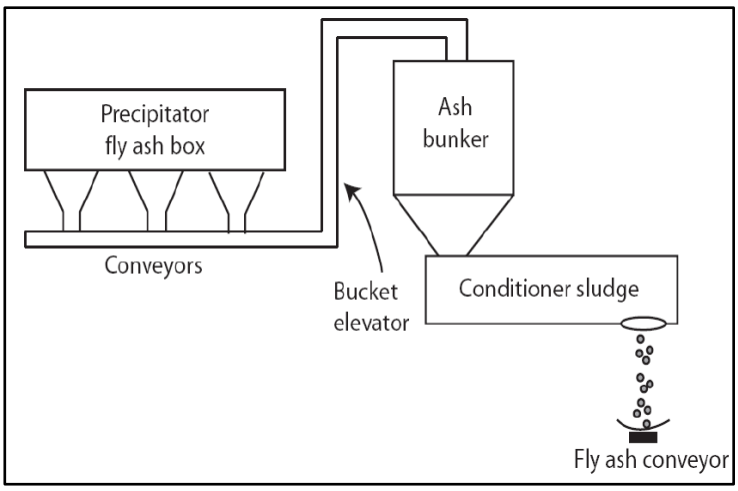


Figure 2.2: Fly ash treatment in the dry ash disposal process (Roberts, 2008)

2.1.2 Coal combustion residue deposition

The majority of the old fleet of power stations in South Africa rely on the wet system for the disposal of ash. In this system of disposal, fly ash collected in the hoppers is taken to the collector tank where it is mixed with water to form a slurry and via pipeline sent to the disposal ponds called ash dams. Similarly, bottom ash falling under gravity as clinker is first ground to below 25 mm size, is mixed with water and then hydraulically transported to disposal facilities along with the fly ash. The method of dry disposal is fairly new (late 1980's) to the coal power generation industry in South Africa. This was critical, as South Africa is a water-stressed region. Any improvements in water use efficiency are required to ensure the long-term disposal of ash.

Irrespective of the method of disposal used, it is imperative to always ensure better management of these systems through compliance with relevant legislation and more importantly, prevent, or at least limit, pollution of the natural environment.

The major possible impacts of ash disposal on terrestrial ecosystems have been reported by Carlson and Adriano (1993). These include:

- Leaching of potentially toxic substances into soils and groundwater.
- Reductions in plant establishment and growth due primarily to adverse chemical characteristics of the ash.
- Changes in the elemental composition of vegetation growing on the ash.
- Increased mobility and accumulation of potentially toxic elements throughout the food chain
- Visual intrusion.

2.1.2.1 Dry ashing

In the case of dry ash disposal, ash is partially wetted at the power station before being transported by conveyor belt to the ash disposal dump. Ideally, the ash on the conveyor belt contains about 15% moisture. The arrangement prevents ash from blowing off the conveyor belt or in the area where it is being disposed of. Disposal occurs by merely tipping the ash at the end of the conveyor belt. Dry disposal is advantageous in that contact with water is reduced. Disadvantages, however, include dust and wind erosion as well as stability of the ash pile in the case of surface disposal (Troskie, 2005). There is no compaction of the ash that occurs during the disposal. The stability of the ash dump relies on compaction by its weight and the weight of the machinery being used at the top of the ash dump. In addition to the moisture added to the ash within the power station, a watering gun is available in the area where the ash is being tipped to prevent the ash from drying out and creating a dust problem (Hodgson and Krantz, 1998). Figure 2.3 is a photograph image of dry ash disposal taken at Matimba Power Station.



Figure 2.3: Matimba power station dry ash dump (Photograph: 2018)

2.1.2.2 Wet ashing

In the case of wet ash disposal, ash is generally being pumped from the power station to the ash dams in ash-to-water ratios of 1:5 to 1:10 by volume (Hodgson and Krantz, 1998). Wet placement (dense slurry disposal) is any method that results in an excess of water that must be handled after the ash has been placed, that is, the fly ash is transported as slurry through pipes and disposed of in an impoundment called an ash pond or commonly known as ash dam. The ash slurry is continuously pumped through pipes to the ash dam where the ash particles immediately settle out and the ash-water

is either drained away via a penstock to the clear ash effluent dam or percolates through the ash dam and is collected in a toe drain. The ash water goes to the clear ash effluent dam, where it mixes with other wastewaters.

2.2 FLY ASH PROPERTIES

Fly ash is the finely fused inorganic and organic residue material formed by heating, vaporisation, and combustion of pulverised coal (Bin-Shafique *et al*., 2002). The inorganic material is mostly dominated by the finely divided glass phase. The glass phase reacts as pozalans of siliceous and aluminous material in the presence of moisture, to chemically react with calcium hydroxide resulting in cementitious compounds (Campbell, 1999). Pozzolan is an additive used in the cement and construction industries for enhancing the setting and cementitious properties when combining with other cement products.

2.2.1 Physical and mineralogy of fly ash

Fly ash particles range from 0.074 – 0.005 mm, classified as silt size (Bin-Shafique *et al*., 2002). The fly ash particles fuse while in suspension with flue gases, melting and dropping forming small particles. Morphology and microscopic structures of fly ash are mostly studied using a scanning electron microscope (SEM). SEM is capable of producing images similar to Figure 2.4 by scanning the surface with a focused beam of electrons. Microscopic structures seen under SEM are regular and irregular shaped spheroidal particles. These shapes are either of the Ceno-, Plero, Derma-, and Ferro-spheres (Matshitse, 2016).

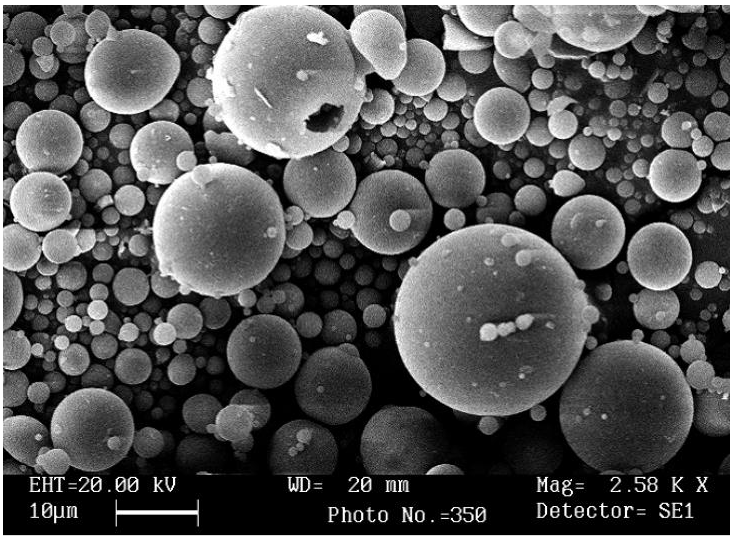


Figure 2.4: A typical scanning electron microscope image of fly ash (Terzano *et al*., 2005)

Plerospheres are typically large hollow particles that may contain insertions of minor particles. Cenospheres tend to lack insertions insides the hollow sphere, while ferrospheres which are

spheroidal particles known to exhibit magnetic properties since they are rich in iron (Matshitse, 2016). Landman (2006) suggests the hollow spherical particles are a result of carbon dioxide and water-gas expansion, forming bubbles the molten inorganic particles cool down rapidly and falls to the furnace against the flue gas streams while maintaining the equilibrium shapes.

Fly ash may exhibit different colours due to varying chemical and mineralogical constituents present and the temperature the furnace is operated under during combustion. Dark grey to black colour is mainly a result of elevated unburned content found in the ash matrix. Tan colour in ash is associated with high lime content whereas the reddish to brown is attributed to high iron content.

The specific gravity of fly ash is known to vary with coal rank, higher rank coals (sub-bituminous) have low specific gravity when compared with bituminous coals known for higher specific gravity values. The specific gravity of most coal ash will vary between 1.6 -3.1 m^2/kg. Microscopic structures such as cenospheres due to hollow structures generally have low bulk density. The low permeability of fly ash is attributed to the high (170- 1000 m^2/kg) specific surface area of fly ash particles (Ahmaruzzaman, 2009). Liquids are known to flow gradually within the fly ash particles matrix due to the high specific surface area, the overall texture of fly ash as well as presence of clay particles.

2.2.1.1 Mineralogy

The amorphous phase dominates the bulk mineral composition of fly ash followed by the crystalline phase and to a lesser extent the unburned coal content (Mokhahlane, 2013). Matshitse (2016) showed major mineralogical phases found in South African fly ash as determined through different analytical techniques including the XRD as quartz, mullite, hematite, and anhydrite (see Table 2.3). During coal combustion, some of the mineral phases in coal remain unaltered and some are thermally altered. As the coal is combusted, its mineral matter is thermally altered into different forms. Carbonates are calcined and sulphides are oxidized, and the clay minerals are hydrated and decomposed. Marcasite, pyrite, and siderite which are found in coal, on combustion alter to form ferrite and hematite phases along with CO_2 and SO_2 respectively. Gypsum dehydrates consequently forming anhydrite mineral while calcium sulphate remains stable. Since the melting point of quartz mineral is above 1700^oC and the boiler furnace operates at a temperature range (1400-1500^oC), less than the melting temperature of quartz, quartz minerals present in coal are generally left unaltered in their crystalline form in fly ash. Coals rich in calcium bearing minerals will consequently lead to lime and sulphates enriched fly ash. Table 2.3 depicts some of the major thermal changes coal underwent during coal combustion.

Table 2.3: Common minerals in coal and their thermal transformation (in fly ash), After (Mattigod, 1983)

Minerals in Coal	Transformed Minerals in Fly ash
Phyllosilicates (clay minerals: e.g. kaolinite)	Glass, mullite ($Al_6Si_2O_{13}$), quartz
Quartz	Glass, quartz
Pyrite (FeS_2), siderite ($FeCO_3$), iron sulfates	Hematite (Fe_2O_3), magnetite (Fe_3O_4)
Calcite ($CaCO_3$)	Lime (CaO)
Dolomite [$CaMg(CO_3)_2$]	Lime (CaO), periclase (MgO)
Gypsum ($CaSO_4.2H_2O$)	Anhydrite ($CaSO_4$)
Ankerite[$CaMgxFe_{(1-x)}$ $(CO_3)_2$]	Calcium ferrite ($CaFe_2O_4$), periclase (MgO)

During coal combustion, the liberation of some of the inorganic elements occurs. These elements get deposited on the surface of fly ash particles and get concentrated. The ease at which these elements wash away in contact with water is one of the environmental problems linked to fly ash deposition. Mobilisation of these elements as they are washed away may lead to subsequent percolation into the subsurface reaching the groundwater. The hydration and leaching behaviour of fly ash is dependent on the mineral phases present in fly ash. These include the non-crystalline amorphous phase, all the crystalline phases, and the chemical make-up of the different phases, and the size distribution of fly ash particles (Bin-Shafique et al, 2003).

2.2.2 Chemical and classification of fly ash

The chemical composition of fly ash is heavily dependent on the composition of burned coal in terms of its primary mineralogy. The chemical composition of fly ash is not entirely dependent on the inherent mineralogical composition of coal. It has been studied that there exist other influences controlling the final elemental composition of fly ash, these include, the degree of coal preparation, boiler combustion conditions, combustion additives, coal ash handling and disposal, emission control technology (Adriano et al., 1980; Fatoba, 2008; Petrik et al., 2005). (2006).

According to Kruger (2003), South African fly ash is a Ferro-aluminosilicate material dominated by Al, Si, Fe, Ca, K, S, Mg, and Na oxides (see Table2.4). Generally, the concentrations of the major elements are higher than those found in the parent coal along with carbon, nitrogen, and various trace elements which include As, B, Be, Cd, Co, Cr, Cu, Ga, La, Mn, Hg, Ni, Pb, Sc, Ag, Tn, Sr, V, Y, Zn and Zr (Gitari et al., 2006).

Table 2.4: Chemical constituents in South African fly ash (Kruger, 2003)

Constituent	Range (wt. %)
SiO_2	45 – 55
Al_2O_3	28 – 35
Fe_2O3	3.0 - 5.0
TiO_2	1.5 - 2.0
P_2O_5	0,5 -1,5
CaO	4 – 12
MgO	1.5 - 2.0
Na_2O	0.1 – 0.8
K_2O	0.5 - 1.0
SO_3	0.3 – 0.8
Loss on ignition	0.5 - 2.0

Fly ash classification relies on chemical composition and can be grouped as either Class C or Class F by the American Society for Testing and Materials (ASTM). This is based on the sum oxides content of Si, Al, and Fe (III), i.e $SiO_2 + Al_2O_3 + Fe_2O_3$ in the fly ash. ASTM (1998) dictates that fly ash comprising of more than 70wt% ($SiO_2 + Al_2O_3 + Fe_2O_3$) and low CaO content be classified as Class F, while fly ash with between 50-70 wt% ($SiO_2 + Al_2O_3 + Fe_2O_3$) and higher CaO content be classified as Class F. Class F fly ashes are normally as a result of the combustion of anthracite or bituminous coal which gives sum oxide content greater than 70 % in the fly ash. The class C fly ashes are produced due to combustion of lignite or sub-bituminous coal (ASTM, 1998). The lime content of fly ash is important concerning its participation in the hydration reactions involving pozzolanic material of fly ash. Pozzolans are composed of a siliceous and or aluminous substance that possesses little or no cementitious value. The lime content in class F is in the range of 1% to 12% while the range for the self-cementing Class C fly ash is above 20%. This high lime content is the reason it can self-cement in the presence of water (Ahmaruzzaman, 2009).

2.3 ENVIRONMENTAL REGULATIONS: WASTE DISPOSAL

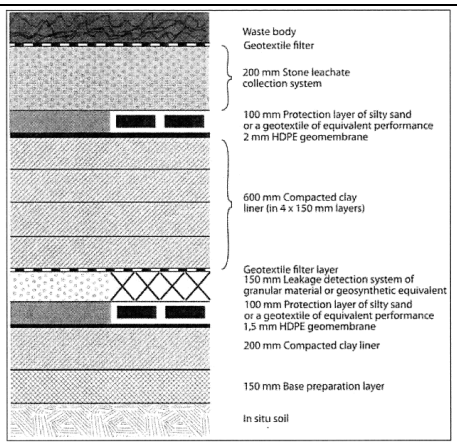
Anthropogenic waste, classified according to its site of generation, constituents, and physical state, is disposed of at specially designated Waste Disposal Facilities (WDFs). WDFs are physical, ground surface-based facilities used for the disposal of municipal and industrial waste. Waste disposal has been practiced for many years as a vital part of waste management and has been linked to various adverse public health effects in the vicinity of disposal sites. In South Africa, impacts on groundwater quality from these facilities are regulated in terms of the National Water Act, No. 36 of 1998 (NWA) and National Environmental Management: Waste Act, No. 59 of 2008 (NEMWA). The NEMWA's

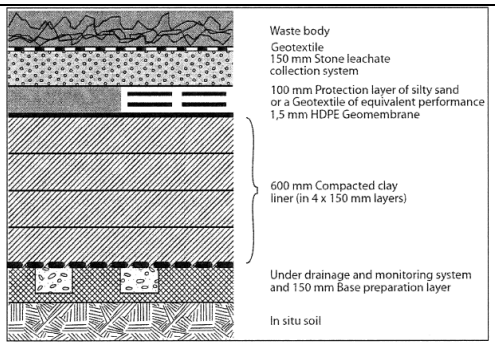
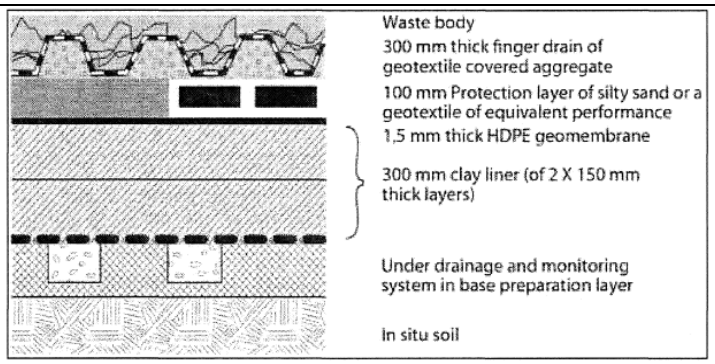
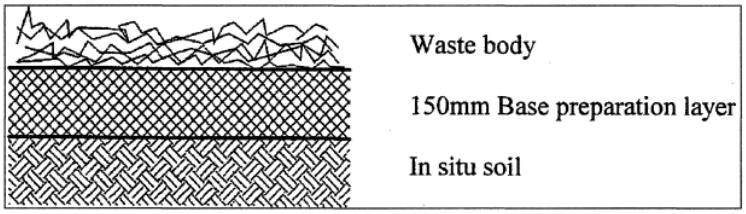
mandate is to protect the environment from waste disposal while NWA focuses on the protection of the water resources which include groundwater.

Best Practice Guidelines (BPGs) for pollution control dams, instituted by the Department of Water Affairs and Forestry [(DWAF, 2007), now the Department of Water and Sanitation (DWS)] guides how to implement the hierarchy of decision making in pollution prevention concerning WDF. The NEMWA Regulations Government Notice No. R.634, R.635 and R.636 on the waste classification (WC) and management, assessment and disposal for landfill regulations instituted by the Department of Environmental Affairs (DEA, 2013) were also developed to direct the process of decision-making in terms of the type of pollution prevention measures for each type of waste.

In terms of waste regulation, waste is classified according to its chemical composition, irrespective of the source, as **Type 0, 1, 2, 3, and 4,** and waste of the same type can be disposed of at the same WDF. The type of waste disposed of leADF to the classification of WDFs as **Classes A-D**, with the corresponding liner requirements as shown in Table 2.5. A liner is a barrier for waste containment, typically underlying the waste body. Considering the current waste regulation, a typical coal-fired power station, regardless of the ash disposal method (i.e dry or wet) used, is expected to have a liner underlying the ash mass. This is dependent on the risk profile as determined by the WC.

Table 2.5: Waste Disposal Facility Classification System (DEA, 2013).

Waste Type	**Liner Requirements**	**WDF**
Type 0	NA	NA
Type 1		Class A

Type 2		Class B
Type 3		Class C
Type 4		Class D

2.4 UNCONSOLIDATED MATERIAL UNSATURATED ZONE AND WATER RETENTION

In this and subsequent sections, the terms unconsolidated material and soil are used congruently to coal combustion residues, loosely termed coal ash. The unsaturated zone is also known as the vadose zone and the zone of aeration is the portion of the subsurface bounded at its top by the soil surface and below by an aquifer and separated by a water table. The unsaturated zone varies in thickness. The lowest (0 m) thickness can be encountered at the groundwater discharge zones where the water table is at the surface during groundwater discharging to the surface (to lakes, marshes streams, *etc.*). Fredlund (2006) refers to the unsaturated zone as a three-phase mixture comprised of solids, air, and water. This zone remains of interest in the scientific and engineering fields, mainly because from a hydrogeological viewpoint the unsaturated zone regulates the amount and quality of water recharging the aquifer. The zone is also critical to the cultivation of plants, designing and construction of civil structures, and disposing of waste. Over the years, the incentive to understand the unsaturated zone originated from the recognition of the critical role it plays in the improvement and protection of the

groundwater qualities, due to anthropogenic influences originating from the top of the unsaturated zone at the surface.

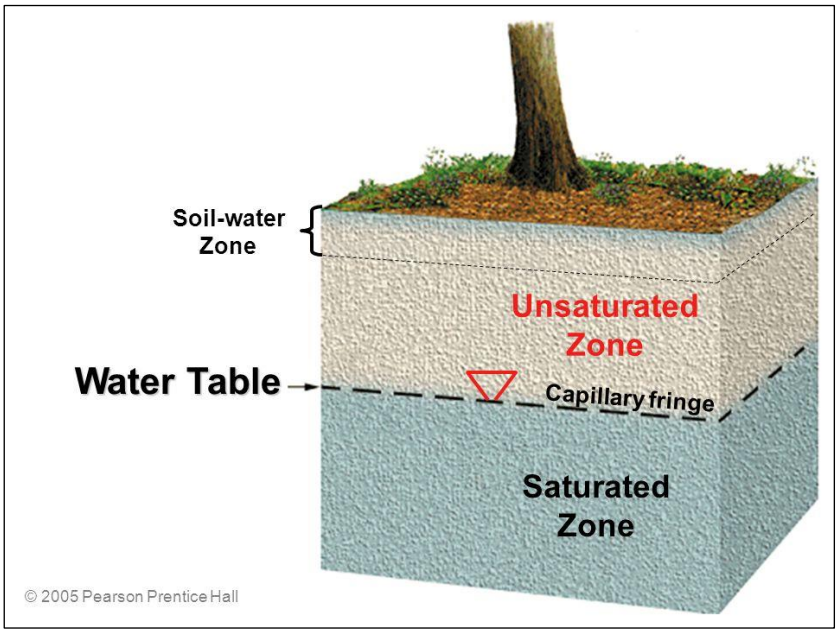


Figure 2.5: Cross-sectional view of the unsaturated zone underlain by the saturated zone (McCauley *et al.*, 2005)

2.4.1 Porosity and soil water content

The porosity of soil is the amount of void space. It depends on the consistency and packing of the soil particles, it is directly affected by compaction. It is given by:

$$n = 100(V_v/V_s) \quad (1)$$

Where n is porosity (in percentage), V_v is volume of void space (L^3, cm^3 or m^3) and V is the volume of the sample (L^3, cm^3 or m^3)

If you let $e = V_v/V$ be the void ratio of the soil, e is dimensionless and V_s has volume units similar to above, then the void ratio is closely related to the porosity by the following equations:

$$n = \frac{e}{1+e} \quad (2)$$

And,

$$e = \frac{n}{1-n} \quad 3$$

The gravimetric water content of the soil is the ratio of the mass of water contained in the pore spaces of soil to the mass of solid dry soil particles.

$$\theta_g = 100(W_w/W_s) \quad 4$$

Where $\theta_g$the gravimetric water is content (in percentage), W_w is the mass of the water in the soil (M; g or Kg) and W_s is the mass of the solid particle (M; g or Kg).

The volumetric water content is the ratio of the volume of water contained in the pore spaces of soil or rock to the total volume of soil and rock.

Where θ_v is the volumetric water content (dimensionless ratio) and V_w is the volume of contained

$$\theta_v = V_w/V \quad 5$$

water (of units; L^3:cm^3 or m^3). 5.2 Water flow in unsaturated soils

The saturation ratio of the soil relates the two water contents by dividing the volume of contained water by the volume of the voids as follows:

$$R_s = V_w/V_v \quad 6$$

2.4.2 Water Flow in Unsaturated Unconsolidated earth material

According to Feddes *et al.* (1988) (cited Buckingham 1907, Gardner and Widtsoe 1921 and Richard 1931) and Prasad *et al.* (2001) water movement in the unsaturated zone, was initially recognised by Edgar Buckinham whose findings related the flow rate to suction gradients. He further introduced a pressure head term which was later confirmed by Gardner and Widtsoe (1921). The mathematical representation of differential equations for soil water flow which is based on heat flow in porous media analogy was introduced by Richard (1931). This is commonly known as Richard's equation. To date, the equation is still used for basic mathematical expression that underlies unsaturated zone flow phenomena.

Water flow in the unsaturated zone is highly nonlinear since the hydraulic conductivity and soil water pressure head depend on the soil water content. The liquid in the unsaturated zone is not pure, rather

a mixture of water and dissolved solids and gaseous constituents (Nielsen and Biggar., 1986). Available voids in the unsaturated zone are mainly filled by gas since most of the liquid phase has been removed by gravitational force (see Figure 2.6). The forces responsible for holding the liquid phase within the porous media voids act by counteracting the gravitational force, these forces are called the matrix forces.

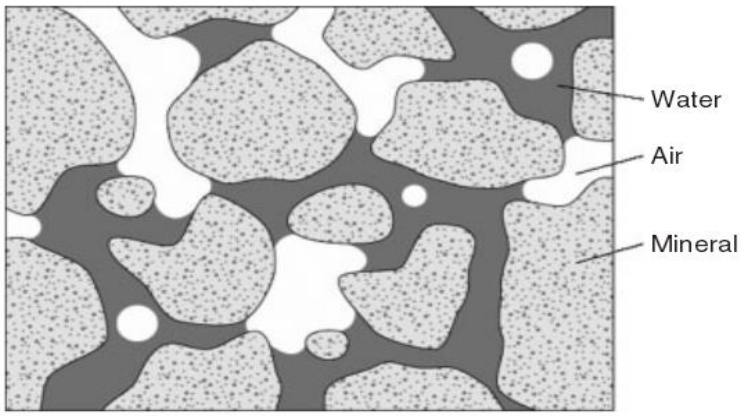


Figure 2.6: Microscopic view through a porous media illustrating the three phases conditions present in the unsaturated zone

2.4.2.1 Mechanical energy concept

Suction gradients are considered to be central and responsible for water movement in the soil when using the mechanical energy concept. But water movement through the unsaturated porous media is also due to other driving forces such as thermal, electrical, or solute concentration gradients (Feddes *et al*., 1988). As a result, an energy concept has been developed which states that unconsolidated earth material water movement is in the direction of depleting energy status. Gibbs' free enthalpy, commonly known as the water potential, best describes the energy status of soil water under a given temperature. The soil water potential is given by according to Feddes *et al*. (1988)

$$\phi = \phi_m + \phi_{ex} + \phi_{en} + \phi_{os} \qquad 7$$

Where:

ϕ_m = Matric potential arising from local interactions between the unconsolidated material matrix and water

ϕ_{ex} = Potential arising from the external gas pressure

ϕ_{en} = Overburden (envelope) potential caused by an external load which is partially carried by the soil water phase

ϕ_{os} = Osmotic potential arising from the presence of solutes in the water

For water at height (above a reference level), gravitational potential does play a role, contributing to the total water potential as given by:

$$\phi_t = \phi + \phi_g \quad (8)$$

Where $\phi_t$and $\phi_g$are total water potential and gravitational potential respectively.

2.4.2.2 Liquid in motion: Darcy equation

The assumption that water moves proportionally to the forces acting on it, is sufficient to define the rate at which water moves one-dimensionally through the unsaturated zone as:
Where q is the volumetric flux density of water, z is the distance, and $K_i$is the proportional constant

$$q = -\sum_i K_i \frac{\partial \phi_i}{\partial z} \quad (9)$$

that relies on the degree of water saturation and temperature. For most field studies, it is generally assumed that ϕ_{os} is constant spatially and temporally (Nielsen and Biggar, 1986). Combining the previous equation with the equation of continuity we get:
The above equation leADF to Richard's equation for liquid flow in the unsaturated soils. The

$$\frac{\partial \Theta}{\partial t} = \frac{\partial q}{\partial z} + \phi \quad (10)$$

equation is in terms of the pressure head for a rigid medium on a vertical flow direction (z coordinates). Assuming positive downward, then the unsaturated flow equation becomes:

$$C(h)\frac{\partial h}{\partial t} = \frac{\partial}{\partial z}\left[K(h)\frac{\partial h}{\partial z}\right] - \frac{\partial K(h)}{\partial z} + \boldsymbol{\Phi} \quad (11)$$

Since$C(h) \equiv \frac{\partial \Theta}{\partial t}$, the water capacity or the slope of the soil water retention curve where Θ is the volumetric water content. K Is the hydraulic conductivity, t is the time and $\boldsymbol{\Phi}$ represents sources and sinks of water in the system.

2.5 COAL ASH WATER RETENTION CHARACTERISTICS

The nonlinear relationship between soil water content and matric suction of a porous material under unsaturated conditions is described by the soil-water characteristic curve (SWCC). Originally

developed for the soil and agricultural fields, however, through vast research work it was introduced to the geotechnical engineering field where it gained popularity (Fredlund *et al*., 1993, Vanapalli *et al.*, 1998; Vanapalli and Fredlun, 2000; Vanapalli and Han, 2019). The SWCC for a given material represents the water storage capability, enabling the determination of varying matric suction with respect to the water content changes (Mahmood and Kareem, 2010). More often, the SWCC is represented using a logarithmic scale (Fredlund and Xing, 1994). Figure 2.7 shows a typical SWCC for a silty soil together with its main components.

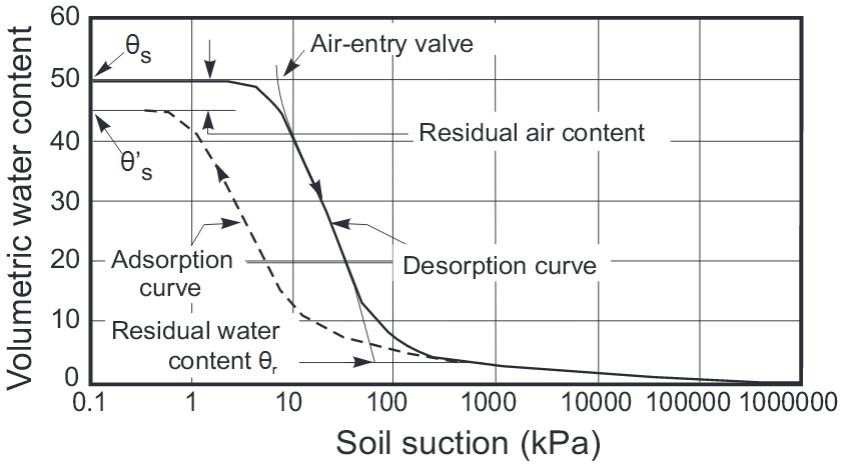


Figure 2.7: A typical SWCC and its main components for a silty soil sample after (Fredlund and Xing, 1994)

The air-entry value sometimes referred to as bubbling pressure represents the matric suction value needed for the largest pore space within the soil to initiate the first draining (Mahmood and Kareem, 2010). The residual water content represents the highest suction required to drain additional water from the soil, while in contrast, the saturated water content corresponds to the lowest matric suction. Through construction of tangent lines as in Figure 2.7, by selecting points of inflection in different parts of the SWCC, it is possible to empirically determine the main components of a SWCC. Different soil textures yield different SWCC shapes as illustrated in Figure 2.8.

Depending on the SWCC determination technique used, SWCC paths may follow the desorption (draining) path or the ADForption (wetting) path. The two paths are represented by curves of similar shapes, however, the starting point of the desorption curve differs from the endpoint of the ADForption one. This is mainly due to the air that is entrapped in the soil and other responsible hysteresis.

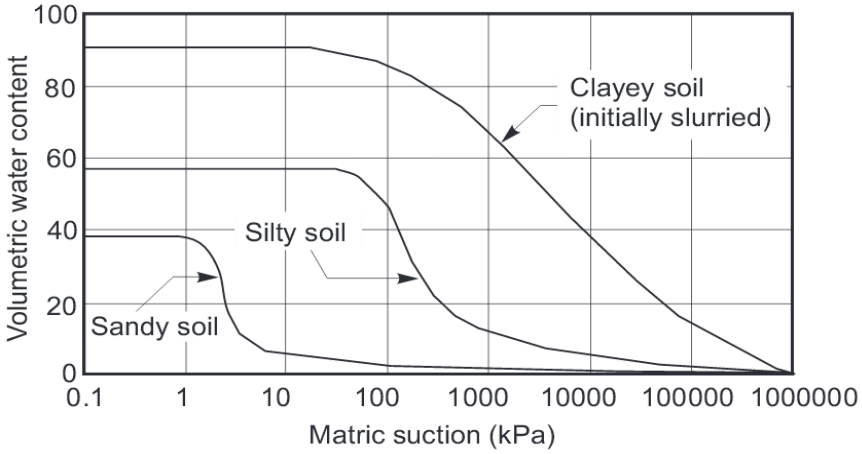


Figure 2.8: A SWCCs for sandy, silty and clayey soils after (Fredlund and Xing, 1994)

Depending on the SWCC determination technique used, SWCC paths may follow the desorption (draining) path or the ADForption (wetting) path. The two paths are represented by curves of similar shapes, however, the starting point of the desorption curve differs from the endpoint of the ADForption one. This is mainly due to the air that is entrapped in the soil as well as another responsible hysteresis.

2.5.1 Soil water characteristics curve hysteresis

The field capacity of waste materials is of critical importance in determining the formation of leachate in landfills which in this case is the coal ash dump facility. It is the field capacity limit when exceeded which gives rise to leachate generation consequently promoting a downward movement of generated leachate. The field capacity varies with the degree of applied pressure. At field capacity, it is the macro-pores of the soil which are drained off initially through gravity, however, water gets retained in the micropores. The soil moisture tension at field capacity varies from soil to soil concerning soil texture class. Figure 2.9 provides field capacity, available water, and wilting point water contents for various soil textures, confirming field capacity as a function of soil texture.

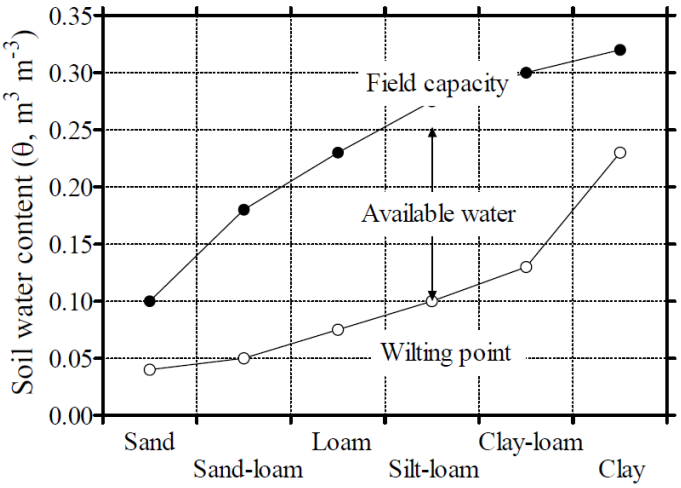


Figure 2.9: Soil-water contents of various soil textures at field capacity and wilting point stages (source: Pardossi et al. 2009)

Additionally, Matsumoto et al. (2016) concluded, in coal ash, it is not only fine fractions that control the water retention but also the coal ash microporous structures enhance water retention capacity.

2.5.2 Soil water characteristics curve hysteresis

Hysteresis in the SWCC refers to the non-unique relationship between the soil's matric suction and its water content, whereby the soil can have two different water contents at the same matric suction value, depending on the preceding sequence of wetting and drying (Tami *et al*., 2004). Hysteresis is thought to be caused by various factors, such as variable and irregular cross-sections of the pores, the different contact angles in the advancing and receding soil-air interface menisci, and the difference in entrapped air volume at different matric suction values. It has been shown that SWCC hysteresis can significantly affect the prediction of flow, redistribution, and storage of water in the unsaturated zone (Fredlund and Xing, 1994).

2.6 SOIL WATER SUCTION MEASUREMENT TECHNIQUES

There exist several suction techniques to measure the suction of a soil sample. The selection of the technique is based on the desired suction ranges. Different methods are used to determine the total suction and matric suction respectively. The most commonly used measurement techniques include; Tensiometers, Pressure Plate Extractors, Conductivity Sensors, Pyschrometers, and Filter Paper Method. In this study, a less common yet effective technique is used, A HYPROP HYPROP (HYdraulic PROPerty analyzer, UMS, 2012). The above techniques can be grouped into two main categories, depending on how the method is employed. These categories are; direct method and indirect method. Pan *et al.* (2013) group these methods (see Table 2.6) according to their suction ranges as well as the period it takes for equilibrium to be reached i.e when no changes in both water content and suction are noticeable for an extended period during the experiment.

Table 2.6: Summary of common water suction techniques (Pan *et al.*, 2013).

		Technique	Suction Range (kPa)	Equilibrium time
Direct suction measurement	Matric suction	axis-transition technique	0-1500	hours
		tensiometer		hours
		suction probe		minutes
Indirect suction measurement	Matric suction	time domain reflectometry	0-1500	hours
		electrical conductivity sensor	50-1500	6-50 hours
		thermal conductivity sensor	0-1500	hours-days
		in-contact filter paper	all ranges	7-14 days
	Osmotic suction	squeezing technique	0-1500	days
		psychrometer technique	100-10000	1 h

	Total suction	relative humidity sensor	100-8000	hours-days
		chilled-mirror hygrometer	150-30000	10 minutes
		non-contact filter paper	all ranges	7-14 days

2.7 CHAPTER TWO SUMMARY

Through the literature studies, coal ash generated from electricity generation is disposed of relying on two methods which are dry and wet ashing. Fly ash is the dominant coal combustion residue found disposed of in the dry ash dump facility. In South Africa, there is legislation that governs the disposal of ash as waste through the waste classification regulations. Water characteristics in ash are comparable to the soil water characteristics as both are systems consist of a three-phase condition. The literature also revealed both the chemical and physical properties of fly ash. Ash water characteristics are explained similarly to that of soil using the principle of soil water characteristic analysis.

CHAPTER 3: SITE DESCRIPTION

Matimba Power Station, a coal-fired power station falls under the Waterberg municipality in the Limpopo province close to Lephalale, formerly Ellisras. Construction of Matimba power station commenced in 1981 with the first unit being synchronized into the national grid in 1987. It consists of six units with a baseload capacity of 3990 MW (6 X 665 MW). Lower yearly rainfall in the area prompted the use of innovative low water consumption technologies which include, direct dry cooling and dry ashing. Figure 3.1 depicts the main land use within the study area consisting of power regeneration, coal mining, and residential. Immediate west of the ash disposal site is Medupi Power Station. The adjacent Grootegeluk colliery, owned by Exxaro, supplies coal to Matimba power station via overland conveyors.

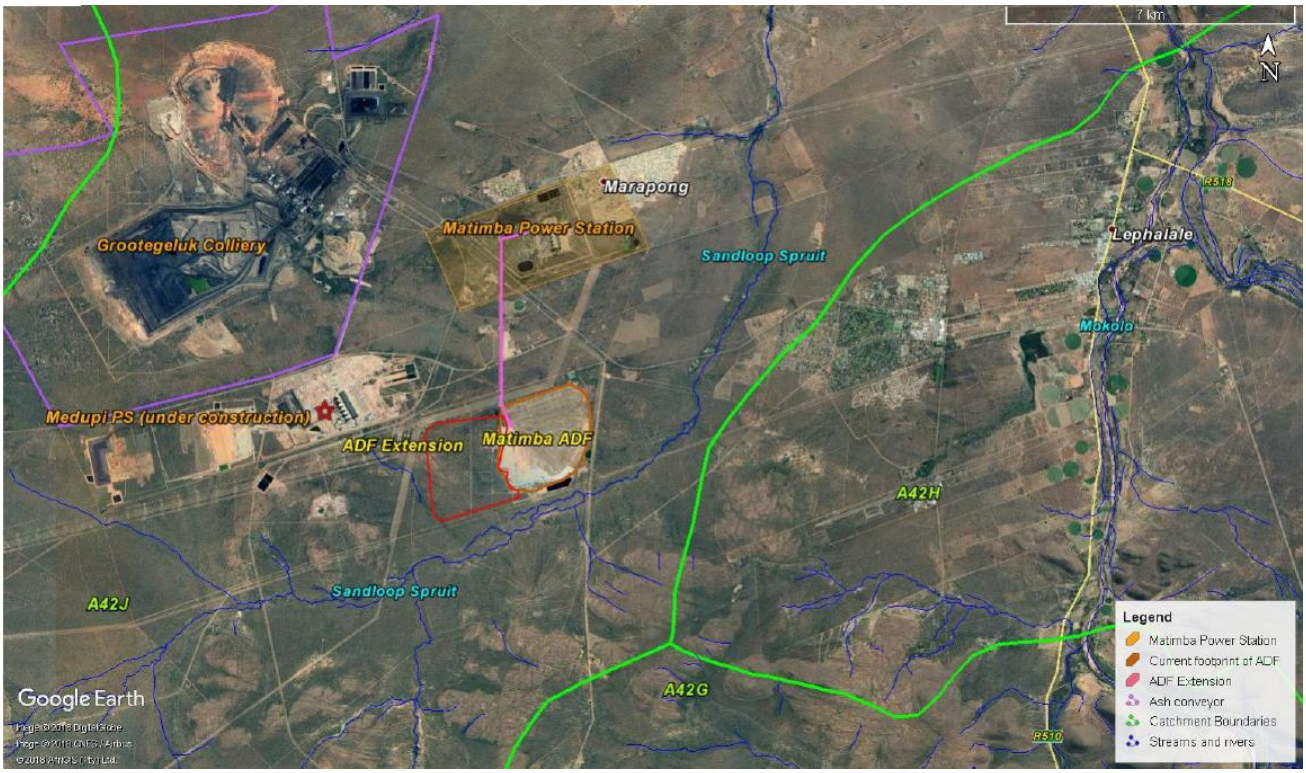


Figure 3.1: Matimba Power station and the Ash disposal site locality map

The Colliery has sufficient coal reserves to guarantee Matimba Power Station a lifespan of 35 – 50 years, extending to around 2055. Consuming coal at a maximum of 2,150 tons per hour, at a combustion rate of 34%, approximately 731 tons of coal fly ash is produced per hour, for a total of around 6.4 megatons (Mt) per annum. Coal ash is transported employing a series of conveyors to an Ash Disposal Site (ADF) where is continuously disposed of through the 'dry ashing' disposal method. The ADF is located approximately 3 km to the south of the Power Station

3.1 MATIMBA ASHING PRACTICES

Fly ash from the boilers is transported to an offsite designated Ash Disposal Facility (ADF) approximately 3 km using the overland conveyor. It is transported with 12% moisture to minimise the mobilising of potential airborne fly ash particulates. Fly ash reaches the ash disposal site using two conveyors in parallel orientation (see Figure 3.2). The spreader (front system) and stacker (back system) are both fed by the two parallel conveyors. The tripper car through a link conveyor is fixed to both the spreader and the stacker. When ash is deposited onto the spreader discharge boom, left and right deposition is achieved since the spreader is mounted with a mobile crawler. The stacker is the most used disposal system due to its maneuverings and that it can deposit more ash per dedicated shift as opposed to the spreader. In Matimba, ash is currently deposited using a radial shifting stacker and spreader system.

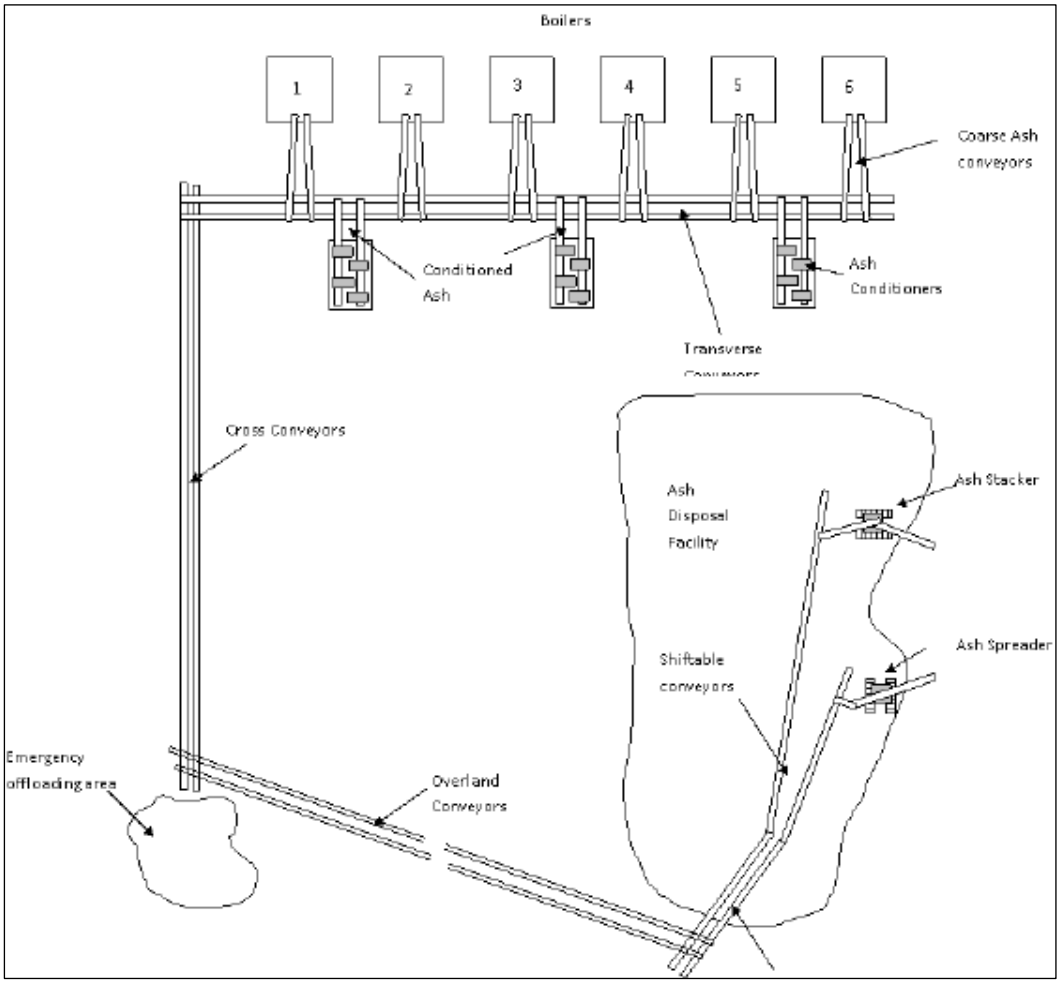


Figure 3.2: Schematic overview of Matimba ash management practices

Spreading of disposed of ash is further carried using construction plant equipment machinery to assist amongst other activities with:

- Moving of ash to locations accessible to the spreader and stacker.
- Moving of soil used for dust suppression and rehabilitation.

Matimba has two emergency ash offloading, one at the power station area, the other located within the ash disposal site as depicted in Figure 3.2. The emergency ash offloading is important in the Matimba ash management system. It provides valuable space to temporarily dispose of ash whilst maintenance or repairs of the conveyor system is on-going. To prevent ash from interacting directly with natural ground, a concrete layer is in place. Once the conveyor system is functional and in operation, the front end loader is used to load ash in the overland conveyors.

Dust suppression is typically achieved using water sourced from pollution control dams within the ash disposal site. Water sprinklers are placed in the advanced slope of the ash dump to suppress airborne ash particles. A combination of ash and water result in ash consolidating within two days of adding water, this typically yields a fairly compacted ash dump. Compaction within an ash dump is increased by the movement and placement of different machinery and equipment above the ash stack. No further compaction is done. A 50 mm thick layer of soil (approximately sand-size particles) is placed as the cover daily for completed sections. This will ultimately be followed by the rehabilitation cover layer of 300 mm thick topsoil. Grasses, plants, and trees are planted to reduce eroding of placed soil through aeolian and water erosion processes. However, this also aids with reducing volumes of water interacting with the ash matrix, as most of the water will be lost through evapotranspiration as well as water loss within the soil voids.

3.2 TOPOGRAPHY AND DRAINAGE

The surface topography of the area where the ADF is located is predominantly undulating. This is mostly represented by cross-section A-B (NW-SE) in Figure 3.3, while cross-section A'-B' (SW-NE) slopes very gently and almost gradually to the Southwest and northeast of the ash dump. The elevation of the site is between 900 meters above mean sea level ("mamsl") in the west, to 875 mamsl in the east, with a total gradient reduction of around 40 m over 6 km from Northwest to Southeast. East of the ADF is a non-perennial stream, Sandloop, with a south to the north flow direction. Sandloop is a tributary of the Moloko River, a major river in Lephalale. Which itself drains into the Limpopo River, about 50 Km in the South Africa Botswana border. The two cross-sections (A-B and A'-B') in Figure 3.3 cuts across the ash dump and reveal that the highest point is at A(900m) which is away from the ash dump. However, cross-section A'-B' shows the topography of the area with ash dump mostly located in high points. Current ashing is happening towards the southwest portion of the ADF.

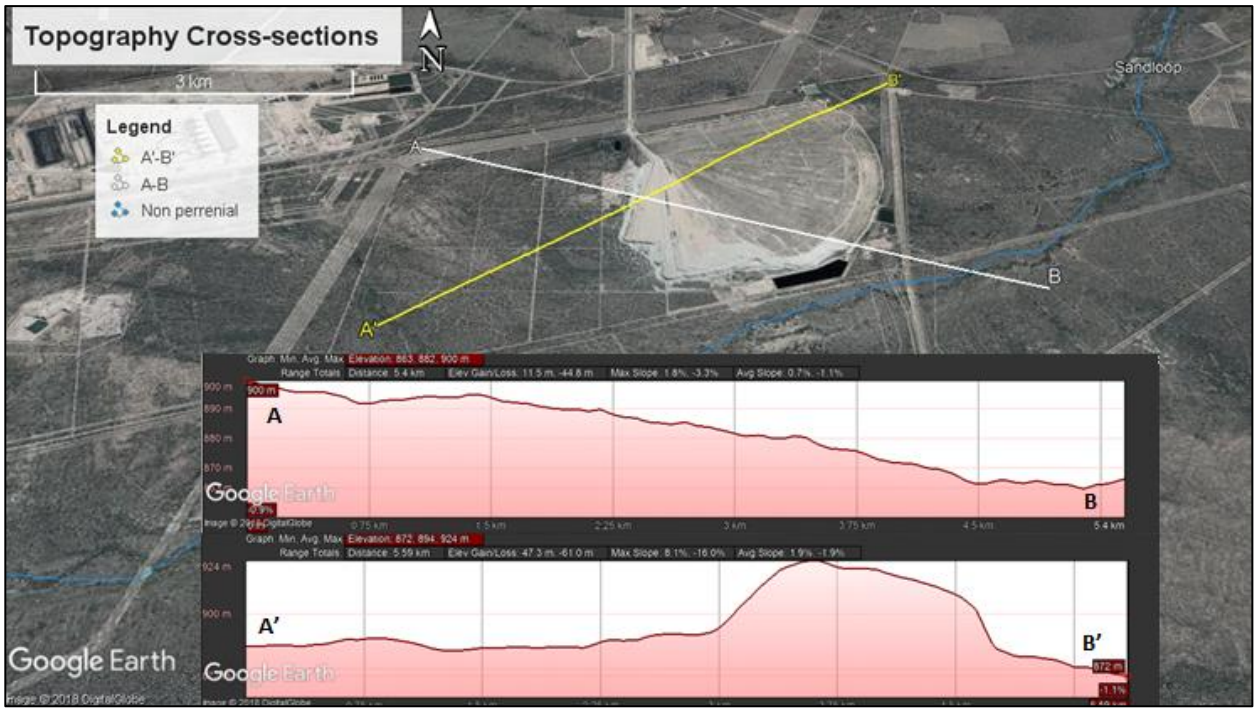


Figure 3.3: Topography sections

The extension portion where future ashing will take place is well developed, trees have been cleared and topsoil disturbed in preparation for the new ashing footprint. Current activities have the potential to influence topography which in turn has an impact on surface run-off. During rainfall events, runoff from the ADF drains towards Sandloop, located downgradient of the ADF.

3.3 GEOLOGICAL AND HYDROGEOLOGICAL SETTING

3.3.1 Regional Geological Conditions

According to the portion of the 1:250 000 geological map (2326 Ellisras) in Figure 3.4, the AD (blue) and Power station area (red) is situated in Zwartwater and Grootestryd farms, respectively. These farms are underlain by different geological units of the Waterberg and Karoo Supergroups. Sandstone, gritstone, mudstone, coal are associated with the power station area. The ADF is underlain by a sequence of distinct coarse-grained purple sandstones as well as conglomerates.

Two major faults with strikes, east-west, and northwest-southeast are heavily faulted ellisras coalfield. Targeted coal seams at the Grootegeluk Colliery occur at fairly shallow depths (to about 60 meters) (Snyman, 1998). This is a result of the horst and graben structures due to the faulting in the area.in some areas, the complex existence of the faults has rendered certain areas un-mineable (Snyman, 1998).

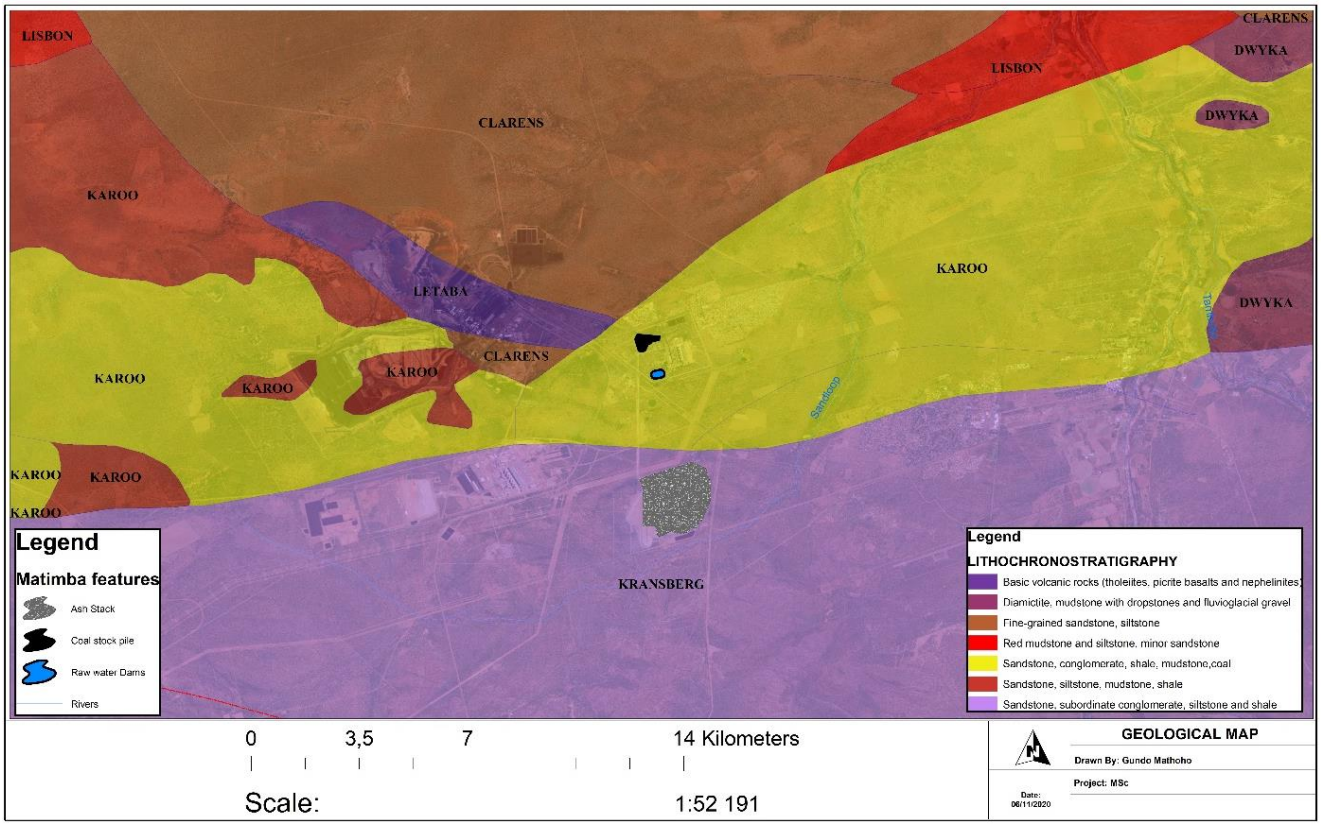


Figure 3.4: Geological setting of Matimba power station and ash disposal Area

The near-vertical Eenzaamheid fault has a throw of 250 m and traverses the area just to the north of the ADF, separating the Mogalakwena Formation (Mm) of the Waterberg Group to the south, from the Swartrant and Grootegeluk Formations of the Ecca Group (Karoo Supergroup) to the north. Two major faults with strikes, east-west, and northwest-southeast are heavily faulted ellisras coalfield. The Grootegeluk Formation consists of mudstone, carbonaceous shale, and coal, which is mined by Grootegeluk Colliery. Further north, the Daarby Fault, a basalt intrusion with a 400 m displacement, separates the Ecca Group from the Clarens Arenite Formation (Stormberg Group), which consists of fine-grained, Aeolian sandstones (Bester, 2009).

3.3.2 Local geological Conditions

Table 3.1 lists volcanic and sedimentary rocks of the Waterberg and Karoo supergroup which underlie the study site. Geology and climate play an important role in the soil types that can be expected to be present in an area, which is mainly derived from the weathering of the parent rocks. A thick aeolian sand layer of approximately 1-2 m fine-grained, silty sand is well exposed around the ADF. The sand deposited around the ADF is typically dry with little or no moisture. The sand is dense and yellowish/orange in colour (Snyman, 1998). The dominant rock type within the ADF is the distinctive conglomerate of the Mogalakwena formation, which outcrops in some parts of the ADF, in particular west of the ADF. The conglomerate bedrock is orange-brown to purplish-grey. The conglomerate is moderate to highly weathered with fine to coarse-grained of numerous sub-rounded to sub-angular

pebbles. In some instances conglomerate is absent, and the aeolian sandy soils are underlain directly by sandstone bedrock (Enviroworks, 2018).

Table 3.1: Local lithography after Snyman (1998)

Age	Stratigraphic unit	Formation	Rock types
Quaternary			Sandy soils
Triassic	Karoo	Clarens	Fine-grained Sandstone
Triassic	Karoo	Eendragtpan	Variegated Shale
Permian	Karoo	Swartrant	Sandstone, Gridstone, Mudstone and Coal
Permian	Karoo	Grootgeluk	Mudstone, Carbonaceous shale and Coal
	Waterberg	Mogalakwena	Coarse grined purplish brown sand stone; Conglomerate

3.3.3 Local Geohydrological Conditions

Geological formations and associated structures dictate the geohydrological make-up of an area to a large extent. Geological structures can improve the groundwater potential in the area by increasing the permeability and transmissivity of the host rock. Fractures or fissures within the host rock, which act as groundwater preferential flow paths and are associated with high groundwater yields, are a result of secondary geological processes such as intrusion, faulting, and fracturing. Based on the drilling information gathered in the area, two aquifers systems were confirmed around the study area, the shallow and deep aquifer systems. The shallow aquifer consists of gravely sand and weathered material existing at depths of approximately 3-12 m below the surface. At this depth, the shallow aquifer is directly recharged by rainfall. The aeolian soils, of the shallow aquifer, have a high percolation rate of 144 mm/h with subsequent high infiltration rates into the lower layers (Bester, 2009). However, the impermeable to slightly permeable shales act as an aquiclude with low percolation rates of between 12-24 mm/h. The deep aquifer consists of fractured sandstone and shale. Groundwater mainly exists within fractures in this zone. The groundwater potential is generally low in the fractured aquifer, and groundwater in this aquifer will typically occur within the joints, bedding planes, and along with dolerite contacts within the Waterberg Group sediments, with yields ranging between 0.5-2 l/s.

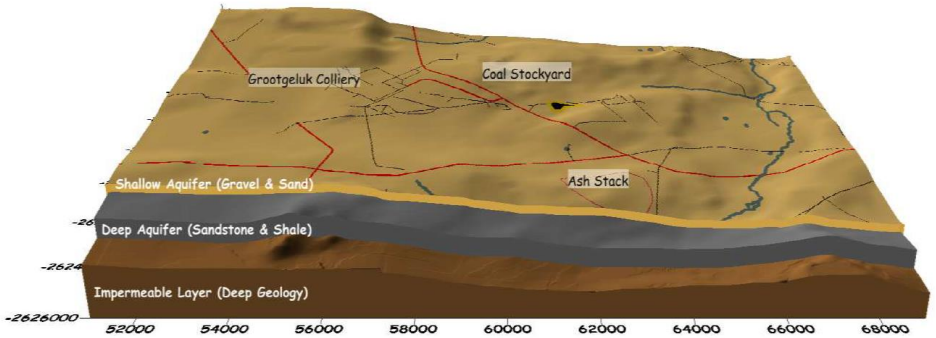


Figure 3.5: Site conceptual model showing distinct aquifer systems (GHT, 2011)

Aquifer testing, mainly based on the slug test has confirmed low transmissivities around the study area, which ranged from 0.04 to 0.06 m^2/day (GHT, 2014). Due to the quick infiltration of rainwater into the gravelly sand, a perched water table will be encountered following rainfall events. Perched aquifers occur between 1-3 meters below ground level (mbgl). Monitoring data consisting of groundwater level elevations surveyed for 38 boreholes within an 8 km radius from ADF indicate that the level of the static water level (water table) generally mimics surface topography. This is concluded after the data yielded a good correlation (R^2=0.86) between surface elevation and water level elevation. The groundwater flow direction is from west to east, towards the drainage line of the Sandloop stream, as depicted in Figure 3.6.

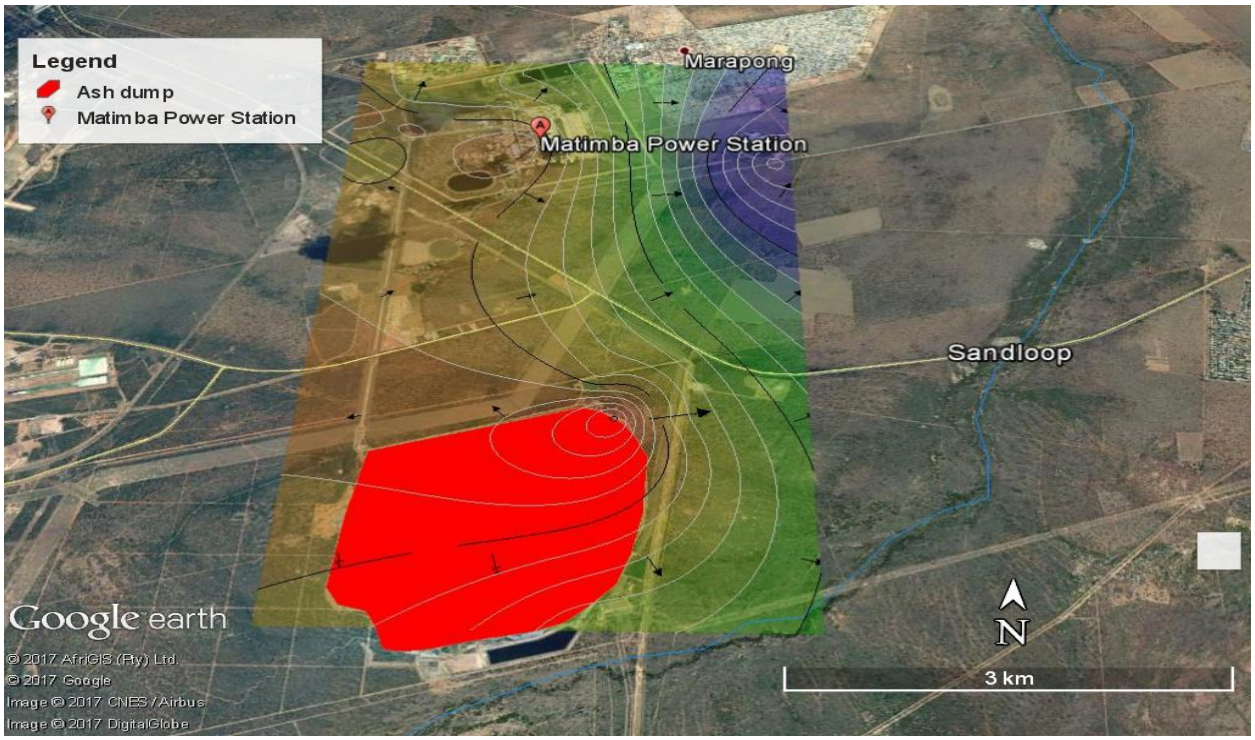
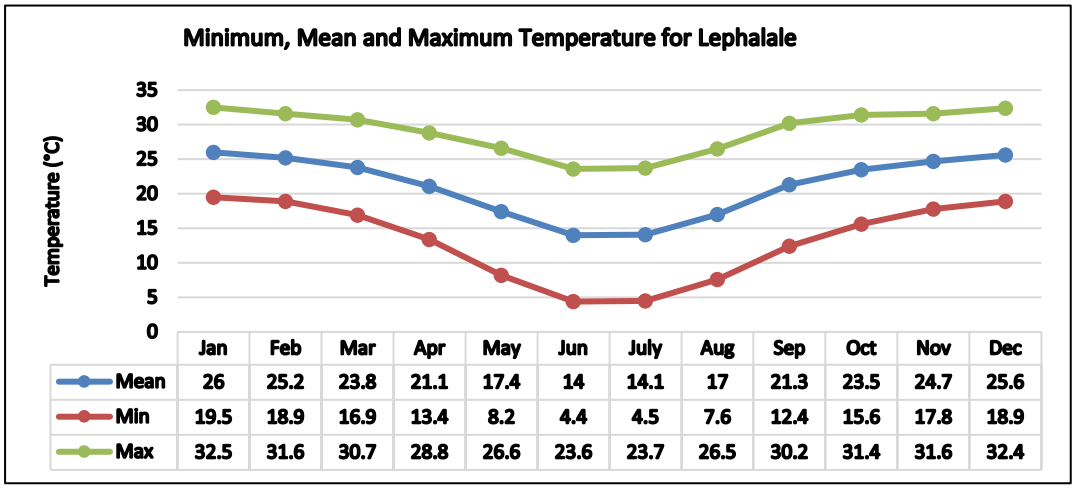


Figure 3.6: Groundwater contour map and flow direction

3.4 HYDROLOGY AND CLIMATIC CONDITIONS

Matimba Power Station including the ADF falls under the Limpopo-Olifants Drainage region. Surface water around the study area drains towards the Sandloop Spruit drainage line, as indicated by the surface topographic cross-sections in Figure 3.3. The study area is characterised by uniformly less undulating plains. The drainage line is located directly south of the study area. Sandloop Spruit, a non-perennial stream flows from west to northeast into the headwaters of the Mokolo River, northeast of the site. The study area falls within the quaternary catchment A42J of the Limpopo Water Management Area (WMA).

According to DWA (2006), the Mean Annual Precipitation (MAP) for A42J is 428mm. This is significantly lower than the country's mean annual rainfall of 437mm. Figure 2-2 presents monthly mean rainfall data collected for a total of 30 years (1982-2012) for the Lephalale area (climate-data.org). In the context of water management around the ash disposal site, November through to April is an important period. These months accounts for approximately 95% of rainfall in the area. Consequently, November to April can be referred to as 'wet-season' for the area, while May to September is the 'dry-season'. Any water balance developed for the site should consider this periodic variation in rainfall viz; water excess and water deficit periods. Data from (climate-data.org) consisting of annual mean, minimum and maximum temperatures of Lephalale (approximately 31 km away from the study area) are presented in a time-series graph (see Figure 3.7). The data indicates December and January as the hottest months with maximum temperatures of 32.4°C and 32.5°C respectively. While June records the lowest temperature of 4.4°C.



	Jan	Feb	Mar	Apr	May	Jun	July	Aug	Sep	Oct	Nov	Dec
Mean	26	25.2	23.8	21.1	17.4	14	14.1	17	21.3	23.5	24.7	25.6
Min	19.5	18.9	16.9	13.4	8.2	4.4	4.5	7.6	12.4	15.6	17.8	18.9
Max	32.5	31.6	30.7	28.8	26.6	23.6	23.7	26.5	30.2	31.4	31.6	32.4

Figure 3.7: Lephalale Town's Annual Mean, Maximum and Minimum Temperature

3.5 CHAPTER THREE SUMMARY

Matimba Power Station, a coal-fired power station consisting of six units with a baseload capacity of 3990 MW (6 X 665 MW). It falls under the Waterberg municipality in the Limpopo province close to Lephalale, formerly Ellisras. The Matimba ash disposal site (ADF) is located approximately 7km south of the power station area. The ADF is sited on predominately undulating surface topography. To the east of the ADF is a non-perennial stream, Sandloop, with a south to the north flow direction. The area receives annual average precipitation of between 449-472 mm (GHT, 2014) mostly in the summer periods. Land use and the geological makeup in the area influence the groundwater quality. The site is underlain by the conglomerates of the Mogalakwena formation of the Waterberg group. There exist two groundwater aquifer systems on site which may be prone to pollution emanating from the ADF and its associated activities. Groundwater flow direction is towards the Sandloop River.

CHAPTER 4: METHODOLOGY

Research Methodology is a continuing process; a continuum that is ever-changing and ever developing. A detailed description of the research methodology informs the reader exactly how the researcher acquired and handled the data (Leedy and Ormrod, 1993).

4.1 SAMPLING

Samples were periodically (every 10 minutes) sampled from a motional conveyor belt on top of the ash dump. A 15 kg heavy-duty plastic bag was used to hold bulked composite samples from Matimba and Tutuka Power stations (henceforth referred to as Matimba and Tutuka respectively) sampled at different dates. Tutuka sample was included to compare some of the physical and geochemical properties with that of Matimba which is the principal sample in this study. Both samples originate from the top of the ash dump, targeting fresh samples straight from the on-land conveyor belt. The bags were sealed and secured at the top to avoid any moisture escape using cable tyres. As a precaution measure to avoid losing a sample through tearing or puncturing of sample bags during sampling and transporting, the sample was double bagged with the same type of sampling bag used. The samples were kept away from direct sunlight during sampling and transporting back to the Laboratory.

Figure 4.1 shows the two sizes of rotary splitters used during the size reduction of the composite sample. The splitters were used to give each particle from the composite sample the same statistical chance for them to be sampled into smaller sizes. This will ensure representative samples of smaller sized samples is extracted from each bag.



Figure 4.1: Two different size rotary splitters used for sampling (size reduction)

4.2 PARTICLE SIZE AND DISTRIBUTION

Studying of unconsolidated soil texture has remained important in the agriculture and engineering fields because the appropriate application of any type of soil is subject to the soil type and associated texture. The distribution of different grain sizes affects the engineering properties of soil. Grain size analysis provides the grain size distribution, and it is required in classifying the soil. Soil texture refers to the size and amount of particles in a given soil and is related to the proportion of sand, silt, and clay (Zhang *et al*., 2005). The amount and distribution of pores are determined by soil texture, therefore, the ability of soil to hold and transmit both liquid and gas phases relies on soil texture amongst other physical properties. The particle size distribution of soils is often used to estimate soil moisture characteristics and hydraulic conductivity, thus accurate estimation of soil properties relies on the accuracy of particle size determination (Gunal *et al*., 2011). Irrespective of the classification system used, the general size sequence is as follows;

Sand> Silt>Clay

The (United States Department of Agriculture) USDA-system has been adopted in South Africa (MacVicar, 1977) for classifying various soil fractions as set out in Table 4.1. Due to the inconsistency of soil particle geometrical shape, a single shape cannot be used to indicate the actual size. The particle size is referred to in terms of the equivalent spherical diameter (e.s.d).

Table 4.1: Soil particle size classification according to the South African system (MacVicar, 1977)

Size class	Diameter (mm)
Stones	>250.0
Cobbles	250.0 - 75.00
Gravel	75.00 - 2.00
Very coarse sand	2.00 - 1.00
Coarse Sand	1.00 – 0.50
Medium sand	0.50 – 0.25
Fine sand	0.25 – 0.10
Very fine sand	0.10 – 0.05
Silt*	0.05 – 0.002
Clay	<0.002
**Silt is sometimes divided into coarse silt (0.05 – 0.02 mm) and fine silt (0.02 – 0.002 mm)*	

4.2.1 Sieving and hydrometer analysis

The hydrometer or pipette method based on sedimentation principles defined by Stoke's law is commonly used to measure clay and silt particles. Sand is measured with the sieving method, involving soil separation according to particle size classes using different sieves of different apertures. The sieving belongs to the mechanical method based on agitation of different sieves staked according to the standard used. There exist various international-based standard methods used across different soil and geotechnical laboratories in South Africa. The most used and referenced standard is the American Society for Testing and Materials, D422 and ASTM C136 / C136M – 14: Standard Test Method for Sieve Analysis of Fine and Coarse Aggregates. The hydrometer method is widely used to estimate particle distribution of soil particles retained from No. 200(0.075 mm) sieve after the sieving process has been concluded. The simplified arrangement of both methods is illustrated in Figure 4.2.

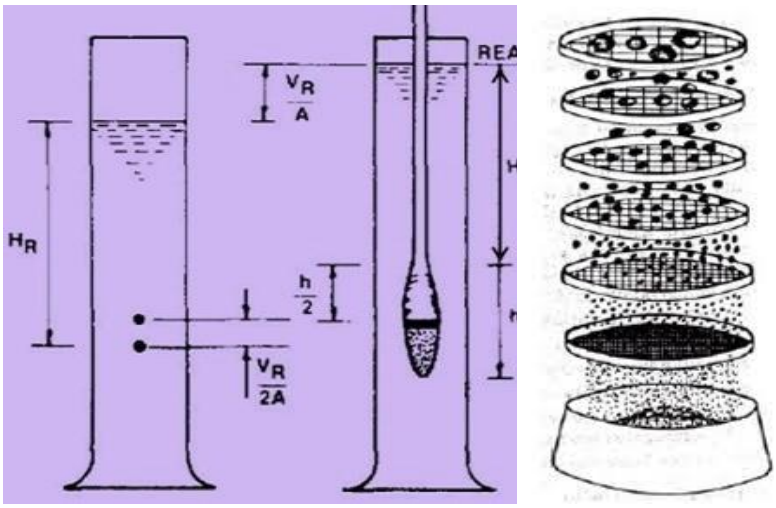


Figure 4.2: Schematic illustration of Hydrometer (left) and sieving (right) configurations

A hydrometer is an instrument used to measure the relative density of a liquid. A hydrometer is made of glass usually consist of two parts;

- A cylindrical flask with graduation marks and,
- A bulb at bottom weighted with mercury.

The density variation will cause the hydrometer to sink due to the lower density of the liquid compared to the hydrometer. Hydrometer analysis is defined by Stoke's Law, which relates the velocity of the suspended falling sphere particle with the diameter of the sphere, the specific weights of the sphere, and the fluid viscosity. The relationship is described by Equation 12 as;

$$V = \frac{2}{9}\frac{(G_s - G_f)}{\eta}\left(\frac{D}{2}\right)^2 \qquad 12$$

v = velocity of fall of the spheres (cm/s)

$\mathbf{G_s}$ = specific gravity of the sphere

$\mathbf{G_f}$ = specific gravity of fluid (varies with temperature)

η = absolute, or dynamic, viscosity of the fluid (g / (cm * s))

D = diameter of the sphere (cm)

All particle size analysis was performed according to the ASTM-D422 (1985): Standard test method for particle-size analysis of soils. Some of the major procedure steps effected are described sequentially as follows:

Sieve analysis

- Weighing of all sieves including the bottom pan was done and all weights were written down.
- The weight of the dry coal ash sample was measured using a scale balance.
- Before the coal ash was placed on the top sieve, the stacking of sieves in ascending order was done. The no. 4 sieve was at the top and no.200 at the bottom.
- The sieves were secured in the mechanical shaker and agitated for 10 minutes.
- Sieves were carefully removed and all sieves weighed separately, including the bottom pan for the retained ash particles.

Hydrometer analysis

- Ash from the bottom pan was placed into a beaker and mixed thoroughly with 125 ml of dispersing agent i.e sodium hexametaphosphate (40g/l). The mixture was let to soak for 10 minutes.
- During the soaking period, 125 ml of the dispersing agent was poured into a control cylinder and then filled with distilled water. The reading at the top of the meniscus formed by the hydrometer stem and the control solution was taken. A reading less than zero is recorded as a negative (-) correction and the reading between zero and sixty are recorded as a positive (+) correlation.
- The ash slurry was transferred into a mixer by adding more distilled water. The solution was thoroughly mixed for at least two minutes.
- Soon after, the ash slurry was poured into the empty sedimentation cylinder follow by filling to the mark of distilled water.
- The cylinder was tightly sealed at the open end followed by a series of upside-down inversions lasting at least one minute each for a total of 30 inversions.

- While the cylinder is placed down a waiting period of about 1 minute 40 seconds before carefully placing the hydrometer. The hydrometer is swiftly and gently placed to avoid any possible sediment disturbance.
- The reading is taken by observing the top of the meniscus formed by the suspension and the hydrometer stem. The hydrometer meter was gently removed and placed back into the control cylinder. The attached particles were removed by slowly spinning the hydrometer in the control cylinder.
- Hydrometer readings were taken after 2, 5, 8, 15, 30, 60 minutes and then after 24 hours using a stopwatch.

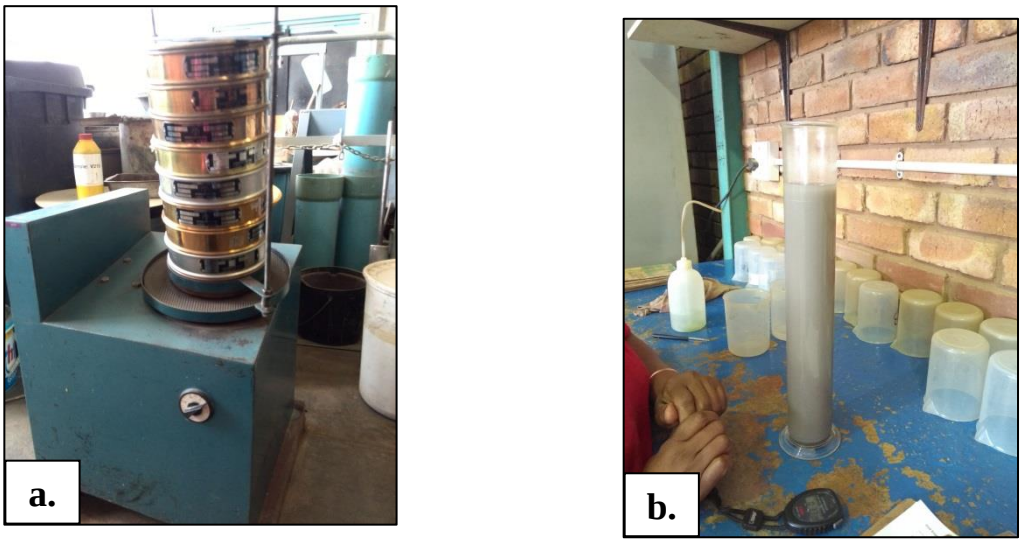


Figure 4.3: Sieve stack configuration (a) and hydrometer measurements setup (b)

Results from the two methods are combined as a percentage of sand, silt, and clay of the analysed soil. This is preceded by some calculation steps as described in the ASTM-D422 standard test method procedure. The data can be presented on a semilog graph of particle size versus particle diameter presenting both sieve and hydrometer analysis data on a single plot.

4.3 MINERALOGICAL ANALYSIS: QUANTITATIVE EVALUATION OF MINERALS BY SCANNING ELECTRON MICROSCOPY (QEM SCAN)

QEMSCAN is an acronym for Quantitative Evaluation of Minerals by Scanning Electron Microscopy. QEMSCAN was developed by CSIRO, Australia for originally determining the mineral proportions and characteristics of base metal and precious mineral samples. It is capable of measuring mineralogical variability based on chemistry at a micrometer scale. A typical QEMSCAN system is comprised of a base scanning electron microscope, consisting of four light element energy-dispersive

X-ray detectors, a microanalyser, and software for controlling and managing data acquisition (Eduafo, 2013). Principally, the QEMSCAN system relies on both the backscatter electron (BSE) signal intensity as well as Energy Dispersive X-ray Signal (EDS) at each measurement to create a mineral composition map (Eduafo, 2013). The Eskom system can acquire 5000 005 000 count X-ray spectrum in an hour for coal and 1.2 million 1000 count X-ray spectrum in an hour for ash or clinker samples.

4.3.1 Sample preparation procedure

The samples were again reduced to smaller sizes. A micro riffler by Quantachrome instruments was used to ensure the representativeness of the sample. The mass of each divided sample was measured using a mass balance. Once the required sample mass is obtained, the sample was then ready for potting.

During potting, samples were prepared using carnauba wax. Carnauba wax was preferred to an epoxy medium since epoxy and coal have very similar backscatter response signals. 30mm Teflon silicon-coated sample molds were coated with silicone oil before being labeled and placed in an oven at 60 ^{0}C for half an hour to dry. Carnobular wax flax was then poured into the sample molds and returned to an oven (at 120 ^{0}C) for 20 min. once the wax is melted the divided ash samples were thoroughly mixed with the wax before being returned to the oven. The samples were left in the oven for an additional 90 minutes before taken out to cool at room temperature (at 25 ^{0}C). After cooling down the samples were then ready for polishing.

The samples were polished using a polishing instrument, Struers TegraPol-21. The instrument applies a 10N/60N force with a rotation speed of 300rpm when in operation. Table 4.2 gives a summary of the polishing procedure. After polishing, the sample was then washed with soapy water and air-dried to ensure the surface is smooth and clean.

Table 4.2: Summary of the polishing process

Polishing Step No.	Polishing Surface	Polishing Paper	Time (s)	Lubricant
1	Sample back	MD Piano 80	10	Water
2	Sample surface	1200 SiC grit	10	Water
3	Sample surface	2400 SiC grit	10	Water
4	Sample surface	4000 SiC grit	10	Water
5	Sample surface	MD Chem	60	Water

The final stage of sample preparation before analysis was carbon coating using a carbon coater. The samples were then loaded into the instrument for analysis.

4.4 ELEMENTAL COMPOSITION: XRF

X-ray fluorescence (XRF) analyses were conducted to measure the chemical composition of Tutuka and Matimba coal ash. Sample preparation for XRF major elements analysis was as follows;

- Drying of the coal ash overnight using an oven at 105 °C was done at the Eskom Research Development and Innovation Centre (RT&D) facilities
- The dried ash was passed through a 45 µm sieve followed by removal of excess moisture
- A fluxing agent (lithium tetraborate 66% + lithium metaborate 34%) was mixed with 0.9 g of coal ash
- The mixture was then melted at a temperature of 1050 °C for seven minutes using the flux instrument
- The hot fused mixture was poured into the molds and allowed to cool for 10 sec
- The cooled mixture was in the form of discs and there were further analysed using the Axios max by PANalytical

4.5 LEACH TEST: CHARACTERIZATION LEACHING TEST PROCEDURE (TCLP)

Coal-fired power stations in South Africa produce a million tonnes of coal combustion residues which end up in dedicated disposal sites. The generated coal ash is viewed as the major potential source to release several sensitive elements to the environment (Izquierdo and Querol, 2012), in particular the groundwater. Toxicity Characterization Leach Test Procedure (TCLP) (EPA, 1992) by the United States environmental protection Agency (USEPA) is widely used as a standard procedure to assess the toxicity of solid waste. TCLP and other available standard leaching procedures are used to simulate the landfill scenario for metal leaching under laboratory environment conditions (Yadav and Yadav, 2014). It is important to interpret read TCLP results with caution as they represent laboratory conditions as opposed to real landfill conditions, as the results may vary. TCLP relies on the use of one of two acid-base extraction fluids (Fluids #1 and Fluid #2) based on the determination steps below (Liu *et al.*, 2019):

- If pH is <5, proceed to the extraction step using extraction fluid #1.
- If pH is >5, add 3.5 ml IN HCI, slurry briefly, cover and heat at 500 C for 10 minutes. Allow the solution to cool and measure the pH.
    - If pH is <5, proceed to the extraction step using extraction fluid #1.
    - If pH is >5, proceed to the extraction step using extraction fluid #2.

Fluids #1 and #2 were prepared using reagent grade chemicals as follows:

- Fluid #1 – by adding 5.7 mL of glacial acetic acid to 500 mL of reagent water. Add 64.3 ml of 1N sodium hydroxide, and dilute to a volume of 1L. The final pH reached was about **4.93.**
- Fluid #2 – by diluting 5.7 mL of glacial acetic acid with reagent water to a volume of 1 L. The final pH was about **2.88.**

This procedure is well summarised graphically by Liu et al, (2019) and illustrated in Figure4.4. Before the section of the appropriate extraction fluid, 5 g of coal ash was added into 96.5 ml of reagent water and thoroughly mixed for at least 5 minutes using a magnetic stirrer. The pH was then recorded followed by selecting the appropriate fluid as described above. The final pH of the ash remained between 8.2 and 8.7, and therefore, fluid 1was selected. TCLP tests were conducted on a capped glass container. After mixing the solution for 24 hours, it was filtered using the 0.45 mm filter paper. The filtered solution was kept on a Teflon bottle and immediately sent to the laboratory for various chemical analyses.

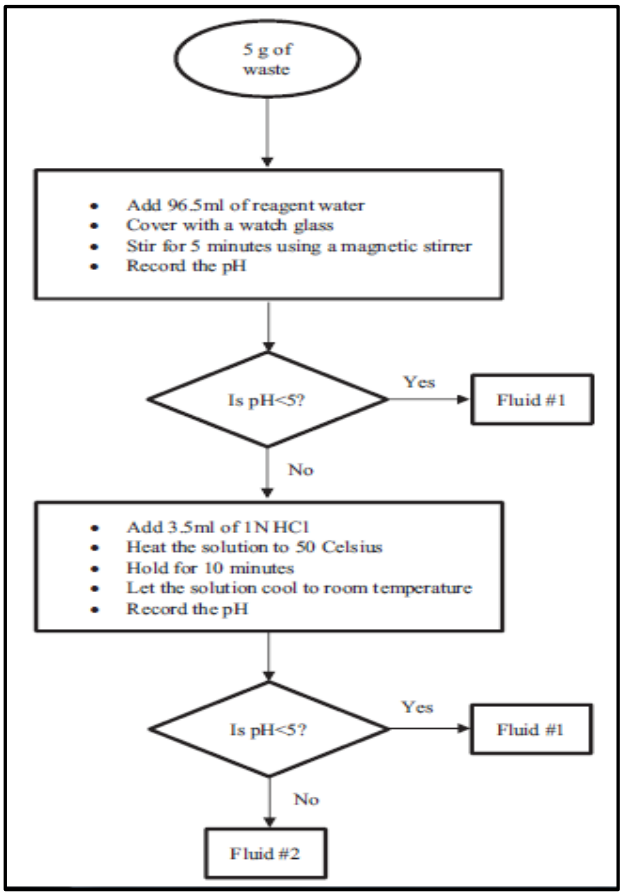


Figure 4.4: Summarized TCLP (EPA, 1992) steps by Liu *et al,* (2019)

4.6 HYPROP WIND/SCHINDLER METHOD: EVAPORATION METHOD

The evaporation method was initially developed by Wind (1966). Many international laboratories have adopted and continue to apply the basis of this method to other developed methods as standard practice. Due to high methodological effort and associated costs of the evaporation method by Wind (1966). A simplified Wind (1966) method was implemented in the HYPROP (**HY**draulic **PROP**erty analyzer, UMS, 2012) measurements, as proposed by Schindler (1980), was introduced. A typical work range for a HYPROP system is 0 to 100 KPa as read out from the two high capacity tensiometers installed at different heights. For ranges above 100 KPa, an extension of measurements related to the HYPROP can be performed.

An undisturbed or disturbed ash sample was acquired using a stainless steel ring (250 cm^3, height 6 cm). Two tensiometers were simultaneously installed at depths of 1.5 and 4.5 cm from the surface. The sample was saturated with degassed water from the bottom by placing the core sample in a pan of water. The saturated sample was then be sealed at the bottom and placed on a weighing scale. The sample was left open at the top exposing the surface to evaporation. Measurements were performed under standard laboratory conditions *i.e.* temperatures (18 -25^{0}C) and atmospheric pressures (19-108KPa). Measurement reading intervals was initially a 2 minutes interval for the first few measurements and later increased to 10 minutes to several hours (Figure 4.5).

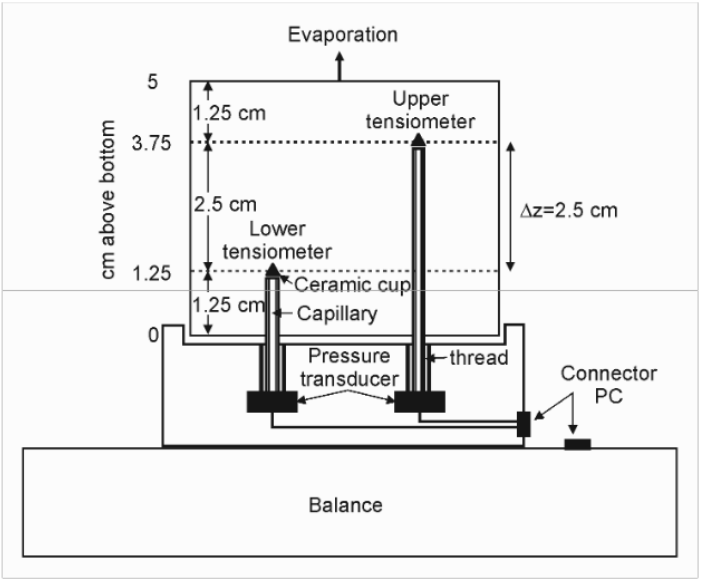


Figure 4.5: Schematic cross-section trough HYPROP evaporation method device (Schindler et al., 2010)

The measurement procedures including sample preparation and data analysis followed are summarised in the following subsections. Figure 4.7 depicts some of the major steps as performed in the laboratory.

4.6.1 Sampling and sample saturation

The core ring sampler which is supplied with the HYPROP system was used to sample the ash straight from the ash sample bag as illustrated in Figure 4.6 (Step 1). The sharper end of the ring was used to cut the sample, while the other end was kept closed using the plastic cap to avoid losing any loose ash particles.

The non-woven cloth was used to replace the cap and placed into the provided saturation plate which was then placed inside a beaker filled with 2 cm of degassed waster as shown in Figure 4.6 (Step 2). The sample was let to self-saturate through sample capillary forces for at least 6 hours.

4.6.2 Degassing the device using syringes

Before the degassing procedure commenced, the tips of the two tension shafts were placed inside a beaker upright overnight. This was done to ensure the degassing procedures are efficient and swiftly executed.

A syringe was filled with 10 ml of demineralised water and residual air was kept out by turning the syringe upside down and ejecting it out while the outlet nozzle was partially closed. The tube piece was carefully placed in the syringe followed by the tension shaft piece. The other tube piece was placed on a filled vacuum syringe containing gas-free 5 ml of demineralised water. The two syringes were joined by connecting both ends of the tension shaft. The plunger of the vacuum syringe was pulled and then released by pressing the plunger stopper and allowing the plunger to gently move on its own. The tension shaft was removed and any residual air was removed from the syringe. This was repeated for the second syringe.

4.6.3 Filling the sensor unit

The sensor unit holes were filled as indicated in Figure 4.6 (Step 3) with bubble-free demineralised water, using the provided droplet syringe. A refilling attachment was used to fill the unit. Approximately 15 ml of demineralised water was filled using a bubble-free vacuum syringe. Air was removed by pulling the plunger out until the stopper snapped-in. Residual visible bubbles were brought to the top of refill by gently knocking the filling vessel to displace the bubbles. The plunger was then released to fill the device.

4.6.4 Assembling the sensor unit and the ash sample

After the sample is confirmed to be fully saturated, two holes for the tension shafts were drilled using the provided auger guide and mini-auger. The mini auger was rotated three cycles and then gently removed, retrieving ash and creating holes for the two tension shafts. The holes were then filled as illustrated in Figure 4.6 (Step 7) with demineralised water using a droplet syringe.

The sensor unit fitted with the tension shafts was turned upside down to ensure that both shafts are slotted in the augured holes, ensuring the correct shaft is in the correct hole. The sample was then firmly secured to the sensor unit. The sensor unit was placed on a scale and measurements began reading off measured value from the connected laptop. The sample was left for at least 13 days at room temperature. Once the 13 days have elapsed, the ash sample is collected from the ring sampler and placed into an oven at 105° C for 24 hours to determine the dry mass of the ash.

4.6.4.1 Determination of soil water retention characteristics and hydraulic conductivity

Tension (φ) and mass (m) are recorded according to the preferred time interval. According to Schindler et al., 2010 the pressure difference between atmospheric pressure and water pressure inside a tensiometer is referred to as tension and normally expressed as an absolute value in pressure units (KPa). Hydraulic gradient (i_m) data is related to the tension measurements observed within the time interval. The flux (V) is derived from soil water volume difference ΔV per surface area (A) and time interval Δt. The Hydraulic conductivity (K) was calculated according to the Darcy-Buckingham

Where φ_{mean} for K is the mean tension averaged between the upper tensiometer positioned 3.75 cm

$$\mathrm{K}(\varphi_{mean}) = \frac{\Delta V}{2Ad\Delta t i_m} \qquad 13$$

(z_1) above the base and the lower tensiometer positioned 1.25 cm (z_2) above the base, this is averaged across time intervalΔt. Heights z_1 and z_2 represent the total height of the two tensiometers completely covered within the soil column as depicted in Figure 5. ΔV is the total evaporated water volume of the complete sample which is equal to the sample mass difference. A is the cross-sectional area of the sample, and i_t is the mean hydraulic gradient in the time interval, given by;

$\varphi_{ti\ upper}$ and $\varphi_{ti\ lower}$ are the upper and lower tensiometer values at time ti and $\Delta z = z_1 - z_2$ is the vertical

$$i_m = \frac{1}{2}\left(\frac{\varphi_{t1\ upper} - \varphi_{t1\ lower}}{\Delta z} + \frac{\varphi_{t2\ upper} - \varphi_{t2\ lower}}{\Delta z}\right) \qquad 14$$

distance between the tensiometers.

Schindler et al.,(2010) further suggested that retention curve data obtained through mapping the mean volumetric water contents of the sample, $\Theta_{i,}$ to the corresponding mean tensions in the sample, $\varphi_{mi} = 0.5(\varphi_{ti\ upper} + \varphi_{ti\ lower})$ at each measurement time. Single points on the water retention curve are calculated based on the water loss per volume of sample at time *t* and mean tension in the sample at this time (Figure 4.3). The residual amount of storage water is represented by the water loss during oven drying at 105^{o}C, determined after all measurements have been recorded. It is important to note that due to short time intervals between measurements and the size of the sample, temporal and spatial nonlinearity is assumed negligible. As a result, the following assumptions can be made:

I. Water flows through the soil core sample is in steady-state conditions *i.e.* the flux and hydraulic gradient are approximately constant through the time interval

II. The water content from the bottom to the top of the sample core diminishes linearly. Similarly, the flux through the depth compartment delimited by the two tensiometers is half of the total flux and can, therefore, be calculated from the total evaporative soil water volume (mass) difference in the time interval (Schindler et al., 2010)

III. HYPROP-FIT is a software tool by USM which is compatible with Windows^{TM}. The software was used to access and read experimental data recorded by the data acquisition software HYPROP-View. The file is stored with (tvp) file extension. Both softwares are freely available from the UMS website. Some of the supported functions listed in the software manual (Peters and Durner, 2015) include:

- Specification of all required parameters for the evaluation of the recorded experimental data with the simplified evaporation method, such as column length, positions of tensiometers, tare weights of the measurement device components, and so on.
- Visualization of the measured raw data, i.e., tensions and weight changes, and specification of starting and stop points for the data evaluation.
- Re-calculation of tensions and net weight data as a base for the calculation of retention and conductivity data. This includes the temporal interpolation for data in low temporal resolution and the aggregation of data in very high temporal resolution
- Calculation and visualization of the data for the retention characteristic and the conductivity characteristic
- Fitting of state-of-the-art hydraulic functions to the data, visualization of the functions, and listing of the values and confidence limits of the hydraulic parameters
- Export of graphs, raw data, calculated data, fitted functions, and other parameters of interest.

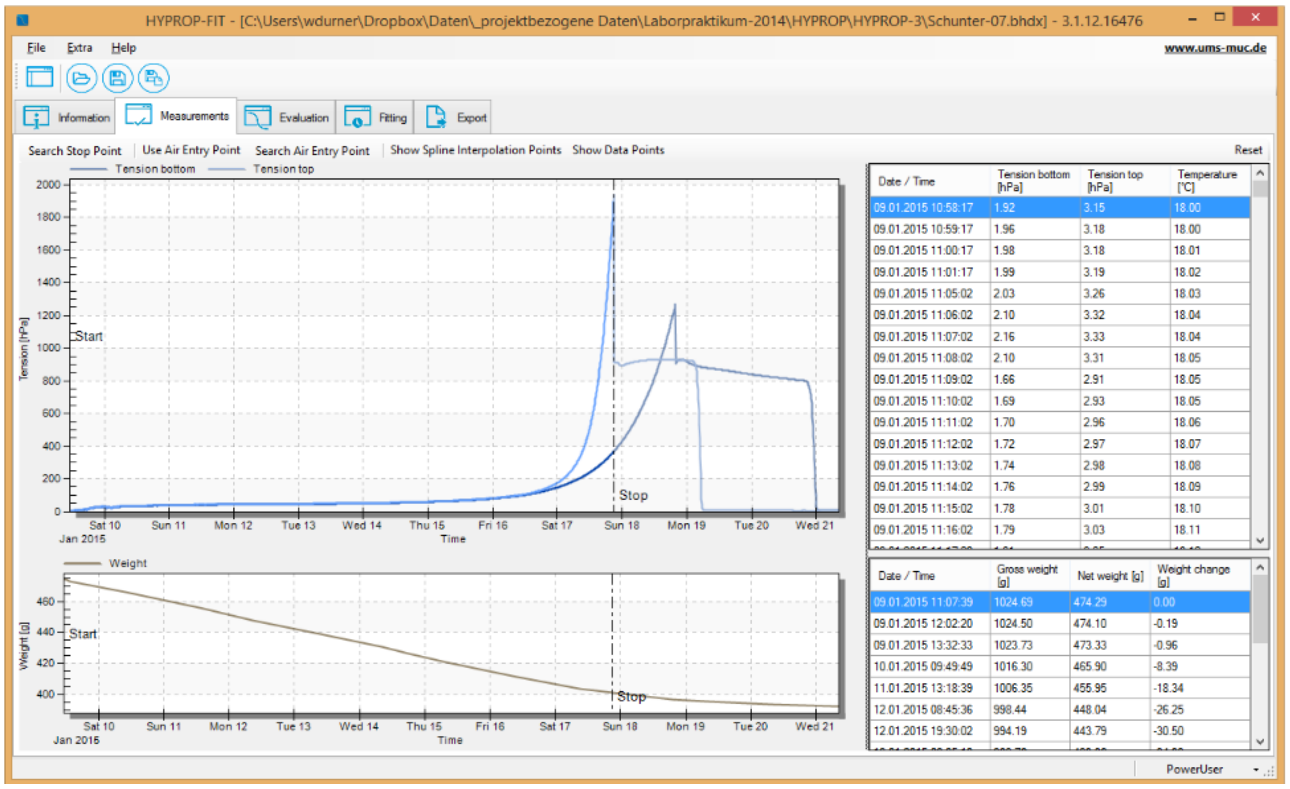


Figure 4.6: HYPROP-FIT sample page showing visualization and editing of measured data (from Peters and Durner, 2015)

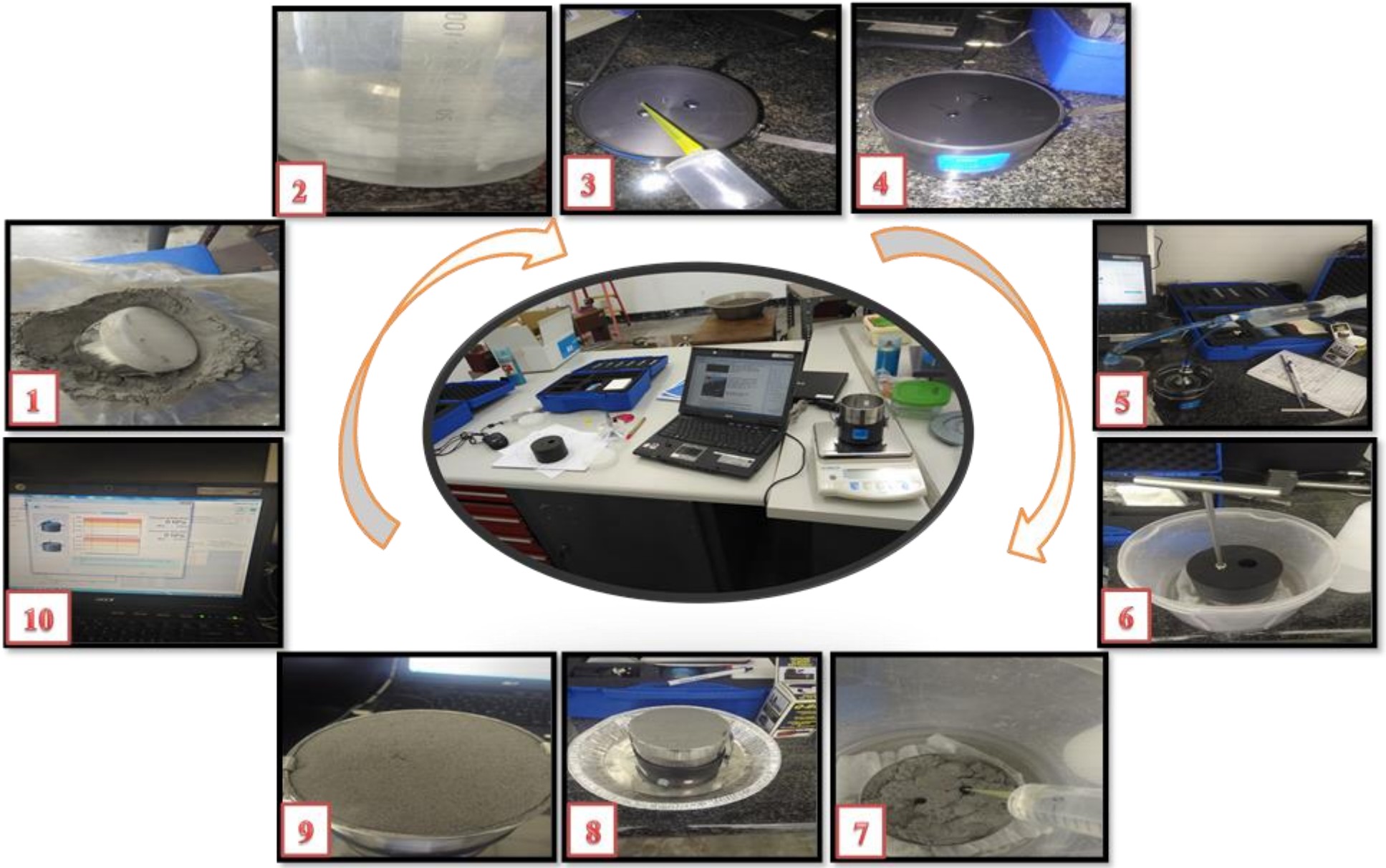


Figure 4.7: HYPROPs sample preparation, setup and measurement

4.7 CHAPTER FOUR SUMMARY

This study set out to investigate the Matimba ash dump water retention characteristic. The ash used in this study originated from Matimba, Tutuka ash was included to provide a comparative analysis of some properties. Several methods were used to characterise chemically, physically and geochemically the ash, to meet the study objectives. Most of the analyses were laboratory-based (particle size and distribution determination, mineralogy and chemical composition, leach test, and ash water retention). Particle size determination revealed information on the size of the ash particles and the distribution of the grains which contributes to the overall texture class. The Mineralogical determination seeks to study potential minerals possessing water retention capabilities. It also seeks to study the potential formation of new minerals and their contribution to the overall water retention. The leach test predicts the geochemistry of ash-water interaction to determine the likely chemistry of potential seepage from a dry ash dump. The Hyprop was the main experiment that relied to determine the ash water characteristics.

CHAPTER 5: RESULTS

This chapter presents the results of coal ash subjected to different analyses. This chapter will also include a discussion of the results.

5.1 MINERALOGICAL AND ELEMENTAL COMPOSITION COMPOSITION

Quantitative analysis of two samples originating from Matimba and Tutuka power stations was carried out using QEMSCAN (Quantitative Evaluation of minerals by scanning electron microscopy). Tutuka sample was included for comparative purposes with the main sample of Matimba. The results for both mineralogical and elemental characterisation are presented in Figure 5.1 and Table 5.1. The analysis was carried out according to Section 4.3. The behaviour and water holding capacity of ash will rely on the types of minerals and their properties. Mineralogical characterization of coal ash also reveals the processes and conditions the parent coal underwent during milling and combustion. Characterisation may help in predicting behaviour of identified mineral groups like the behaviour of clay mineral groups. The mineralogical composition of coal ash is characteristically reflected in the composition of the original parent coal, which is dominated by a high proportion of aluminosilicate, quartz, and glass cenospheres. Matimba coal ash is characterised by a high proportion of quartz and aluminosilicate and a lower proportion of cenospheres relative to Tutuka. A low proportion of a plagioclase group mineral anorthite in Matimba fly ash sample, suggests that the proportion of coarse ash is comparatively low.

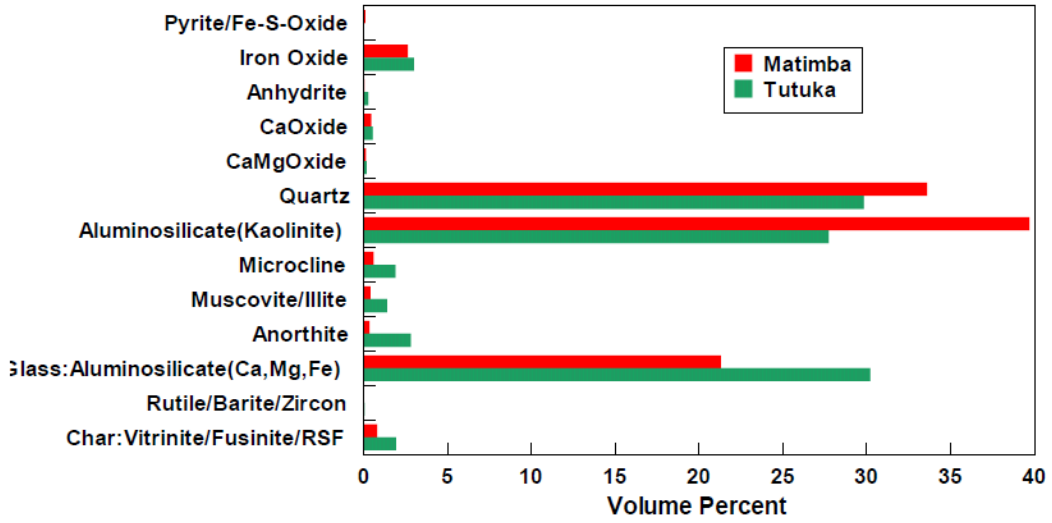


Figure 5.1: Matimba power station dry ash dump

The average particle size of "stone" (aluminosilicate/quartz), iron/calcium/calcium magnesium oxide, and cenospheres in fly ash is 55, 32, and 31 microns respectively. This is relatively coarse for a pulverised fuel which is typically milled to about 70 to 75% passing 75 microns. The mineralogical

composition for Matimba and Tutuka is in general agreement with the mineralogy reported for South African fly ash.

Table 5.1: Matimba and Tutuka chemical constituents

Constituent	Matimba (wt. %)	Tutuka (wt. %)
SiO_2	59.54	55.08
Al_2O_3	25.79	28.85
Fe_2O3	7.25	5.43
TiO_2	1.27	1.51
P_2O_5	0.37	0.34
CaO	3.16	4.91
MgO	0.94	1.76
Na_2O	0.22	0.24
K_2O	0.87	0.97
SO_3	0.29	0.52
MnO (Cal)	0.03	0.02

The combined composition of (SiO_2+Al_2O_3 + Fe_2O_3) for both samples is more than 70%, while the lime (CaO) content is less than 5%. According to the classification prescribed by the American Society for Testing and Materials (ASTM, 1998) both ash samples classify as class F fly ash. This classification suggests the ash possesses less Cementous properties unless an additive is added. This may either promote or reduce the ash water holding capacity, depending on the rate of drying after being exposed to moisture. Cementing of ash may reduce the available pore water storage, resulting in low permeability, restricting moisture movement within the ash matrix. Drying may sometimes result in cracking of ash, which then creates preferential flow paths. This flow is difficult to predict as it relies on the connectedness of the created cracks. Since both samples lack the Cementous ability due to lack of lime, ash from the two stations may provide ideal volume space to lock disposed liquids and allow evapotranspiration to occur. Some of the clay minerals like kaolinite are inherently from clays incorporated into the coal seam and escape any temperature transformation and still be detected in coal ash. Kaolinite, a non-swelling clay mineral is the dominant clay mineral present on both samples. Generally, soils with a predominance of 2:1 clay minerals water retention and availability are higher than in kaolinitic soils (Gaiser et al., 2000). Kaolinite is characterised by a 1:1-type layered structure with high crystallinity and unique structure (Benco *et al.,* 2001). The structure consists of one side of the interlayer space covered with hydroxyl groups of the $Al_2(OH)_4$ octahedral sheets and the other side is covered by oxygens of the SiO_4 tetrahedral sheets (Benco *et al.,* 2001). Since kaolinite is a non-swelling clay mineral, this reduces water uptake through ADForption. The hydrogen bonding that keeps the kaolinites from swelling does not allow for water to enter the interlayers and water predominantly ADForbs to the outer surface (Schuttlefield *et al.,* 2007).

5.2 LEACH TEST RESULTS: TOXICITY CHARACTERIZATION LEACH TEST PROCEDURE (TCLP)

Leach test was done to simulate the ash dump geochemistry concerning the potential release of environmental and health sensitive elements, in particular, mobile elements with impending fate into the groundwater system overlain by the ash dump disposal facility where the coal ash samples originated. Samples from Matimba and Tutuka Power Stations were subjected to Toxicity Characterization Leach Test Procedure (TCLP) (EPA, 1992) as described in Section 4.5.

Leaching of elements from fly ashes is mainly controlled by two different mechanisms solubility (dissolution, precipitation) and sorption mechanisms. Leachate composition of coal ash is expected to vary per country and even per different power stations within the same country using varying coal qualities possessing inherently different chemical and mineralogical compositions due to contrasting depositional settings during the coal genesis. Izquierdo and Querol (2012) in their study, even though coal properties, combustion conditions, and other factors vary, concluded that there are similar trends in the behaviour of leached elements from different coal combustion residues across the globe. The findings by Izquierdo and Querol (2012) become an important basis for interpreting the leach test results of this research, as their study involved an extensive literature review. The review considered a range of global studies on ash leaching of samples originating from different plants around the world. The leachate of both samples, post-filtration were submitted to Eskom Research, Testing and Development (RT&D) in Rosherville, Johannesburg for analysis of a combined list of minor and major elements. The Eskom RT&D laboratory is an accredited laboratory by the South African National Standard (SANS), authorizing the acceptability of their analysis methods and results of Ion chromatography (IC) and Inductively Coupled Plasma (ICP) performed on the samples. TCLP results in Figures 5.2 – 5.5 are according to the extraction fluid used; fluid #1 is a buffered solution of acetic acid and sodium hydroxide while fluid #2 is an un-buffered acetic acid solution.

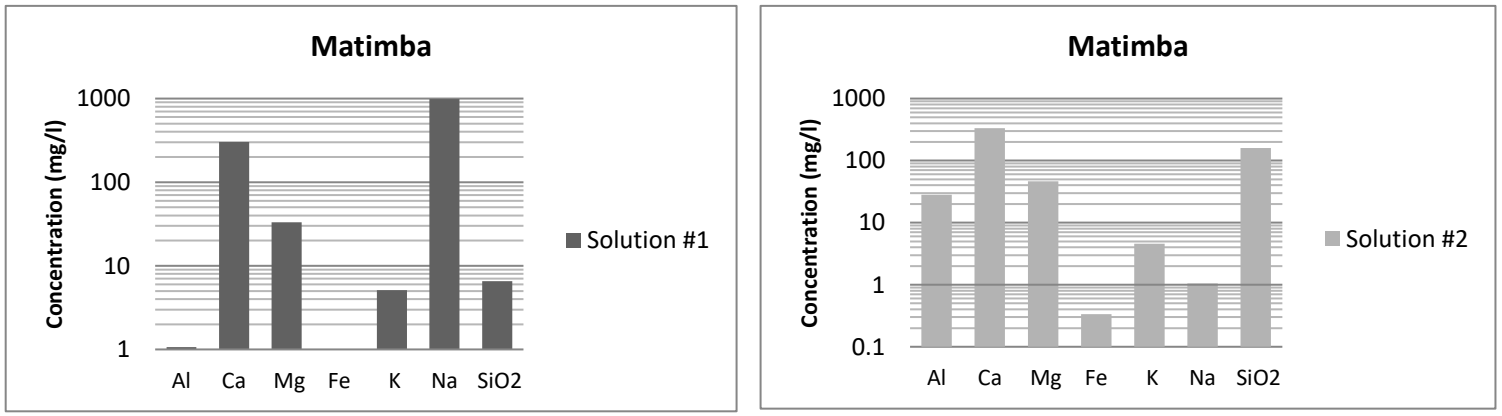


Figure 5.2: Matimba ash TCLP major elements results of using Fluid #1 and 2

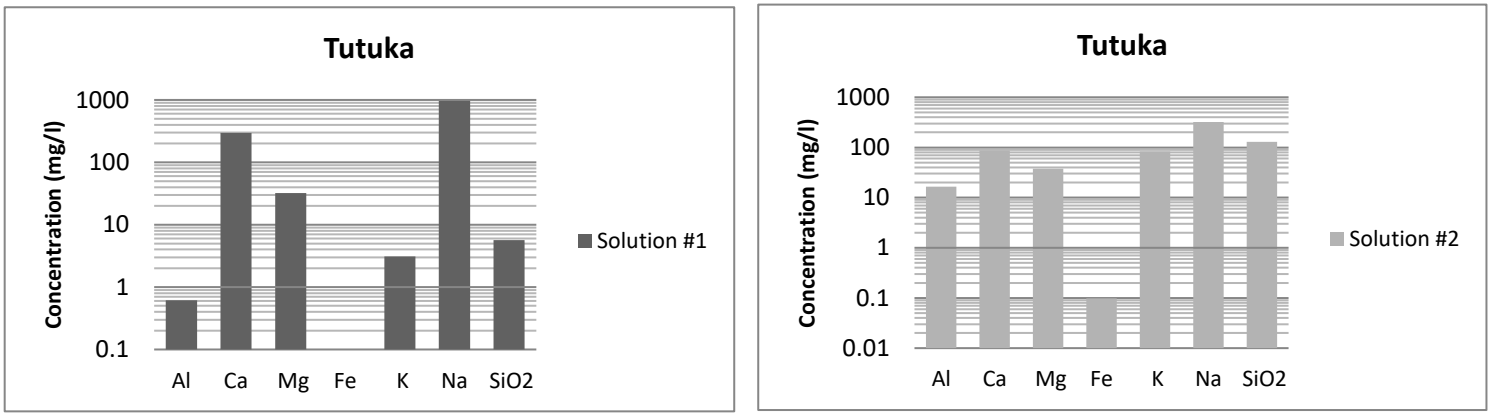


Figure 5.3: Tutuka ash TCLP major elements results of using Fluid #1 and 2

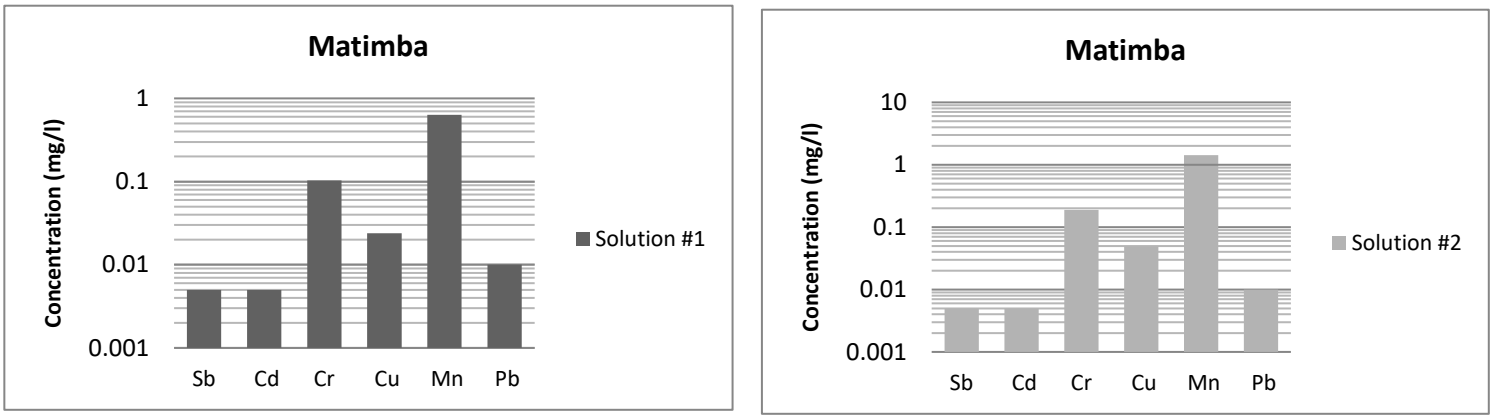


Figure 5.4: Matimba ash TCLP trace elements results when using Fluid #1 and 2

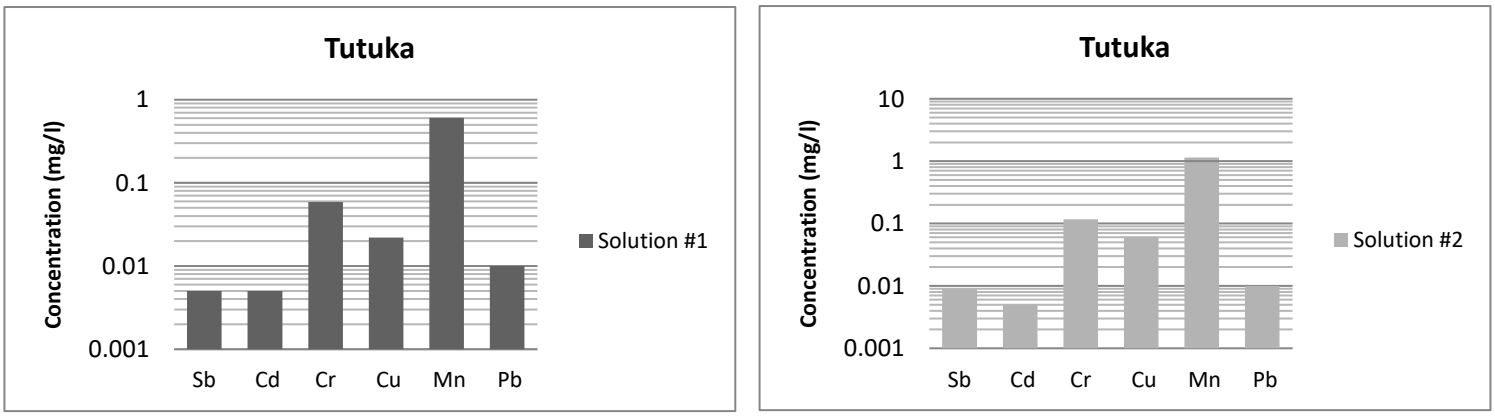


Figure 5.5: Tutuka ash TCLP trace elements results when using Fluid #1 and 2

5.2.1 Leach test results compared with drinking standard

Laboratory analyses results received from a SANAS accredited laboratory were compared to the South African National Standard (SANS) 241:2015 (See Table 5.2) to determine the possible risks associated with water use. This is considering the worst-case scenario, assuming the leachate from the ash dump migrates to the groundwater systems as it is determined by the leach test. This might not be the case considering site conditions, where the leachate takes a long journey through the ash dump, into the vadose zone, and ultimately into the saturated zone.

The limits and associated risks for domestic water as determined by the SANS 241:2015 are as follows, where:

- **Health risks:** parameters falling outside these limits may cause acute or chronic health problems in individuals.
- **Aesthetic risks:** parameters falling outside these limits indicate that water is visually, aromatically, or palatably unacceptable.
- **Operational risks:** parameters falling outside these limits may indicate that operational procedures to ensure water quality standards are met may have failed.

The majority (more than 45 %) of the major and minor elements from the leachate results exceeded the aesthetic and operational risk levels set by the South African national drinking water standard (SANS 241: 2015).

Noticeably, three parameters, namely; manganese, chromium (VI), and total organic carbon exceeded the health risk criteria of the SANS 241: 2015. Even in low-level concentrations, these parameters cause irreversible effects on human health. Generally, as precautionary measures, water with detectable levels of chromium is not advisable for drinking purposes.

The analysis only considered total chromium, usually as screening for the presence of any chromium species in solution. As such, chemical speciaciation analysis will be required to further ascertain the individual chromium ion concentration, in this case, chromium(VI). Occupational exposure of chromium is associated with a nasal septum and skin rashes and at times skin ulcers, while ingestion may lead to more adverse health effects like lung cancer. The total chromium detected ranges from 0.06 – 0.19 mg/l, at these levels the possible risk of induction of gastrointestinal cancer after long-term exposures.

Manganese shows levels higher than the aesthetic criteria of the SANS 241: 2015. At these levels (0.61 – 1.43 mg/l) water will be highly stained or discoloured and it will also affect the taste of the water.

Table 5.2: Chemical analysis compared to the SANS 241 drinking standard

Parameter	Unit	Risk	SANS 241:2015	Leach Test Results			
			Standard Limits (SANS 241-2006 and 2015)	Matimba A	Matimba B	Tutuka A	Tutuka B
pH (at 25°C)	pH units	Operational	≥5.0 - ≤ 9.7	5.21	4.09	5.22	4.06
Conductivity	mS/m	Aesthetic	≤ 170	507.2	170.5	500.8	159.3
Turbidity	NTU	Operational	< 1	0.131	0.17	0.093	0.134
		Aesthetic	< 5				
Total Alkalinity (as $CaCO_3$)	mg/L		-	1964	<1	1969	<1
Calcium (as Ca)	mg/L	Aesthetic / Operation	≤ 150	304	334.4	296.4	87.38
Magnesium (as Mg)	mg/L	Aesthetic / Health	≤ 70	33.2	46.23	32.21	37.84
Sodium (as Na)	mg/L	Aesthetic	≤ 200	988	1.05	971	322
Potassium (as K)	mg/L	Operational / Health	≤ 50	5.1	4.55	3.09	83.34
Zinc (as Zn)	mg/L	Aesthetic	≤ 5	0.083	0.2	0.061	0.192
Chloride (as Cl)	mg/L	Aesthetic	≤ 300	403	553	389	692
Fluoride (as F)	mg/L	Chronic Health	≤ 1.5	<0.030	<0.030	<0.030	<0.030
Sulphate (as SO^{2-})	mg/L	Acute Health Chemical	≤ 500	201	250	110	215
		Aesthetic	≤ 250				
Total Dissolved Solids	mg/L	Aesthetic	≤ 1 200	2842	1232.3	2461.8	1137
Ammonia Nitrogen (as N)	mg/L	Aesthetic	≤ 1.5	<0.005	<0.005	<0.005	<0.005
Nitrate Nitrogen (as N)	mg/L	Acute Health Chemical	≤ 12	0.12	<0.02	0.85	0.88
Iron (as Fe)	mg/L	Chronic Health	< 2	<0.005	0.336	<0.005	0.098
		Aesthetic	< 0.3				
Manganese (as Mn)	mg/L	Chronic Health	< 0.4	0.633	1.432	0.605	1.147
		Aesthetic	< 0.1				
Aluminium (as Al)	mg/L	Operational	<0.3	1.063	28.08	0.614	16.64
Cadmium (as Cd)	mg/L	Chronic Health	≤ 0.003	<0.005	<0.005	<0.005	<0.005
Chromium (as Cr)	mg/L	Chronic Health	≤ 0.05	0.103	0.189	0.059	0.117
Cobalt (as Co)	mg/L	Chronic Health	≤ 0.5	< 0.003	< 0.003	< 0.003	< 0.003
Copper (as Cu)	mg/L	Chronic Health	≤ 2	0.024	0.049	0.022	0.061
Lead (as Pb)	ug/L	Chronic Health	≤ 0.01	<0.010	<0.010	<0.010	<0.010
Total Organic Carbon	mg/L	Chronic Health	≤ 10	2442	2388	2414	2398
Acute Health Chemical							
Acute Health Microbiological							
Chronic Health							
Aesthetic							
Operational Efficiency							

5.2.2 Major elements

Following Izquierdo and Querol (2012), the above results were grouped according to major and trace elements. The amount of each element is either presented in mg/l or µg/l for major elements and trace elements, respectively. Sodium and calcium dominated the major element composition on both Matimba and Tutuka coal ash. The high sodium concentration from samples subjected to fluid #1 is of no surprise since sodium hydroxide was added as part of the TCLP practice. Sodium and potassium are known to be precipitate in coal and from the groundwater as they are mainly linked with feldspar and clays. The second highest major element to be leached from Matimba and Tutuka coal ash is Calcium. The presence of calcium seems to not have relied on pH lowering from fluid #1-2. Matimba coal ash shows similar proportions of calcium when using both fluids. Calcium is known as the most largely released cation, this is despite the type of fluid used. It has multiple modes of occurrences, primarily as lime, anhydrite, and calcite (Izquierdo and Querol, 2012). Generally, high calcium concentration from coal ash may suggest that calcium is present as free lime. Even though on its own

is not regarded as an element of concern, but its role in controlling the quality of ash remains important. Precipitation of metalloid-bearing phases from ash leachate is enhanced by the presence of calcium. It also plays a role in the precipitation of secondary calcium-hydrated phases like ettringite minerals. Environmental and health sensitive elements like arsenic, chromium or selenium are likely to be retained by these secondary ca-hydrated phases. Calcium to a large extent controls the leachate composition and the fate of trace elements (Izquierdo and Querol, 2012).

The formation of ettringite is of interest concerning the evolution of the water retention characteristics of coal ash. Ettringite (Ca_6Al_2 $(SO_4)_3(OH)_{12}\cdot 26H2O$), a hydrated sulphate of calcium and aluminium is rare in nature, but commonly found in hydrated Portland and fly ash with high lime and gypsum content. The formation of Ettringite within the coal ash matrix may lead to a deleterious effect on the mechanical properties of coal ash (Chindaprasirt *et al.,* 2013).

Qemscan scan results did not show any sources of calcium-sulphate, this in combination with alumino-silicate phases is required for ettringite to form. The latter was the dominated mineral phase as seen in the qemscan results (see Figure 5.1). Chindaprasirt *et al.,* (2013) suggested that it is due to its needle-like structure that causes the formation of microcracks, swelling, and eventual failure of the material, as result compromising the mechanical properties of coal ash material. Leach test results provide an opportunity to assess different ions present in coal ash leachate and the probable formation of ettringite can be determined based on the proportion of the present ions (i.e calcium, aluminium and sulphate). Ouhadi and Yong (2008) assessed the role of different ions in the formation of ettringite by studying the intensity of XRD peaks versus variation of concentration of sulphate, calcium, and aluminium. The varied concentrations were between 0.04-0.12 mol. Ouhadi and Yong (2008) concluded that high XRD intensity peaks were consistent with the stoichiometric relations of elements required for ettringite formation.

Leach test results based on TLC for the two samples (i.e Matimba and Tutuka) were used to predict the formation of ettringite mineral. Concentration (in mg/l) of alumium, calcium, and sulphate were all converted to mol concentration as presented in Table 5.3.

Table 5.3: TCLP results of Al, Ca, and SO_4, including their mole equivalent

Ion	Concentration (mg/l)		mass (g)		Molar mass (g/mol)	moles	
	Matimba	Tutuka	Matimba	Tutuka		Matimba	Tutuka
Aluminium as Al	28.08	16.64	56.16	33.28	26.98	2.081542	1.233506
Calcium as Ca	334.4	296.4	668.8	592.8	40.08	16.68663	14.79042
Sulphate as SO4	250	215	500	430	96.06	5.20508	4.476369

Ettringite is likely to form from both Tutuka and Matimba coal ash, even though aluminium concentration for Tutuka was lower than that of Matimba, with time aluminum may be leached out in higher concentration to allow for ettringite to form. Matimba ash shows strongly that ettringite is likely to form as their mol concentrations exceed the minimum stoichiometric requirement for aluminium, calcium and sulphate. This favours the formation of ettringite, but the actual formation will rely on site-specific conditions related to the chemistry of the ash-water system on a specific site.

Ettringite has another important characteristic *i.e* its swelling nature. The swelling of ettringite is confined to two possibilities; crystallization pressure due to crystal growth and expansion due to water absorption. The latter possibility favours the high fluid retention characteristics of ettringite. The formation of ettringite in coal ash thus enhances the water retention of ash.

One of the other major elements observed when fluid #2 (lower pH) is used, reactive silica results indicate a dependence on pH change. Silica (quartz) is a chemical compound silicon dioxide SiO_2. It is the dominant rock-forming mineral on earth and a dominant mineral phase in both coal and ash. Silicon is generally slowly leached from its crystalline structure in ash but can be enhanced by the presence of hydroxide ion (OH^-) (Izquierdo and Querol, 2012). Dissolved silicon largely increases with a decrease in pH, and vice-versa for the pH increase scenario. A high concentration of silicon is generally observed in ash that has undergone advanced glass weathering. In real cases, weathered ash is associated with ash deposited over a prolonged period at the ash disposal facility (Izquierdo and Querol, 2012).

5.2.3 Trace elements

Trace elements are chemical elements present in ash in small amounts, but still at lower levels pose a threat to the environment and human health. Only three trace elements were found present in concentrations above 0.01 mg/l. Tutuka and Matimba ash samples, but dominated by fluid #2. The detected trace elements in an increasing concentration order are Manganese>Chromium>Copper.

Manganese

Various oxides of manganese (Mn) exist in coal ash as a result of coal combustion of different qualities. Common manganese oxidation states include Mn(II), Mn(III), and Mn(IV), while salts associated with Mn(II), are the easily soluble form of Mn (Zhao *et al*., 2018). Mn in coal ash is either associated with the ferromagnetic particles or sometimes the glass phase fraction. Although the study by Querol *et al*. (2001) shows that both ferromagnetic and glass particles are responsible for the low

leaching rates of Mn from coal ash. As the behavior of other metals, Mn is known to be insoluble under neutral to alkaline conditions (pH>7), while soluble in acidic conditions (pH<7). A considerable amount (up to1147µg/l) of Mn was measured from Matimba and Tutuka ash TCLP results. It is unlikely that the values determined by the TCLP laboratory-scale leach test will mimic site conditions as both the power stations rely on a dry ash disposal method. The dry ash disposal facility operates in water deficit conditions as compared to the wet ash disposal system. This will result in a higher solid: liquid ratio, which is generally a prerequisite for metal retardation.

Chromium

Chromium (Cr) exists naturally in the environment in two oxidation states as Cr (III) and Cr (VI), similarly in coal ash. The trivalent Cr (III) is the less soluble form and poses much less health risk to humans than Cr (VI) does (Izquierdo and Querol, 2012). Considering its appropriate levels, Cr is essential for the proper functioning of a living organism, including humans (Sočo and Kalembkiewicz, 2009). The hexavalent Cr (VI) is widely known for its carcinogenic impact and also for being highly soluble in an aqueous environment (Sočo and Kalembkiewicz, 2009). Using both solutions #1&2 the mean archived mobilised Cr (total) was 0.12 mg/l. Cr speciation analysis was not performed for this study, which would have given the different chromium oxidation states present in both Matimba and Tutuka ash. Considering the 0.12 mg/l mean concentration at this level has potential to impact negatively on the environment. Speciation of Cr in coal ash is extremely complex due the some of the following reactions; oxidation-reduction potential, precipitation, adsorption, ion exchange that can occur for both Cr (III) and Cr (VI). In reduced circumstances, in the presence of high sulphates, the oxidation state for Cr would be Cr (III), and not Cr (VI). Generally, groundwater is the most vulnerable water resource environment due to mobilised Cr emanating from ash disposal sites. However, groundwater aquifers are mainly reducing the environment due to lack of oxygen, particularly the deep aquifers. The presence of clay minerals in ash has an important role in the natural scavenging of Cr species through the ADForption reactions between clay minerals like kaolinite and illite with Cr.

Copper

Copper (Cu) is an essential trace element to the existence or support of plants, animals, and humans. Copper occurs in three oxidation states, namely metallic Cu (0), cuprous Cu (I), and cupric Cu (II). Naturally, Cu occurs in semi-precious minerals like malachite, azurite, and turquoise. Cu in coal ash is associated with clay minerals from the coal before combustion. Post-combustion, Cu is associated with glassy mineral phases. The mode of occurrence is linked to the assimilation within the glass

phases, making it not to be easily released. Oxidation of Cu-Iron (Fe)-Sulphides in coal leads to increased mobility of Cu in fly ash (Izquierdo and Querol, 2012). At neutral and alkaline conditions, the concentration of copper in an aqueous solution is usually low, while in acidic conditions copper readily dissolves, and substantially higher concentrations are observed. Solution #2 at final pH of about 2.88 was able to mobilise 0.061 mg/l of Cu, while the less acidic solution #2 was able to mobile maximum amounts of 0.024 mg/l. This confirms the dependence of pH in mobilising copper from coal ash.

5.3 PARTICLE SIZE AND DISTRIBUTION ANALYSIS

Two representative ash coal samples were obtained from Tutuka and Matimba power stations and were subjected to sieve analysis and Atterberg limits test. This was done to try and establish the water retention properties of the ash. This enabled the two samples to be classified.

5.3.1 Particle size and texture analysis

Figure 5.6 presents sieve and hydrometer results in a semi-log plot. The analysis results from both samples obtained from the two power stations suggest that these samples are relatively fine-grained with almost 100% passing of material in sieve 2.0 mm. The grading modulus of these samples was found to be in the range of 0.27 and 0.41 confirming that the samples are relatively fine-grained. However, the results also indicate ash with an insignificant amount of clay particles.

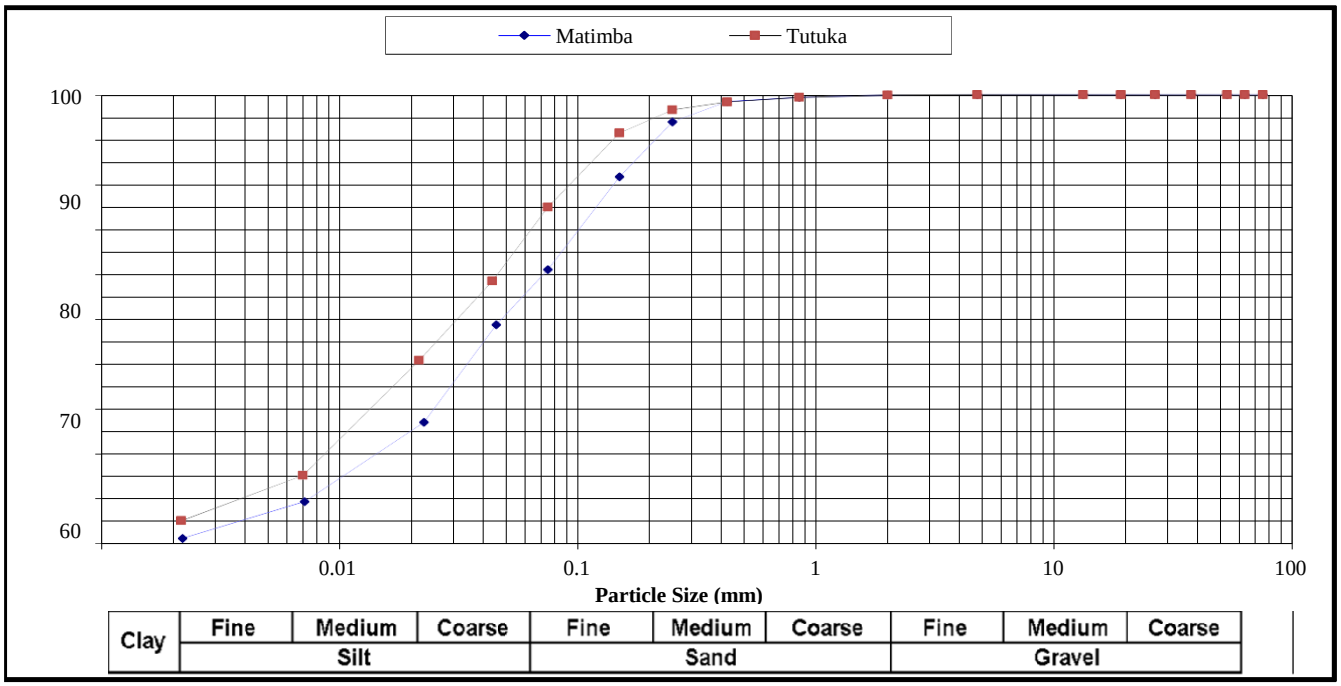


Figure 5.6: Matimba power station dry ash dump

A texture trilinear diagram (Figure 5.7) was used after the particle size determination experiment to determine the texture of two coal ash samples *i.e.* ash from Matimba and Tutuka power stations. The three sides of the triangle represent the percentage proportions of sand, silt, or clay. The intersection points of three lines from each side of the triangle determine the texture class. Both samples consist of considerable (above 50%) amounts of silt-sized particles with very low clay content (less than 5%) clay, hence both samples are classified as silt-loam. As both samples have a high percentage of silt resulting in a larger surface area, thus provides a larger surface area for soil to hold water and exhibits higher water holding capacity.

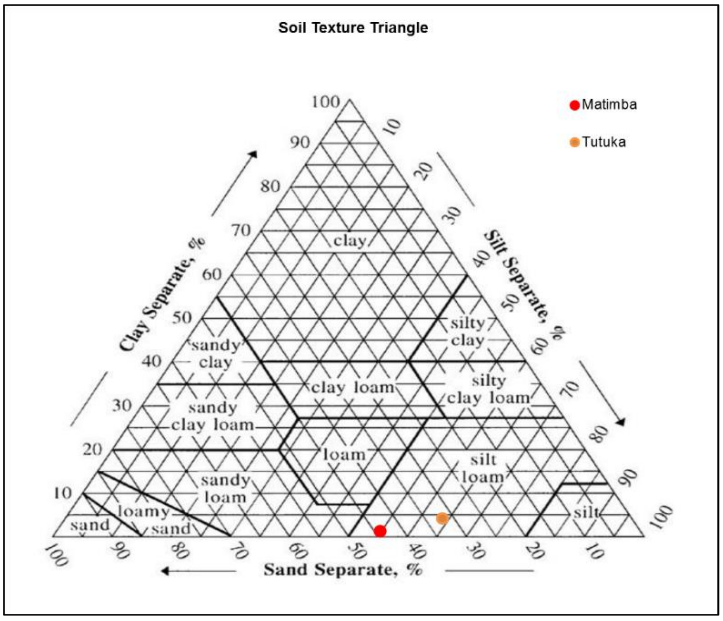


Figure 5.7: Matimba power station dry ash dump

5.3.2 Atterberg limits

The consistency of a fine-grained soil to be transformed from a plastic state to a liquid state, as well as from semi-solid state to liquid state can be explained using the Atterberg limits, Plastic limit(PL), Liquid limit(LL), and shrinkage limit(SL) respectively. The relation between gross Plasticity index (i.e. LL-PL) and gross clay content is explained using the Van der Merwe (1964) chart in Figure 5.4. The chart defines zones of swell potential ranging from low-medium-high-very high. Expansive soil needs to exhibit at least one of the following:

- Clayey in nature
- High Cation exchange capacity
- High liquid limit and low plastic limit
- High specific surface area

The Atterberg results found that the ash samples are “inert” and exhibit a negligible swell potential. The Unified classifications of the samples were found to be ML which means the samples are mostly silts of low activity/ low plasticity. This is particularly important because no microscopically cracking would occur on the clays thus forming a preferential pathway of the water to leak from the ash dump due to expansion and Shrinkage of the clays with variation in moisture content throughout the life span of the ash dump

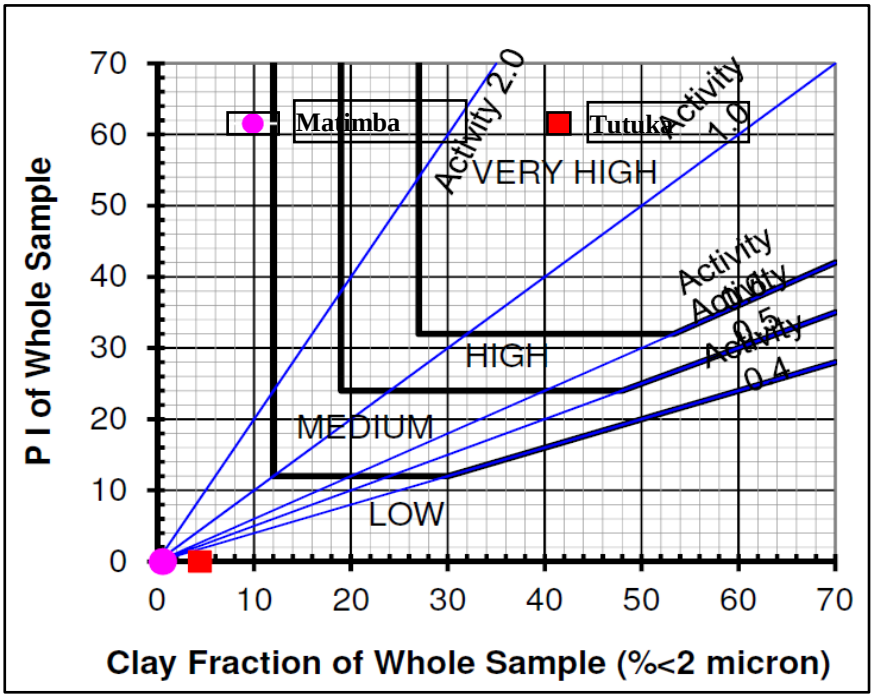


Figure 5.8: Van-der Merwe chart for clay swelling potential

5.4 RETENTION ANALYSIS RESULTS

A range of soil-water characteristic curve (SWCC) models has been proposed over the years to define soil water retention characteristics across the complete range of soil water contents. Measuring the SWCC demands high methodological effort and usually is time-consuming. The modeling approach provides an opportunity to represent the SWCC in a mathematically continuous form. The HYPROP-Fit software contains HYPROP-DES which is a high-class algorithm to fit functional relationships of the retention curve as well as the conductivity. Some of these models are discussed in detail in Appendix 2. Three samples (*i.e.* Samples A-C) from Matimba power stations were allowed to air dry with mass and suction measurements automatically recorded every 10 minutes for 12 days on average. After 36 days, water content and tension data were exported to the HYPROP-Fit software for evaluation and subsequent model fitting, relying on Brook-Corey (1964), unimodal Van Genuchten

(1980), and Kosugi (1996). The measuring campaigns were stopped since no significant mass loss was observed for a prolonged period. This happens after all phases of evaporation have transpired *i.e.* after the third evaporation phase at which both the tensiometers have cavitated. Using the HYPROP-Fit, multiple sample graphs showing the volumetric water content (%) and tension data expressed as pF maybe be viewed in a single plot (see Figure 5.9). All samples yielded a unimodal shape curve of a high peak at lower tensions (0.5-1.0 pF) for the sample, while B and C were observed at relatively higher tensions (0.8-2.0 pF).

Initial water content for sample A was approximately 82%, this is 6% higher than the initial water content of sample B&C. Hyprop-Fit software relies on the initial water content to estimate the porosity of the sample which is estimated at 82% and 76% for sample A and sample B&C respectively. During the saturation of samples, enough time was afforded for the sample to fully saturate through capillary actions. In practice, 100% of water content can never be achieved on a sample. It is for this reason that the calculated water contents are regarded as the best possible approximation of the initial water contents on the three samples during the initial stages of the experiment.

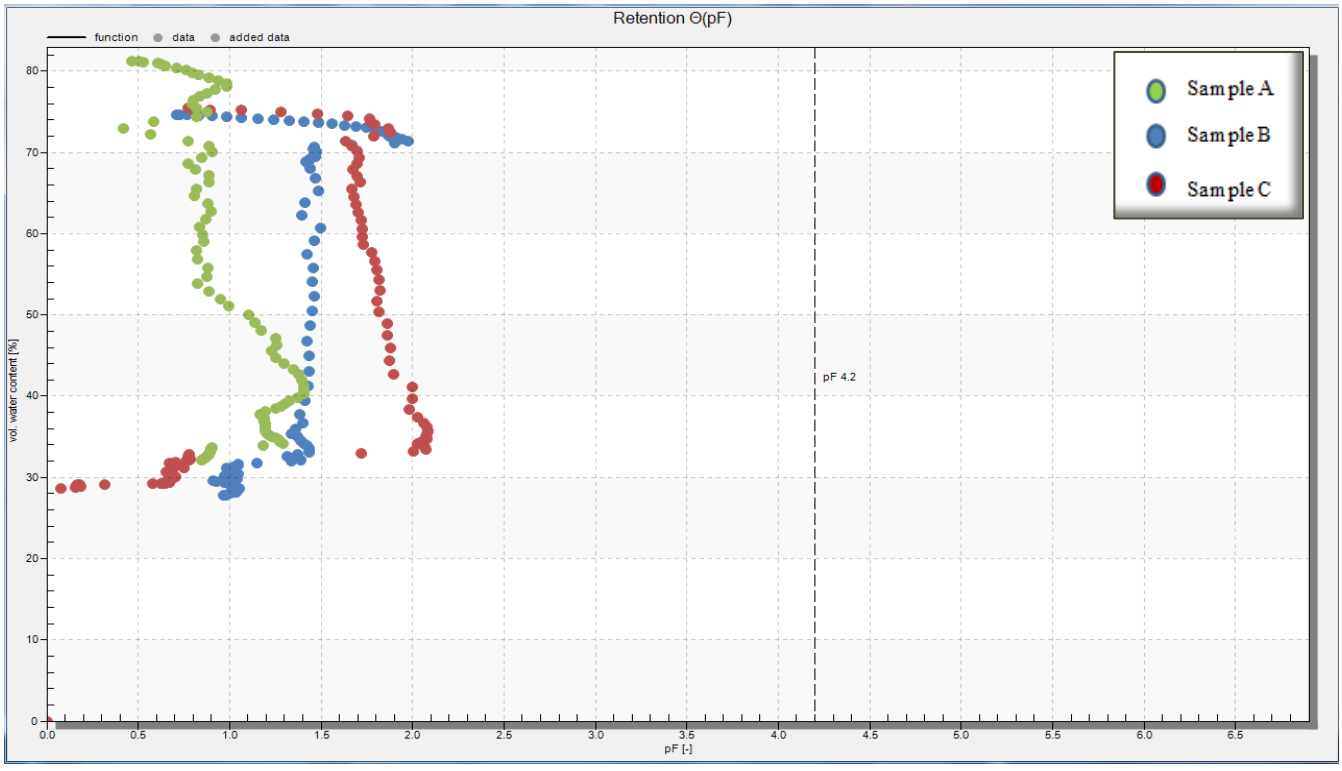


Figure 5.9: Matimba coal ash sample A, B, and C retention measurement

5.4.1 Model selection and parameter estimation

A combination of retention and conductivity models were empirically fitted on Hypro-fit software using measured data. Modeled values together with uncertainties of the individual parameters are presented as an insert in each model (see insert in Figures 5.5 – 5.8). The uncertainties are indicated by 95% confidence limits for the parameter values (expressed by the 2.5% quantiles and the 97.5% quantiles in the two following columns). The fit quality for each fitted model is given in terms of the root mean squares errors. The root mean squares error (RMSE) is an indication of the mean distance between a data point and the fitted function.

RMSE is commonly used to measure the difference between model predicted values and measured values. The difference is referred to as residual, and the RMSE helps to aggregate them into a single measure of predictive power. The RMSE of a model prediction with respect to the estimated variable X_{model} is defined as the square root of the mean squared error given by the following equation:

Where:

$$RMSE = \sqrt{\frac{\sum_{i=1}^{n} (X_{obs,i} - X_{model,i})^2}{n}} \qquad 15$$

X_{obs} is observed values and,

X_{model} is modeled values at time/place i.

Jamieson *et al.* (1992) relied on the following RMSE criteria when Comparing modeled results of ARCWHEAT1 predictions with measured data.

RMSE <10%	-	Excellent
10%<RSME<20%	-	Good
20%<RSME<30%	-	Fair
RMSE>30%	-	Poor

The above criteria were used in this research to determine the quality of each fit model. As an aid to assist with the selection of the best fit model, another statistical analysis tool was relied on, the corrected Akaike Information Criterion (AICc) (Akaike, 1974). AICc features a different number of adjustable parameters when selecting the best fit. Typically the larger the absolute number (value of AICc), the more suitable is the model. Table 5.4 list the statistical summary of each model used, suggesting Brook-Corey as the best fit for the measured retention data. An RMSE of this estimated value indicates about +/- 1.23% error on the estimated value. This value was also achieved by other

functions i.e. Fredlund-Xing, Kasugi, and Van-Genuchten. The average percentage RMSE for samples A, B, and C are 12.3%, 19.1%, and 16.9%, respectively. According to the criteria described above, good fitting was achieved.

This suggests that to interpret the coal ash water retention characteristics, all four functions are likely to yield fairly comparable water retention values. However, Brook-Corey results for sample A will be used further to determine the water retention characteristics of the Matimba ash disposal facility.

Table 5.4: Model selection statistical summary

Statistical analysis	Sample	Brook-Corey	Fredulad-Xing	Kosugi	Van-Genuchten(m=n-1/n)
RMSE-Retention		0.1233	0.1228	0.1229	0.1229
RMSE-Conductivity	A	1.3904	1.1737	0.9534	1.2731
AICc		**-597**	-593	-595	-595
RMSE-Retention		0.1905	0.1905	0.1905	0.1905
RMSE-Conductivity	B	0.3712	0.3751	0.3875	0.3705
AICc		-468	-465	-468	-468
RMSE-Retention		0.1684	0.1689	0.1688	0.1685
RMSE-Conductivity	C	2.7958	4.8247	2.0367	2.6361
AICc		-576	-573	-575	-576

At the same time, a poor parameter estimate for unsaturated hydraulic conductivity is generally observed. The average RMSE values range from 0.376 to 3.073 corresponding to a % RMSE of 37.6 % and 307.3%. This translates to an error range of about 3.76 % to 30.73 %. The % RMSE criteria indicate a poor-fitting effort on all samples for the conductivity function. However, Brook and Corey (1964) is the best possible fit-model amongst the four to estimate the hydraulic conductivity. The model based on Brook and Corey (1964) is used vastly in the geoscience field. It is a four-parameter model suitable to express the soil-water characteristic curve with a sharp air-entry point. The Brook-Corey model is given by the following equation:

$$S_e(h) = \begin{cases} (\alpha\,|h|)^{-\lambda} & \text{for} \quad (\alpha\,|h|) > 1 \\ 1 & \text{for} \quad (\alpha\,|h|) \leq 1 \end{cases} \qquad 16$$

Where S_e is the effective water content

α is the inverse of the air-entry value

h is the matric suction

λ is the pore size distribution index

S_e can be written as:

$$S_e = \frac{\theta - \theta_r}{\theta_s - \theta_r} \qquad 17$$

Where θ is the volumetric water content, θr the residual water content, and θ_s the saturated water content. The uncertainty on the fitted functions can be graphically visualised on the HYPROP-Fit software. The effect of parameter uncertainties due to the Brook-Corey fitting function is illustrated in Figure 5.6. A reduced amount of uncertainty along the desaturation path of sample A is observed between the tension values 0.5-1.5 pF. The highest uncertainty is observed after 1.5pf. At this tension, the sample has reached the residual water content zone.

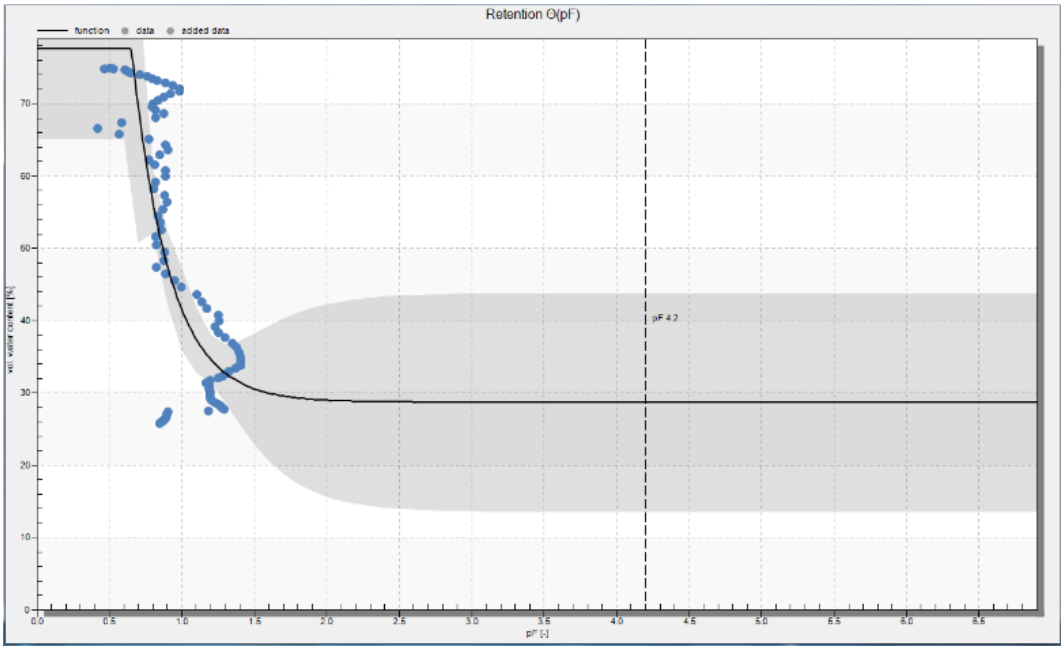


Figure 5.10: Matimba coal ash (Sample A) Brook-Corey fitting uncertainty

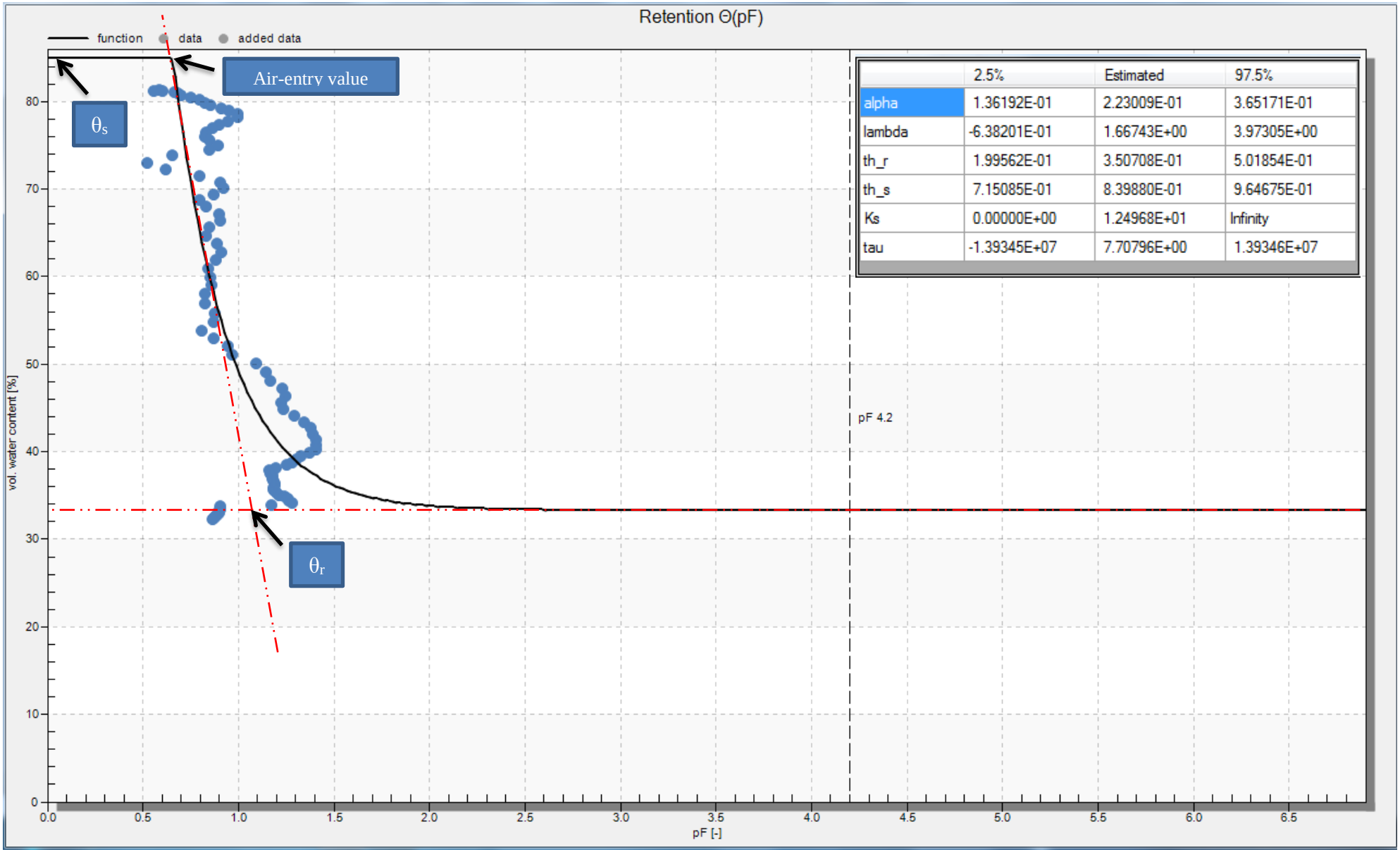
Table 5.5 lists the Brooks-Corey (1964) retention parameters in a symmetric matrix (correlation matrix). Too-high correlation (>0.95) of parameters is undesirable since it indicates an over-parameterization of the selected model. This confirms that this study yielded a well-posed fitting problem as most absolute values of retention parameters are below 0.95.

Table 5.5: Correlation matrix of estimated retention parameters

	α	**λ**	**θ_r**	**θ_s**
α	1.000	-0.915 θ_r	-0.817	0.779
λ	-0.915	1.000	0.957	-0.532
θ_r	-0.817	0.957	1.000	-0.461
θ_s	0.779	-0.532	-0.461	1.000

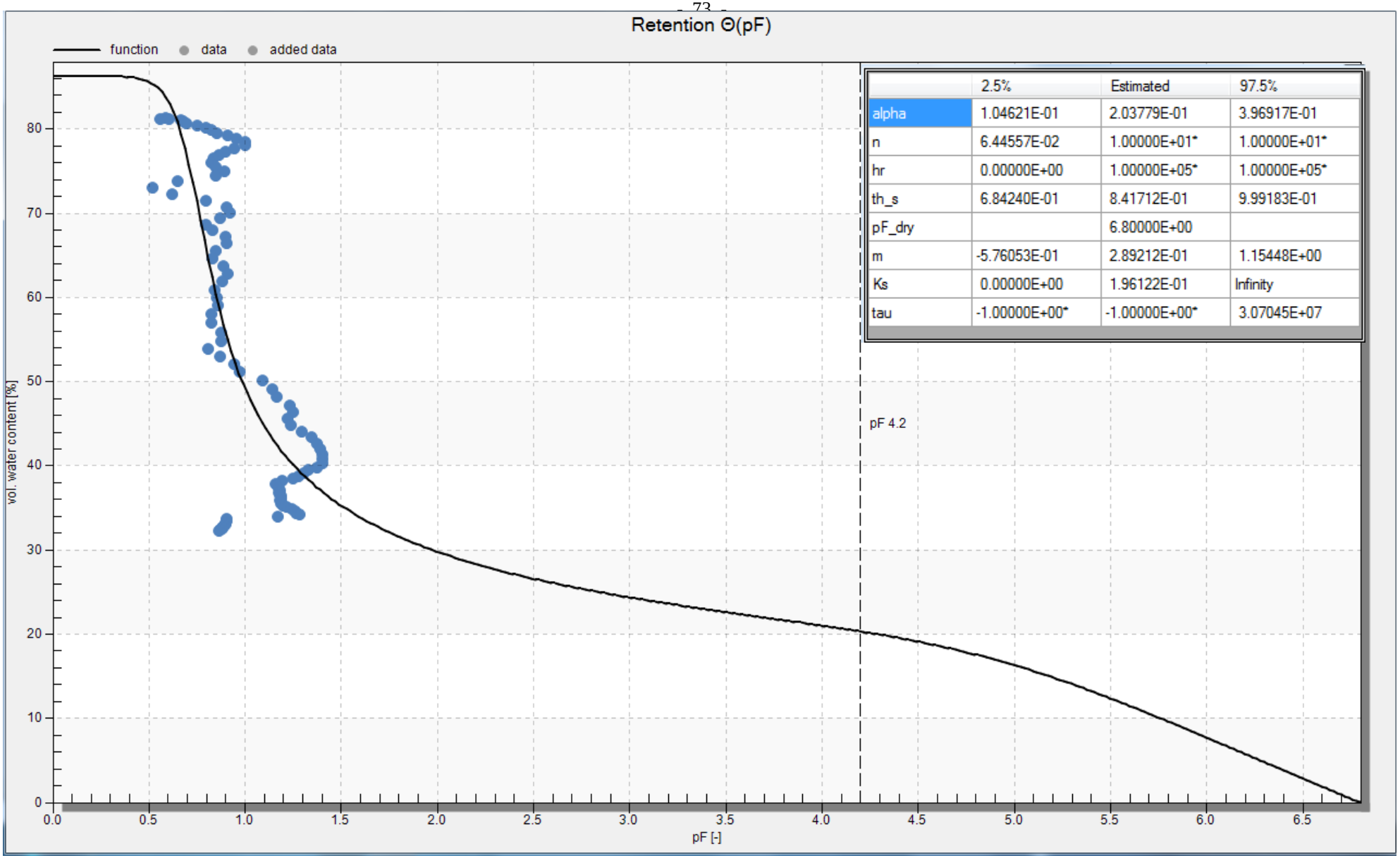
5.4.2 Soil water characteristics curve by Brooks-Corey

The SWCC desorption path of coal ash with a silt-loam texture class was defined by the Brooks-Corey (1964) method (in Figure 5.11) along with its key characteristics. The air-entry is the matric suction value at which a first phase change is observed. It is the matric suction required to ease air entrainment into the largest available pores along the desorption path. This value is approximately 0.65 pf corresponding to the initial water content of 83%. Subsequent the air-entry value is a steep drop in retention as observed in Figure 5.11. This is typically due to the coal ash texture characteristics related to particle size and distribution. At approximately double the air-entry matric suction is the residual water content, defined as a water content corresponding with the large suction change required to remove excess from the coal ash. Fredlund and Xing (1996) provided an empirical approach to determine this value as indicated in Figure 5.5. It is a point of two lines intersecting drawn from two inflection points on the curve as indicated in Figure 5.11. The value is 33 %(at 1.2 pf matric suction) which is 2% less than the value determined by the Brooks-Corey model parameter estimate of 35.07%.



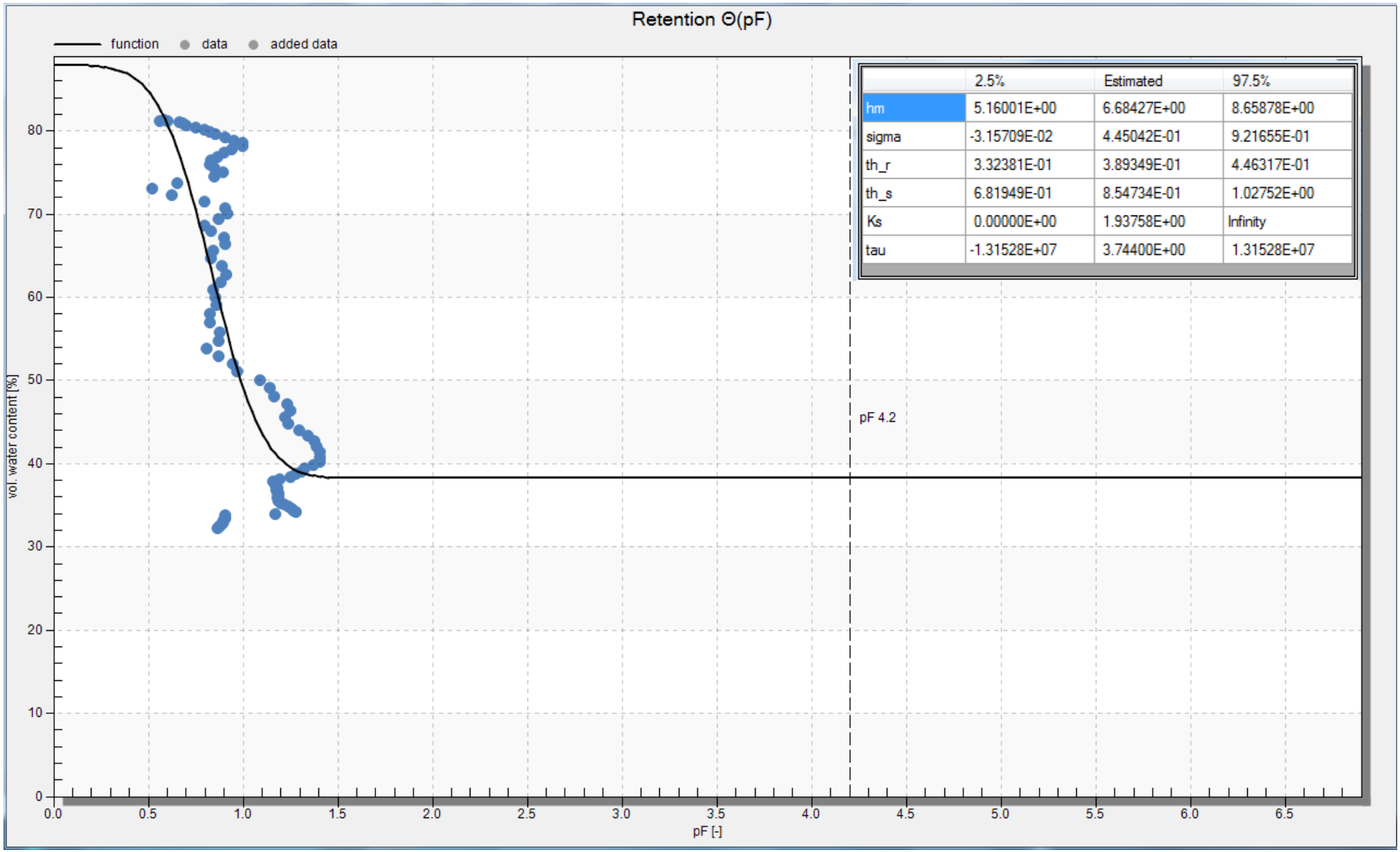
	2.5%	Estimated	97.5%
alpha	1.36192E-01	2.23009E-01	3.65171E-01
lambda	-6.38201E-01	1.66743E+00	3.97305E+00
th_r	1.99562E-01	3.50708E-01	5.01854E-01
th_s	7.15085E-01	8.39880E-01	9.64675E-01
Ks	0.00000E+00	1.24968E+01	Infinity
tau	-1.39345E+07	7.70796E+00	1.39346E+07

Figure 5.11: Matimba coal ash (Sample A: Silt-loam) Brook-Corey fitting results



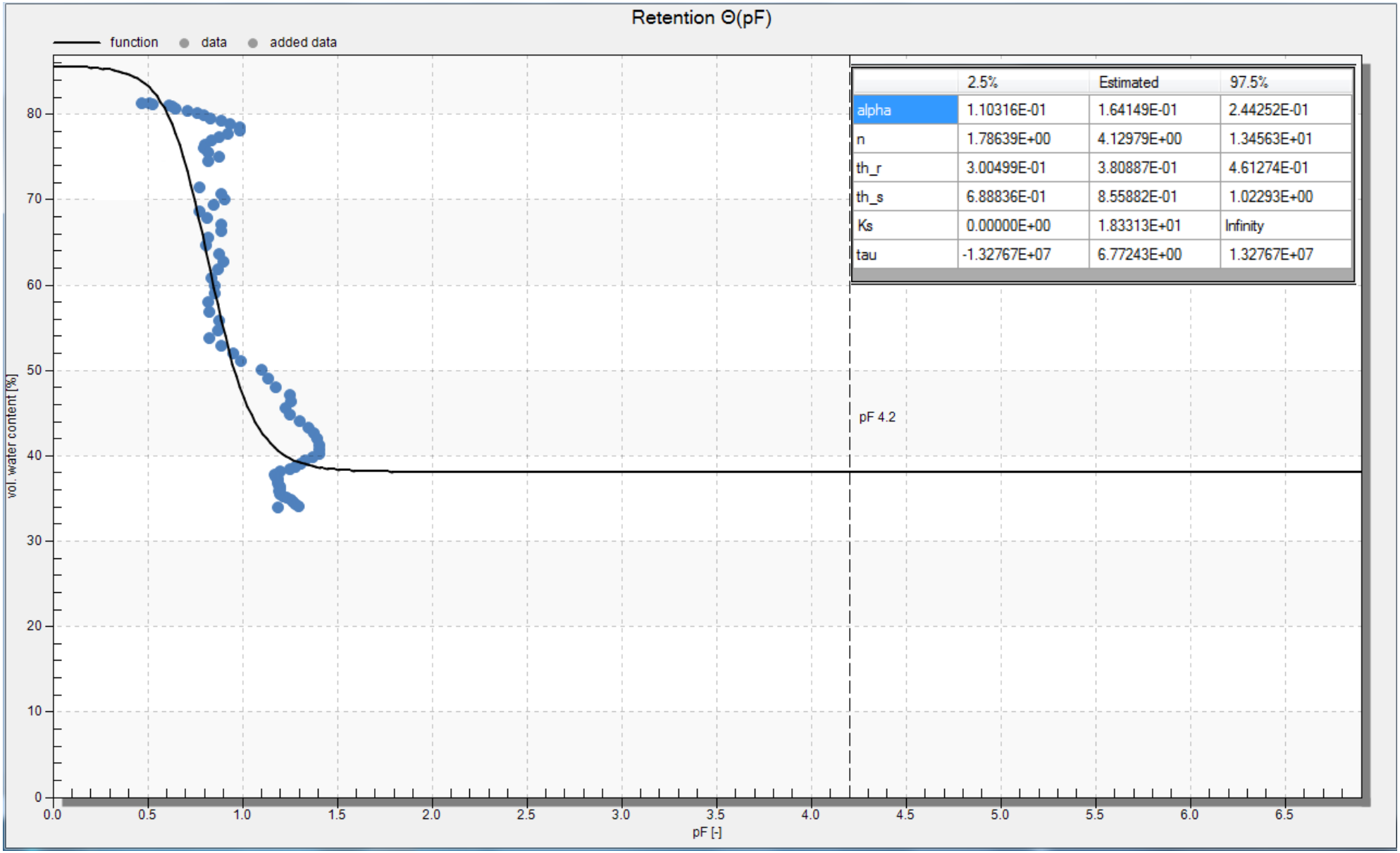
	2.5%	Estimated	97.5%
alpha	1.04621E-01	2.03779E-01	3.96917E-01
n	6.44557E-02	1.00000E+01*	1.00000E+01*
hr	0.00000E+00	1.00000E+05*	1.00000E+05*
th_s	6.84240E-01	8.41712E-01	9.99183E-01
pF_dry		6.80000E+00	
m	-5.76053E-01	2.89212E-01	1.15448E+00
Ks	0.00000E+00	1.96122E-01	Infinity
tau	-1.00000E+00*	-1.00000E+00*	3.07045E+07

Figure 5.12: Matimba coal ash (Sample A: Silt-loam) Fredulad-Xing fitting results



	2.5%	Estimated	97.5%
hm	5.16001E+00	6.68427E+00	8.65878E+00
sigma	-3.15709E-02	4.45042E-01	9.21655E-01
th_r	3.32381E-01	3.89349E-01	4.46317E-01
th_s	6.81949E-01	8.54734E-01	1.02752E+00
Ks	0.00000E+00	1.93758E+00	Infinity
tau	-1.31528E+07	3.74400E+00	1.31528E+07

Figure 5.13: Matimba coal ash (Sample A: Silt-loam) Kasogi fitting results



	2.5%	Estimated	97.5%
alpha	1.10316E-01	1.64149E-01	2.44252E-01
n	1.78639E+00	4.12979E+00	1.34563E+01
th_r	3.00499E-01	3.80887E-01	4.61274E-01
th_s	6.88836E-01	8.55882E-01	1.02293E+00
Ks	0.00000E+00	1.83313E+01	Infinity
tau	-1.32767E+07	6.77243E+00	1.32767E+07

Figure 5.14: Matimba coal ash (Sample A: Silt-loam) Van-Genuchten(m=n-1/n) fitting results

5.4.3 Ash dump water retention

Coal-fired power stations rely on disposing of some of their surplus water through spraying over the ash dump surface. This practice fulfills dual purposes i.e. for suppressing dust of potential airborne coal ash particles and to dispose of water by evaporation loss and capillary storage within. Blight *et al*. (2000) suggest, for a dry ash dump to be optimally used as sinks, input water applications should be matched with evaporation rates and capillary storage. This will ensure the moisture storage of the ash dump is not exceeded and consequently avert leachate generation at the base of the ash dump. The waste balance principle has been widely used to predict changes in moisture in a waste body relying on the principle of conservation of mass to water movement within the waste body. The balance can be loosely stated as water input is equal to water output including the amount of water left in storage. Figure 5.15 shows a simplified water balance of a dry ash dump, depicting main input and output water streams.

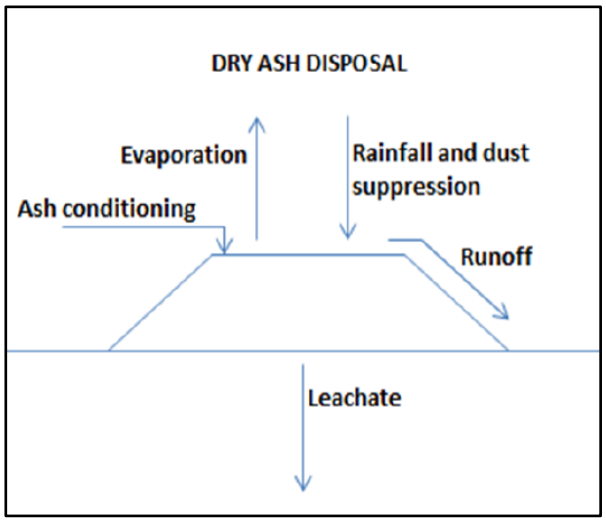


Figure 5.15: A typical simplified water balance of a dry ash dump

Considering the components in Figure 5.15, a mathematical relationship may be summarised and written similar to the soil water balance by Blight *et al*. (2000) as follows:

$$R = ET + LE + LO + \Delta ST \qquad 18$$

Where R is rainfall

ET is water loss by evapotranspiration

LE is water loss as leachate from the base of the waste body

RO is water lost as runoff

ΔST is the change in water stored in the waste by capillary

A lot of work has gone into studying water balance at landfill sites as opposed to dry coal ash disposal facilities. This trend is observed for international as well as local ash dump disposal facilities. Not to say work has not been done, but due to confidentiality, most work remains within the responsible power generation entities managing these facilities. Both landfill and dry coal ash dump behave similarly concerning moisture movement within the solid waste body. Both these facilities pose a risk of groundwater pollution due to the downward percolation of leachate generated within the waste body. Blight *et al.* (1995) suggested that the potential for a landfill to generate leachate regularly or not can be investigated employing the water balance method. Both systems exhibit similar behaviour regarding liquid movement and to some degree, the leachate generated. This can also be said for a dry ash dump under unsaturated conditions.

Figure 5.15 depicts some of the major water balance components for a dry ash dump. Even though is not represented in Figure 5.15, infiltration is the amount of water entering the waste body through the surface of the waste body. Irrespective of the source of water, be it from natural precipitation or any input liquid stream as a disposal effort. All this liquid will enter the waste body through infiltration processes. But a close inspection of Figure 5.15 reveals that not all input liquid streams into the waste body are accounted for through infiltration processes, but some of it ends up as runoff. Also, some part of infiltration is lost due to seasonal variations and geographical differences as a wide temperature range prevails. This loss can be attributed to evaporation. Depending on the stage of ash disposal practice and the existence of vegetation, some water loss might be attributed to evapotranspiration. Vegetation can intercept some water through plant intake and loss as water vapour into the atmosphere. For this study plant, moisture transpiration is disregarded as the focus of the study was mainly at a portion where rehabilitation efforts have not commenced. Suggesting that the study targeted an active ashing portion where dust suppression is on-going and the ash is susceptible to interact with the environment as there is no soil layer applied to the top of the waste body.

5.4.3.1 Matimba liquid retention potential

A dry ashing system is currently in operation at Matimba power station. The area between the toe of the ash stack slope and the ash stacker is referred to as the front stack, and this currently defines the southern face of the ash dump (see Figure 5.16). The active ashing portion refers to areas where rehabilitation has not begun. At the Matimba ash disposal facility, the area is delineated in green in Figure 5.16. The amount of water that an ash dump facility can store is dependent on the capillary storage potential of coal ash. Capillary storage is related to the field capacity of solid waste. Zornberg et al. (1999) define the field capacity of solid waste as the moisture content that a porous material, in this case, coal ash, will store within its pores by capillary stress. This can also be formally defined as the amount of water held in the soil after the excess gravitational water has drained away and after

the rate of downward movement of water has materially decreased (Veihmeyer and Hendrickson, 1931).



Figure 5.16: Matimba ash disposal active ashing portion (2018) (in green)

Pardossi et al. (2009) provided a physical definition of Field capacity and wilting point as water contents at 33 and 1,500 kPa respectively. Table 5.6 present field capacity values estimated by the four models at varying pressures (Pertassek *et al.*, 2015):

- 6 kPa = water content at pF 1.8, i.e., field capacity for conditions with close groundwater level,
- 33 kPa = water content at pF 2.5, i.e., field capacity for conditions distant to groundwater,
- 1500 kPa = water content at pF 4.2, i.e., at the wilting point,

Table 5.6: Model estimated field capacity values for different samples

Sample	Field Capacity pressure	Model Estimated Field Capacity (%)				Sample Mean
		Brook-Corey	Freduland-Xing	Kosugi	Van-Genuchten(m=n-1/n)	
A	6 kPa	29.30	27.10	32.50	31.70	**29.54**
	33 kPa	28.70	22.80	32.50	31.70	
	1500 kPa	28.70	17.70	32.50	31.70	
B	6 kPa	49.50	49.50	49.50	49.50	**44.90**
	33 kPa	49.50	49.50	49.50	49.50	
	1500 kPa	32.70	47.80	31.20	49.50	
C	6 kPa	47.00	46.90	46.90	47.00	**27.43**
	33 kPa	32.80	20.20	26.80	33.90	
	1500 kPa	32.80	12.20	26.80	33.90	

El-Nesr (2006) in his Ph.D. thesis relied on a collection of data from several sources (Keller and Karmeli., 1974; Saxton *et al*., 1986; Van Genuchten *et al*., 1991) to classify soil physical properties according to its texture class. The table of his results is presented in Appendix 4. Using data from El-

Nesr (2006), silt loam texture soils are characterised by the following physical properties expressed in volumetric water content:

- Saturated water content: **Min = 38.20%, Max=50.70% and Mean=45.30%**
- Residual water content; **Min = 6.4%, Max=30.76% and Mean=13.74%**
- Field capacity: **Min = 23.40%, Max=40.19% and Mean=30.76%**
- Wilting point: **Min = 6.45%, Max=19.69% and Mean=11.36%**

This research, using Matimba coal ash Sample A, B and C yielded mean water contents of 29.4%, 44.90%, and 27.43% respectively at 6 and 33 kPa. The determined coal ash mean-field capacity values were further compared to the literature-based value by El-Nesr (2006) in Figure 5.17. Hyprop based filed capacity for Sample A and C are comparable with literature values, while sample B field capacity was overestimated when compared to both mean and maximum field capacity values for the same texture class (silt-loam). This finding was earlier confirmed by two statistical methods used to determine the best fit model. Using RMSE and AICs, sample A was found as the best suitable representative of Matimba coal ash retention characteristics.

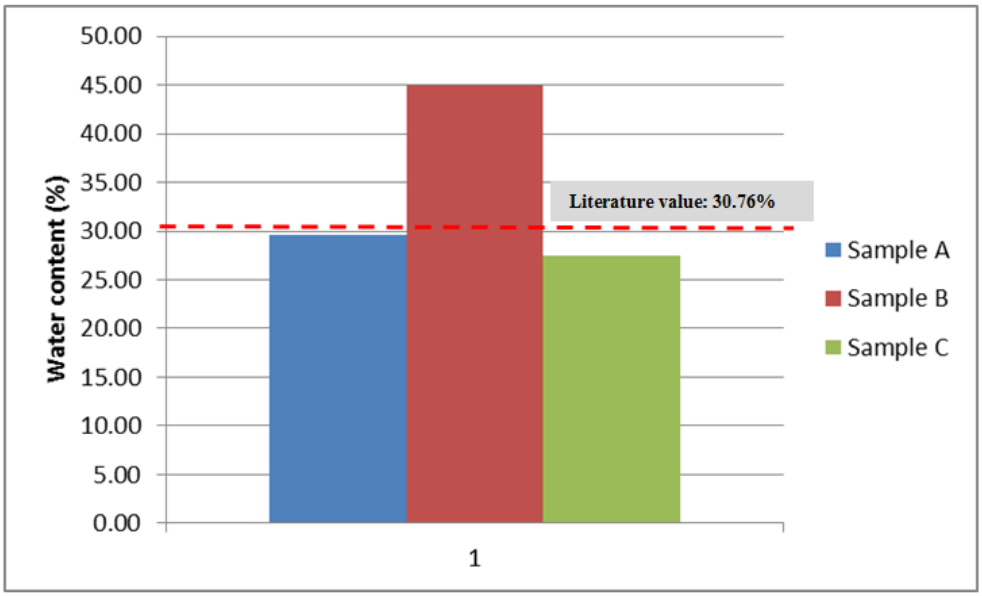
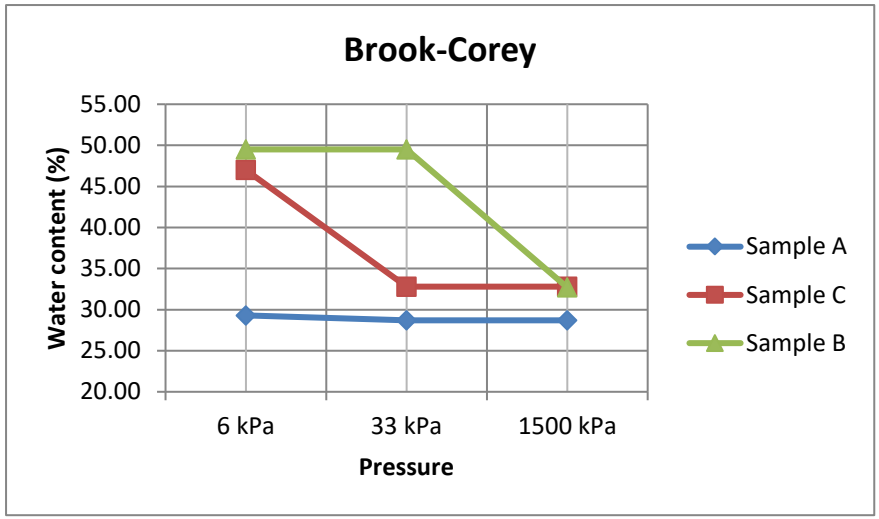
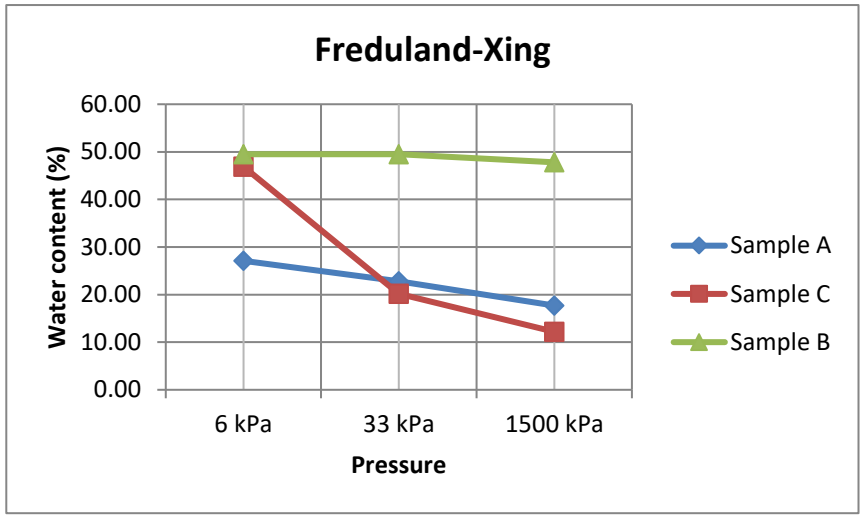
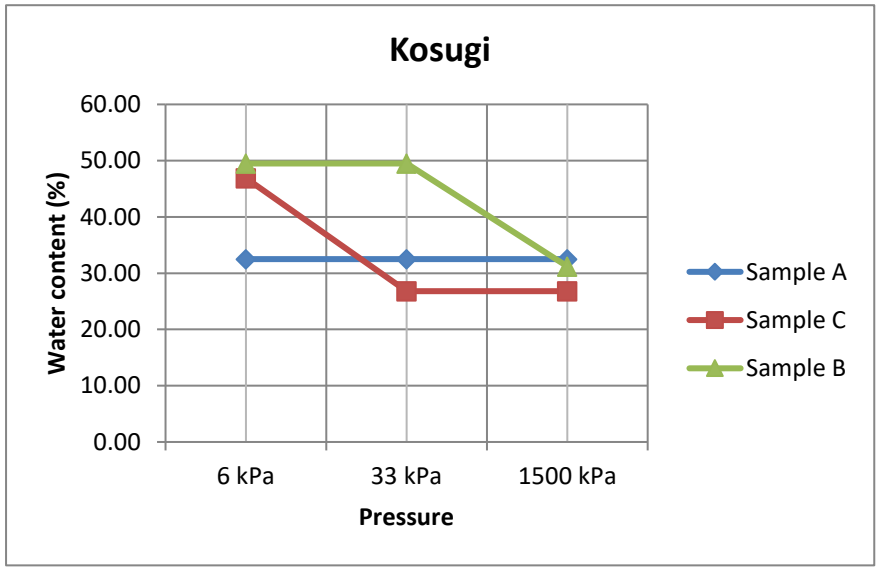


Figure 5.17: Hyprop determined mean-field capacity values compared to mean literature value

Sample B estimated water content at field capacity as 44.90 % this is an overestimate of more than 14% compared to literature value for the same texture class. While Sample A and B underestimated by 1.22 % and 3.33% respectively. AIC analysis did confirm that samples A and B as best represented by the four models used.







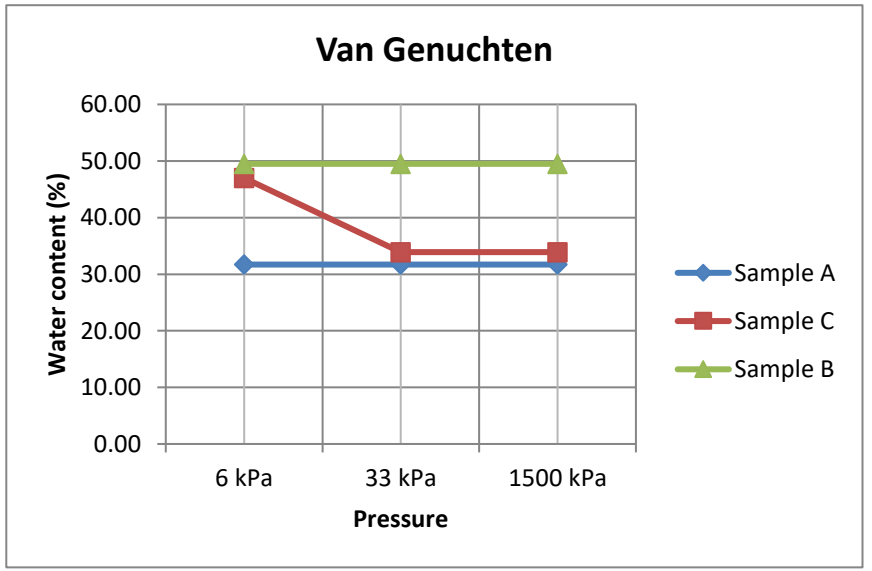


Figure 5.18: Hyprop-Fit estimated field capacity values at different pressures for different Matimba ash samples

The minimum estimated field capacity value was 22.80% at 33 kPa by Kosugi (1996), while the largest field capacity was estimated at 38.9% by the unimodal Van Genuchten model (1980) at all three pressures (6, 33 and 1500 kPa respectively). However, for this study, the selected model was the Brooks-Corey model (1964) (see section 5.3.1 above). The Brooks-Corey model yielded field capacity ranges of 35.1% to 35.7% at a pressure range of 6kPa to 1500 kPa. These values suggest that field capacity was not strongly influenced by pressure change. This might not be true in a real case scenario, since field capacity is known to be influenced by other factors prevalent conditions.

Previous work by GHT (1998) at the Tutuka power station dry ash dump disposal site, suggest that the ash dump field capacity is influenced by the following factors:

- ***Ash characteristics***

  This includes the physical and chemical properties of ash as well as its engineering characteristics.
- ***Input water composition***

  The chemistry of any input water stream (e.g. Dust suppression, precipitation, and irrigation) going into the ash dump. The chemistry is related to the osmotic pressure between the coal ash particles and the solvent of the input water.
- ***Height of the dump***

  The height of the ash dump is important, as gravity and capillary suction are major role players in the retention capacity of the ash.
- ***Boundary conditions***

  This relates to the site-specific geological setup underlain by the ash dump disposal facility. It also includes the groundwater piezometric levels or water table depth below the ash dump.

Table 5.7 lists the field capacity values determined theoretically by three independent institutions GHT (2014) at Tutuka ash disposal facility, also, the average value determined in this study was included to compare the retention potential of the two disposal facilities.

Table 5.7: Comparison of Tutuka and Matimba field capacity values

Study by	Field capacity	Mean Value
SRK	35-42%	38.50%
Rudolph, Van Niekerk	38%	38%
Department of soil science (UFS)	35-40%	37.50%
This research: Sample A	22.80-32.50%	29.54%
This research: Sample B	49.50-49.50%	44.90%
This research: Sample C	**20.20-47.00%**	**27.43%**

The field capacity value determined for Matimba ash dump is lower compared to all the theoretical values determined for the Tutuka ash dump. This accounts for about 3.2% difference when compared with the highest estimated value at Tutuka. This difference might be due to different approaches followed in measuring the ash water retention characteristics. In addition, the targeted portion of the ash dumps during sampling. With all these factors the value is still comparable to the Tutuka field capacity values, even though site-specific conditions will have the ultimate say in the total retention of any coal ash disposal facility.

Site-specific data is required to provide a more realistic water retention value. Relying on the ash dump dimensions as illustrated in Appendix 3, collectively with site-specific climatic data, it was possible to determine a more realistic water retention value. The step-wise calculations performed on an Excel spreadsheet to arrive at a value for Matimba ash dump is presented in Table 5.9. Two essential parameters were sourced from various databases are discussed below.

Evaporation

The Monthly evaporation data were available for two Department of Water and Sanitation (DWS) stations namely A4E003 Zandpan situated some 30km southeast of the site and A4E007 Mokolo Nature Reserve at Mokolo Dam (23°58'32.49"S and 27°43'28.89"E some 35km southeast of the site). The mean annual evaporation (MAE) for station A4E003 is 2 572 mm while station A4E007 is 2 014 mm. Monthly mean, minimum, and maximum evaporation depths are shown in Figure 5.19. The mean annual evaporation between the two stations is 2 293 mm, it is this value that was used as representative for Matimba Power Station ash disposal area.

Table 5.8: Stations A4E003 and A4E007 monthly mean evaporation data

Month	Station-A4E003	Station-A4E007
Jan	256.27	213.56
Feb	261.40	186.99
Mar	228.37	179.34
Apr	180.00	138.32
May	155.00	122.51
Jun	113.00	98.83
Jul	122.97	105.45
Aug	196.33	139.85
Sep	270.00	184.88
Oct	255.75	219.38
Nov	270.00	211.21
Dec	262.47	213.81
Total	**2 572**	**2 014**

Figure 8 shows that the highest evaporation occurs in the summer months from September to March. This is verified in Table 5.7 which shows the average monthly evaporation for the two stations.

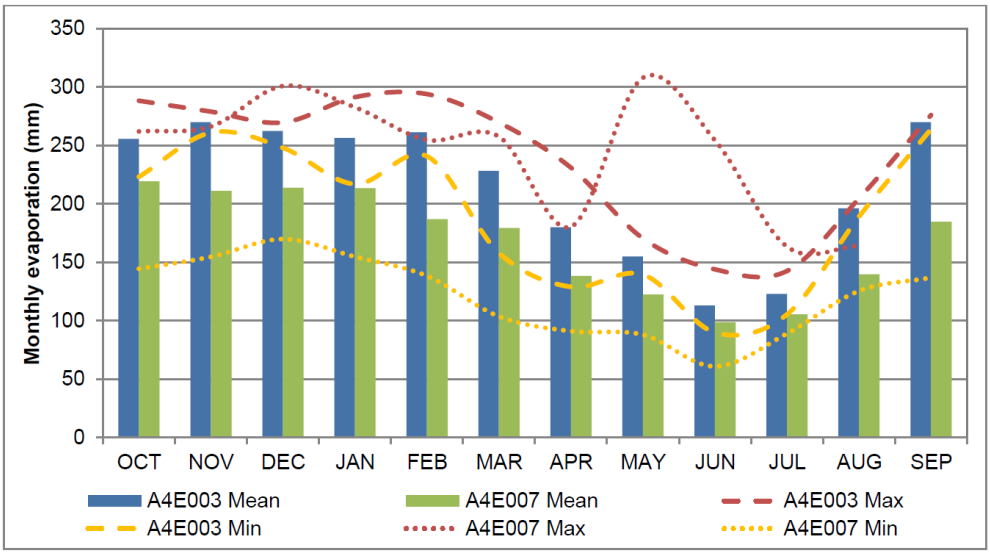


Figure 5.19: Evaporation monthly mean, minimum and maximum of stations A4E003 and A4E007

Rainfall

Rainfall data in the area around Matimba Power Station was sourced from the Daily Rainfall extraction utility (Kunz, 2004). The South African Weather Services (SAWS) station Stockport number 0717595_W was chosen as the station. The mean annual rainfall for Stockport is 416.09 mm. The lowest rainfall year was 1913 with 98.6 mm and the highest rainfall year was 1980 with 747.9 mm

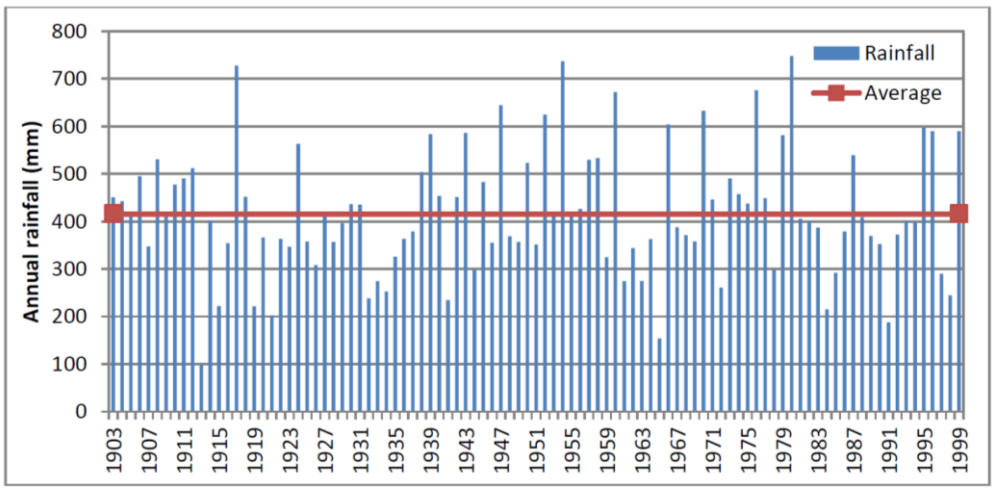


Figure 5.20: Station Stockport yearly and mean rainfall

Table 5.9: Matimba ash dump liquid retention calculations

Description	Calculations			Data Source
Ash Front Stack Length (m)	1000			Measured
Ash Front Stack Width (m)	80			Measured
Ash Front Stack Area (m^2)	80000	8 ha		Calculated
Standby Stack Lenth (m)	900			Measured
Standby Stack Widht (m)	120			Measured
Ash Standby Stack Area (m^2)	108000	10.8 ha		Calculated
Total Area that can be irrigated/Evaporated (m^2)	188000	18.8 ha		Calculated
Height (m)	40			Measured
Volume of ash m^3	7520000	7520 ML		
Retention (%)	33,93%			Hyprop Experiment
Retention volume (m^3)	2654560	2655 ML		Calculated
Average Yearly Rainfall (m)	0,416			(Kunz, 2004) - SAWS database
Yearly Rainfall Volume on area (m^3)	78208	78,21 ML		Calculated
Yearly Evaporation (m)	2,293			DWS
Total Volume of brine that can be encapsulated without taking evaporation into acount (m^3)	2473328	2473 ML	6,78 ML/day	Calculated
Irrigation / day without taking evaporation into acount	36			Calculated
Yearly Evaporation Volume (m^3)	431084	431,1 ML		Calculated
Total Volume of liquid that can be stored taking evaporation into acount (m^3)	**2904412**	**2904,4 ML**	**7,96 ML/day**	**Calculated**

Matimba ash dump liquid retention calculations only considered the south active portion, as discussed above and depicted in figure 5.16. The calculated area of this potion is approximately 18.8 hectares, considering the combined front ash stack and standby ash stack areas. The average ash stack height is 40m above the ground surface. This translates to a total volume of ash of 7520000 m^3, which is equivalent to a liquid volume of 7520 megalitres (ML). Considering the volume occupied by the ash particles and the determined mean total liquid retention of ash (at 33.93%), the amount of liquid that can be stored within the ash matrix is 2655 ML. This water resists gravity draining, remains interlocked within the pore spaces and absorbed within the ash grains. It is important to consider the water balance of the ash dump, as discussed above, rainfall, evaporation, and dust suppression or irrigation. Considering these water streams into and absent from the ash dump, 7.96 ML per day of liquid can be stored in the current Matimba ash portion. With this rate, an entire year can be reached without exceeding the field capacity of the ash dump. This does not account for a more than average rainfall event, also the quality of water applied during dust suppression or irrigation, the water quality will influence in terms of the water holding capacity due to the osmotic pressures. Compaction characteristics and ash density variation are other properties not factored into this calculation due to the limitation of data and not being part of the study's scope. But individually or cumulative effects of all these do play a role in the holding capacity of an ash dump, as such, the value calculated in this study should be used as an overestimate and may aid in terms of realistically determining dust

suppression or irrigation volumes considering the prevalent climatic conditions as experienced on site.

5.5 CHAPTER FIVE SUMMARY

Three set of samples (A, B, and C) were subjected to the Hyprop for an average of 10 days per sample. The Hyprop-fit software was used to estimate the full desorption path of the soil characteristic curve. Sample A was estimated using the Brook-Corey (1964) model. A 29.4 % filed capacity value which is well comparable with that from literature 30.76%. Was estimated considering the full desorption path. The determined field capacity value is consistent with the silt-loam texture class determined in this study. The presence of less active clays like kaolinite could have contributed to the estimated retention value. The formation of new minerals like ettringite might improve the current determined water holding capacity value. The Matimba ash dump has the potential to impact the groundwater resource. This is due to the leach test results exceeding the South African drinking water standard (SANS 241:2015).

CHAPTER 6: CONCLUSIONS AND RECOMMENDATIONS

This chapter provides the key findings from this research and how it relates to the specific objectives of the study. Recommendations for supplementary research are also outlined.

6.1 CONCLUSIONS:

- Sieving together with the hydrometer analysis was conducted to determine the coal ash particle sizes and distribution. The texture of Matimba coal ash is silt-loam and can be generally characterised as fines. Fine-grained materials generally exhibit better water retention properties than coarse-grained materials due to the high surface area available for possible ADForption of water molecules. However, the results also indicate ash with an insignificant amount of clay particles(<0.002 mm) but rather dominated by silt-sized particles (0.05-0.002 mm).
- QEMSCAN, a scanning electron microscope was used to analyse the bulk mineral composition of the coal ash samples. The mineralogical composition of coal ash is characteristically reflected in the composition of the original parent coal, which is generally dominated by the high proportion of aluminosilicate, quartz, and glass cenospheres. The mineralogical analysis on both samples yielded appreciable quantities of clay mineral, with Kaolinite as the dominant mineral phase.
- TCLP tests were conducted to determine the leachability of the ash. Trace elements are chemical elements present in ash in small amounts, but still at lower levels pose a threat to the environment and human health. The detected trace elements from TLCP results in an increasing concentration order are Manganese>Chromium>Copper.
- HYPROP-FIT software was used to access and analyse the ash retention experimental data recorded and acquired using HYPROP-View software. After plotting of various desorption ash water characteristic curves the following were determined:
    - The tested ash material suggests a high moisture retention capacity at low suction, with a progressive decrease in retention apparent with increasing negative head pressures.
    - The study found the Brooks-Corey model as a suitable representative of the Hyprop measured data, confirmed by AICc and RMSE analysis. The Brooks-Corey estimated retention function parameters within +/- 1% error.

- A mean value of 35.3% for the three samples was determined as the water retention or field capacity value for Matimba Coal ash.

After considering site-specific conditions like rainfall and evaporation rate within Matimba ash disposal facility, the active ashing portion can hold about 7.96 megalitres per day of liquid through its capillary storage. If the ash dump is operated in excess of this value, the chances of groundwater pollution are high. It is essential to treat this value as an overestimate, and be used to aid in terms of realistically determining dust suppression or irrigation volumes, for overall effective water management at a dry coal ash dump.

6.2 RECOMMENDATIONS:

Future works should consider the following to complement the current research:

- Retention values should be tested on a laboratory scale physical model of an ash dump, mimic site prevalent conditions to validate this research. This should be done before any results of this study are incorporated into any operational procedures for the ash disposal facility.
- The Study of coal ash morphology and microstructures using a scanning electron microscope (SEM) might aid in identifying micropores and microcracks that will likely increase the water holding capacity of coal ash.
- Alternatively, the Construction of a 2-D/3-D unsaturated numerical based flow model, relying on determined retention values should be considered.
- Considering a different water retention measuring method from the Hyprop with a longer pressure length that covers a longer WCC path.

REFERENCES

Adriano, D.C., Page, A.L., Elseewi, A.A., Chang, A.C. and Straughan, I., 1980. Utilization and Disposal of Fly Ash and Other Coal Residues in Terrestrial Ecosystems: A Review 1. *Journal of Environmental Quality*, *9*(3), pp.333-344.

Ahmaruzzaman, M., 2009. Role of fly ash in the removal of organic pollutants from wastewater. *Energy & Fuels*, *23*(3), pp.1494-1511.

Akaike, H., 1974. A new look at the statistical model identification. *IEEE transactions on automatic control*, *19*(6), pp.716-723.

ASTM D 6836-02., 2003. Test methods for determination of the soil water characteristic curve for desorption using a hanging column, pressure extractor, chilled mirror hygrometer, and/or centrifuge, Annual Book of ASTM Standards, 04.08, *ASTM International, West Conshohocken, PA*

ASTM, C., 1998. Standard specification for coal fly ash and raw or calcined natural pozzolan for use as a mineral admixture in concrete. *1998 Annual Book of ASTM Standards*, *4*, pp.pp-293.

ASTM, D422., 1985. Standard test method for particle-size analysis of soils.

Bashir, R., Sharma, J. and Stefaniak, H., 2015. Effect of hysteresis of soil-water characteristic curves on infiltration under different climatic conditions. *Canadian Geotechnical Journal*, *53*(2), pp.273-284.

Benco, L., Tunega, D., Hafner, J. and Lischka, H., 2001. Orientation of OH groups in kaolinite and dickite: Ab initio molecular dynamics study. *American Mineralogist*, *86*(9), pp.1057-1065.

Bester, M., 2009. *Groundwater resource assessment of the Waterberg coal reserves* (Masters' dissertation, University of the Free State).

Bin-Shafique, M.S., Benson, C.H. and Edil, T.B., 2002. *Leaching of heavy metals from fly ash stabilized soils used in highway pavements*. Geo Engineering Program, Department of Civil and Environmental Engineering, University of Wisconsin-Madison.

Bin-Shafique, M.S., CRAIG, H.B. and TUNCER, B., 2003. Leaching of heavy metals from fly ash-stabilized soils used in highways. *Ashlines*, *4*(4), pp.1-14.

Blight, G.E., Ball, U.T.M., Blight, J.J. and Vorster, K., 1995. Moisture conditions in landfills situated on the South African Highveld. *Journal of the South African Institution of Civil Engineering= Joernaal van die Suid-Afrikaanse Instituut van Siviele Ingenieurswese*, *37*(2), pp.6-10.

Blight, G.E., Troncoso, J.H., Fourie, A.B. and Wolski, W., 2000, November. Issues in the geotechnics of mining wastes and tailings. In *ISRM International Symposium*. International Society for Rock Mechanics and Rock Engineering.

Brooks, R. and Corey, T., 1964. HYDRAU uc properties of porous media. *Hydrology Papers, Colorado State University*, *24*, p.37.

Brooks, R. H., and Corey, A. T., 1964. Hydraulic properties of porous Media. *Colorado State University, Fort Collins*, Hdrol Paper 3.

Campbell, A.E., 1999. *Chemical, physical and mineralogical properties associated with the hardening of some South African fly ashes* (Mastoral thesis, University of Cape Town).

Carlson, C.L. and Adriano, D.C., 1993. Environmental impacts of coal combustion residues. *Journal of Environmental quality*, *22*(2), pp.227-247.

Carlson, C.L., Adriano, D.C, *Enviromental impacts of coal combustion residues* Journal of Enviromental Quality, 1993. **22**: p. 227-247.

Chindaprasirt, P., Thaiwitcharoen, S., Kaewpirom, S. and Rattanasak, U., 2013. Controlling ettringite formation in FBC fly ash geopolymer concrete. *Cement and Concrete Composites*, *41*, pp.24-28.

Department of environmental affairs., 2013, National Norms and Standards for the assessment of waste for landfill disposal. *Government Gazette 36784*, Regulation 635 of 23 August 2013.

Department of Water and Forestry., 2007, *Best Practice Guideline A4: Pollution Control Dams*, , Pretoria, South Africa.

Eberhard, A., 2011. The future of South African coal: Market, investment and policy challenges. *Program on energy and sustainable development*, pp.1-44.

Eduafo, P.M., 2013. *Experimental investigation of recycling rare earth elements from waste fluorescent lamp phosphors* (Doctoral dissertation, Colorado School of Mines. Arthur Lakes Library).

EIA, 2005. Energy Information Administration: National Energy Information Center, 1000 Independence Ave., SW Washington D.C., USA. Also available online at: www.eia.doe.gov.

El-Nesr, M.N., 2006. Subsurface drip irrigation system development and modeling of wetting pattern distribution. *Unpublished Ph. D. thesis, Fac. of Agric., Alex. Univ*.

Environmental integrity project (EIP), 2019. Coal's Poisonous Legacy - Groundwater Contaminated by Coal Ash across the U.S. Also available online at: *https://earthjustice.org/*

Enviroworks, 2018. Source-pathway-receptor risk assessment and options analysis for the expansion of the ash disposal facility at Matimba Power Station, Limpopo province.

EPA, U., 1992. Toxicity characteristic leaching procedure USEPA Method 1311. *United States Environmental Protection Agency*.

Eskom., 2016. Ash management in Eskom. *Fact sheet, Revision 12*

Fatoba O.O., 2008. The chemical composition and leaching behavior of some South African fly ashes. VDM Verlag Dr Muller Aktiengesellschaft and Co.Kg USA.

Feddes, R.A., Kabat, P., Van Bakel, P., Bronswijk, J.J.B. and Halbertsma, J., 1988. Modelling soil water dynamics in the unsaturated zone—state of the art. *Journal of Hydrology*, *100*(1-3), pp.69-111.

Ferreira, A.M., Soeiro, F.J.C. and Gerscovich, D.M.S., 2010. Parameter Identification of the Soil-Water Characteristic Curve of Brazilian Residual Soils Using Hybrid Optimization Methods. In *2nd International Conference on Engineering Optimization September* (pp. 6-9).

Fredlund, D.G. and Xing, A., 1994. Equations for the soil-water characteristic curve. *Canadian geotechnical journal*, *31*(4), pp.521-532.

Fredlund, D.G., 2006. Unsaturated soil mechanics in engineering practice. *Journal of geotechnical and geoenvironmental engineering*, *132*(3), pp.286-321.

Fredlund, D.G., Rahardjo, H. and Rahardjo, H., 1993. *Soil mechanics for unsaturated soils*. John Wiley & Sons.

Gaiser, T., Graef, F. and Cordeiro, J.C., 2000. Water retention characteristics of soils with contrasting clay mineral composition in semi-arid tropical regions. *Soil Research*, *38*(3), pp.523-536.

Gardner, W. and Widtsoe, J.A., 1921. The movement of soil moisture. *Soil Sci*, *11*(3), pp.215-232.

GHT Consulting Scientists, 1998. *Tutuka Power Station – Ash dump water holding capacity REPORT NO.: RVN 142/194*

GHT Consulting Scientists, 2011. *Matimba Power Station – Numerical Pollution Plume Model Report – November 2011* ("2011 GHT Model")

Gunal, H., Ersahin, S., Uz, B.Y., Budak, M. and Acir, N., 2011. Soil particle size distribution and solid fractal dimension as influenced by pretreatments. *J. Agr. Sci*, *17*, pp.217-229.

HODGSON, FDI.and KRANTZ RM. (1998). Groundwater Quality Deterioration in the Olifants River Catchment above the Loskop Dam with Specialized Investigation in the Witbank Dam Sub-Catchment.-WRC Report No.-291/1/98.

Holdich, R.G., 2002. *Fundamentals of particle technology*. Midland Information Technology and Publishing.

International Energy Agency (IEA). 2007. Fossil fuel-fired power generation- Case studies of recently constructed coal- and gas- fired power plants. Also available online at: www.iea.org

Izquierdo, M. and Querol, X., 2012. Leaching behaviour of elements from coal combustion fly ash: an overview. *International Journal of Coal Geology*, *94*, pp.54-66.

Jamieson, P.D., Porter, J.R. and Wilson, D.R., 1991. A test of the computer simulation model ARCWHEAT1 on wheat crops grown in New Zealand. *Field crops research*, *27*(4), pp.337-350.

Keller, J. and Karmeli, D., 1974. Trickle irrigation design parameters. *Transactions of the ASAE*, *17*(4), pp.678-0684.

Kosugi, K.I., 1996. Lognormal distribution model for unsaturated soil hydraulic properties. *Water Resources Research*, *32*(9), pp.2697-2703.

Krüger, J.E., 2003. South African fly ash: A cement extender. *A south African coal Ash Association publication*.

Landman, A.A., 2006. *Aspects of solid-state chemistry of fly ash and ultramarine pigments* (Doctoral dissertation, University of Pretoria).

Leedy, P.D. and Ormrod, J.E., 1993. Practical Research: Planning and Design, Columbus: Merril Prentice-Hall.

Liu, Y., Clavier, K.A., Spreadbury, C. and Townsend, T.G., 2019. Limitations of the TCLP fluid determination step for hazardous waste characterization of US municipal waste incineration ash. *Waste Management*, *87*, pp.590-596.

MacVicar, C.N., 1977. *Soil classification. A binomial system for South Africa*. Department of Agricultural Technical Services.

Mahmood, K.R. and Kareem, A.H.A., 2010. Nature of Soil-Water Characteristics Curves (SWCC) for Soils from Anbar Governorate. *AJES*, *3*(1), p.61.

Matshitse, R.M.S., 2016. *Effect of fly ash composition on the synthesis of carbon nanomaterials* (Mastoral thesis).

Matsumoto, S., Ogata, S., Shimada, H., Sasaoka, T., Kusuma, G.J. and Gautama, R.S., 2016. Application of coal ash to postmine land for prevention of soil erosion in coal mine in Indonesia: utilization of fly ash and bottom ash. *Advances in Materials Science and Engineering*, *2016*.

Mattigod, S.V., 1983. Chemical composition of aqueous extracts of fly ash: Ionic speciation as a controlling factor. *Environmental Technology*, *4*(12), pp.485-490.

McCauley, A., Jones, C. and Jacobsen, J., 2005. Basic soil properties. *Soil and water management module*, *1*(1), pp.1-12.

Mokhahlane, L., 2013. *Composition and performance of multi-layer liner systems to inhibit contaminant transport in a fly-ash dump* (Masters' thesis, University of the Free State).

Nielsen, D.R. and Biggar, J.W., 1986. Water flow and solute transport processes in the unsaturated zone. *Water resources research*, *22*(9S).

Osman, K., Coquelet, C. and Ramjugernath, D., 2014. Review of carbon dioxide capture and storage with relevance to the South African power sector. *South African Journal of Science*, *110*(5-6), pp.01-12.

Ouhadi, V.R. and Yong, R.N., 2008. Ettringite formation and behaviour in clayey soils. *Applied Clay Science*, *42*(1-2), pp.258-265.

Pan, H., Qing, Y. and Pei-yong, L., 2010. Direct and indirect measurement of soil suction in the laboratory. *Electronic Journal of Geotechnical Engineering*, *15*(3), pp.1-14.

Pardossi, A., Incrocci, L., Incrocci, G., Malorgio, F., Battista, P., Bacci, L., Rapi, B., Marzialetti, P., Hemming, J. and Balendonck, J., 2009. Root zone sensors for irrigation management in intensive agriculture. *Sensors*, *9*(4), pp.2809-2835.

Pertassek, T., Peters, A. and Durner, W., 2015. HYPROP-FIT software user's manual, Version 3.0. *UMS GmbH, Munich, Germany*.

Peters, A. and Durner, W. (2015). SHYPFIT 2.0 User's Manual. Research Report. *Institut für Ökologie, Technische Universität Berlin, Germany*

Petrik, L.F., Fatoba, O.O., Missengue, R., Kalombe, R.M., Nyale, S. and Madzivire, G., 2017. Water Research Commission.

Prasad, K.H., Kumar, M.M. and Sekhar, M., 2001. Modelling flow through unsaturated zones: sensitivity to unsaturated soil properties. *Sadhana*, *26*(6), pp.517-528.

Querol, X., Umana, J.C., Alastuey, A., Ayora, C., Lopez-Soler, A. and Plana, F., 2001. Extraction of soluble major and trace elements from fly ash in open and closed leaching systems. *Fuel*, *80*(6), pp.801-813.

Ramme, B.W., Lingle, J.W. and Naik, T.R., 1998, October. Coal combustion products utilization in Wisconsin—an environmental approach. In *Proceedings of the Three-Day CANMET/ACI*

International Symposium on Sustainable Development of the Cement and Concrete Industry. October (pp. 21-23).

Republic of South Africa (RSA). 2013. Waste Classification and Management Regulations. *Government Gazette 36784,* Regulation 634 of 23 August 2013.

Richards, L.A., 1931. Capillary conduction of liquids through porous mediums. *Physics*, *1*(5), pp.318-333.

Roberts, D., 2008. Chromium speciation in coal combustion byproducts: case study at a dry disposal power station in Mpumalanga Province, South Africa.

Royal HaskoningDHV, 2015. *Final Environmental Impact Assessment Report for the Proposed Continuous Ash Disposal Facility for the Matimba Power Station in Lephalale, Limpopo Province*

Saxton, K.E., Rawls, W., Romberger, J.S. and Papendick, R.I., 1986. Estimating generalized soil-water characteristics from texture 1. *Soil Science Society of America Journal*, *50*(4), pp.1031-1036.

Schindler, U., 1980. Ein schnellverfahren zur messung der wasserleitfahigkeit im teilgesattigten boden and stechzylinderproben. *Archiv fur Acker-und Pflanzenbau und Bodenkunde*.

Schindler, U., Durner, W., von Unold, G. and Müller, L., 2010. Evaporation method for measuring unsaturated hydraulic properties of soils: Extending the measurement range. *Soil Science Society of America Journal*, *74*(4), pp.1071-1083.

Schuttlefield, J.D., Cox, D. and Grassian, V.H., 2007. An investigation of water uptake on clays minerals using ATR-FTIR spectroscopy coupled with quartz crystal microbalance measurements. *Journal of Geophysical Research: Atmospheres*, *112*(D21).

Sigh, N., Reynolds-Clausen, K.,2015, 'Eskom's revised Coal Ash Strategy and Implementation Progress, In *Proceedings of the Test and Measurement conference, https://www.home.nla.org.za/*.

Singh, K.R.C.N., South Africa's power producer's revised Coal Ash Strategy and Implementation Progress.

Snyman, C.P. (1998) "Coal". In: Wilson, M.G.C. and Anhaeusser (Ed) The mineral resources of South Africa. Handbook 16, Council for Geosciences, 6th Edition. ISBN 1-875061-52-5.

Sočo, E. and Kalembkiewicz, J., 2009. Investigations on Cr mobility from coal fly ash. *Fuel*, *88*(8), pp.1513-1519.

Standard, A.S.T.M., 2014. C136/C136M-14.(2014). *Standard Test Method for Sieve Analysis of Fine and Coarse Aggregates*.

Tami, D., Rahardjo, H. and Leong, E.C., 2004. Effects of hysteresis on steady-state infiltration in unsaturated slopes. *Journal of Geotechnical and Geoenvironmental Engineering*, *130*(9), pp.956-967.

Terzano, R., Spagnuolo, M., Medici, L., Tateo, F. and Ruggiero, P., 2005. Characterization of different coal fly ashes for their application in the synthesis of zeolite X as cation exchanger for soil remediation. *Fresenius Environmental Bulletin*, *14*(4), pp.263-267.

TROSKIE, K. (2005). GCS ref. NIN.05/469.

Van der Merwe, D.H., 1964. The prediction of heave from the plasticity index and percentage clay fraction of soils. *Civil Engineering= Siviele Ingenieurswese*, *1964*(v6i6), pp.103-107.

Van Genuchten, M.T., 1980. A closed-form equation for predicting the hydraulic conductivity of unsaturated soils 1. *Soil science society of America journal*, *44*(5), pp.892-898.

Van Genuchten, M.T., Leij, F.J. and Yates, S.R., 1991. The RETC code for quantifying the hydraulic functions of unsaturated soils. US Salinity Laboratory. *US Department of Agriculture, Agricultural Research Service, Riverside, California*, *9250*(1).

Vanapalli, S.K. and Fredlund, D.G., 2000. Comparison of different procedures to predict unsaturated soil shear strength. In *Advances in Unsaturated Geotechnics* (pp. 195-209).

Vanapalli, S.K. and Han, Z., 2019. Addressing Transportation Geotechnics Challenges Using Mechanics of Unsaturated Soils. In *Geotechnical Design and Practice* (pp. 91-104). Springer, Singapore.

Vanapalli, S.K., Sillers, W.S. and Fredlund, M.D., 1998, October. The meaning and relevance of residual state to unsaturated soils. In *Proceedings of the 51st Canadian Geotechnical Conference, Edmonton, Alta* (pp. 4-7).

Veihmeyer, F.J. and Hendrickson, A.H., 1931. The moisture equivalent as a measure of the field capacity of soils. *Soil Science*, *32*(3), pp.181-194.

Wind, G.P., 1966. *Capillary conductivity data estimated by a simple method* (No. 80). [sn].

Yadav, S. and Yadav, S., 2014. Investigations of metal leaching from mobile phone parts using TCLP and WET methods. *Journal of environmental management*, *144*, pp.101-107.

Zhang, X., Younan, N.H. and O'Hara, C.G., 2005. Wavelet domain statistical hyperspectral soil texture classification. *IEEE Transactions on geoscience and remote sensing*, *43*(3), pp.615-618.

Zhao, S., Duan, Y., Lu, J., Gupta, R., Pudasainee, D., Liu, S., Liu, M. and Lu, J., 2018. Chemical speciation and leaching characteristics of hazardous trace elements in coal and fly ash from coal-fired power plants. *Fuel*, *232*, pp.463-469.

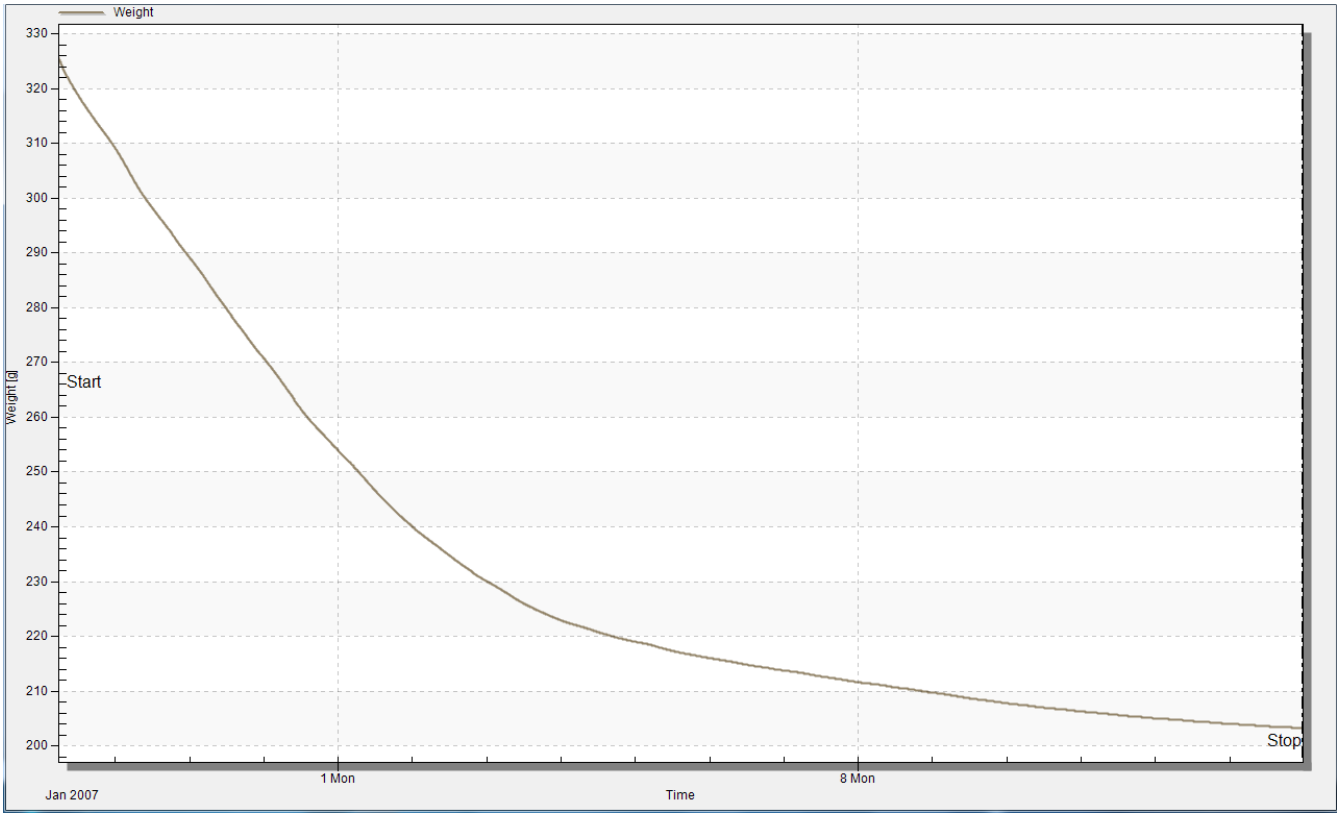
Zornberg, J.G., Jernigan, B.L., Sanglerat, T.R. and Cooley, B.H., 1999. Retention of free liquids in landfills undergoing vertical expansion. *Journal of Geotechnical and Geoenvironmental Engineering*, *125*(7), pp.583-594.

APENDIX 1: EXPERIMENTAL DATA

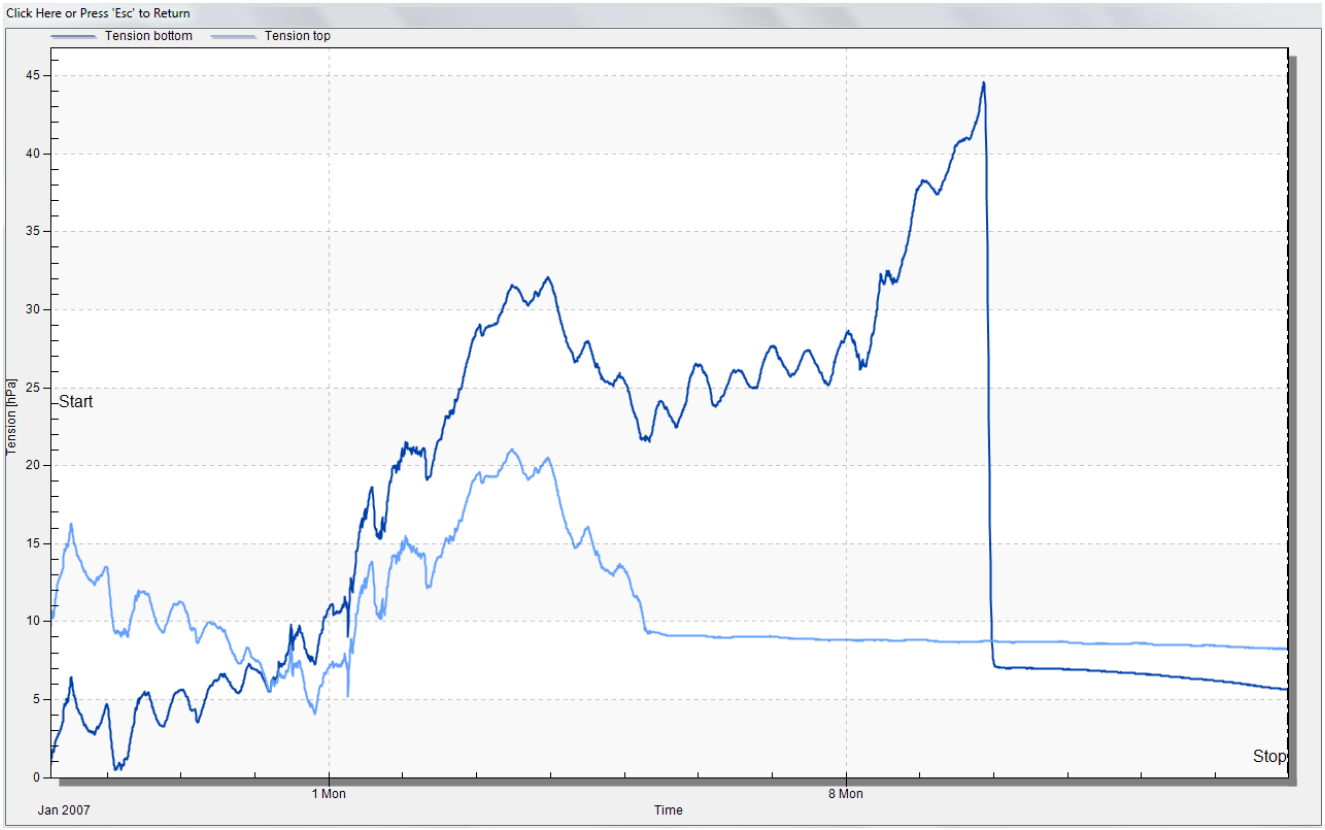
Ambient total water content

Sample ID	Mass of container(g)	Mass of solid particles(g)	Mass of container and oven dried specimen(g)	Mass of container and moist specimen (g)	mass of water (g)	water content(%)	Mean values
RT&D standard*	33.9066	1.0025	34.8876	34.9091	0.0215	2.1446	
RT&D standard*	31.9683	1.0008	32.9480	32.9691	0.0211	2.1083	2.1265
Sample 26	32.4172	1.0012	33.3435	33.4184	0.0749	7.4810	
Sample 36	31.8638	1.0024	32.7860	32.8662	0.0802	8.0008	
Sample 41	28.2182	1.0034	29.1484	29.2216	0.0732	7.2952	
Sample 30	38.4820	1.0018	39.4124	39.4838	0.0714	7.1272	7.3011
***standard= pulvarised coal**							

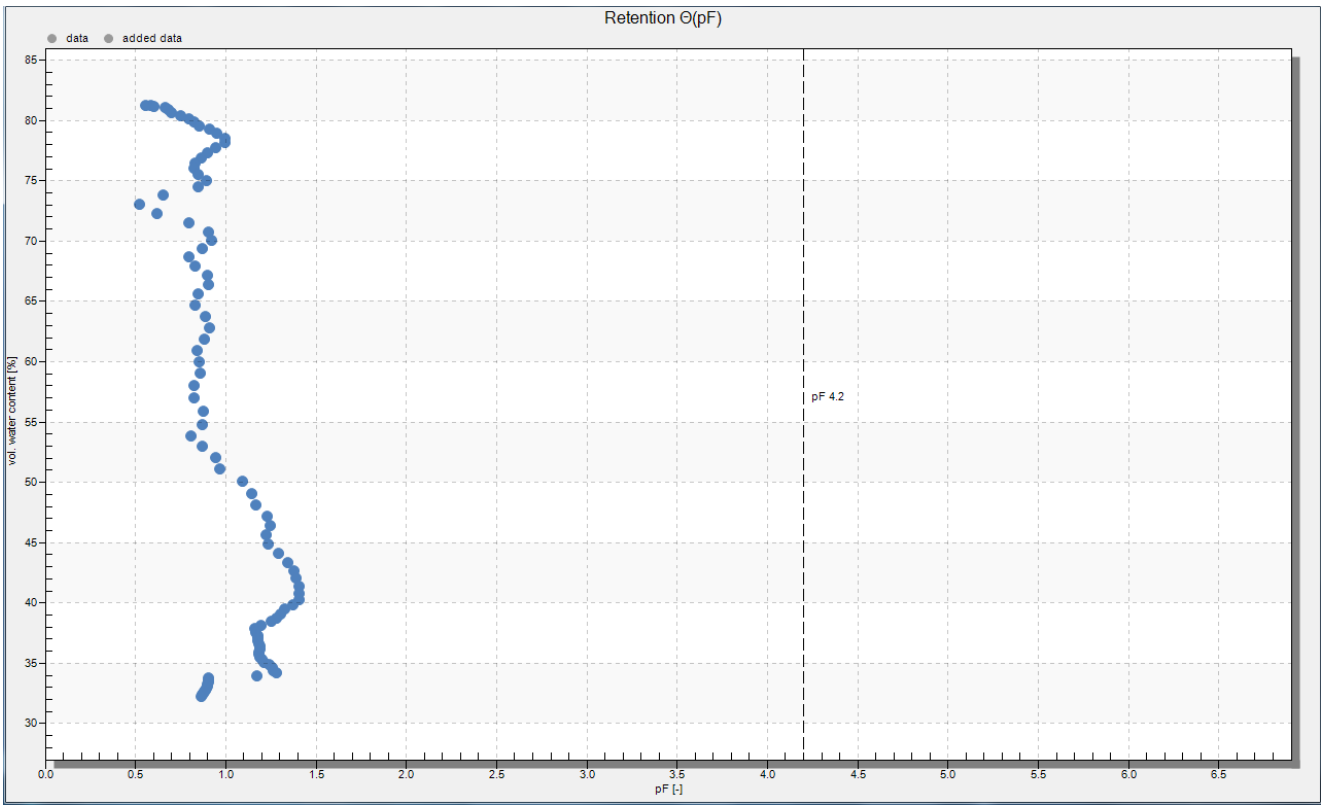
Hyprop weight loss graph



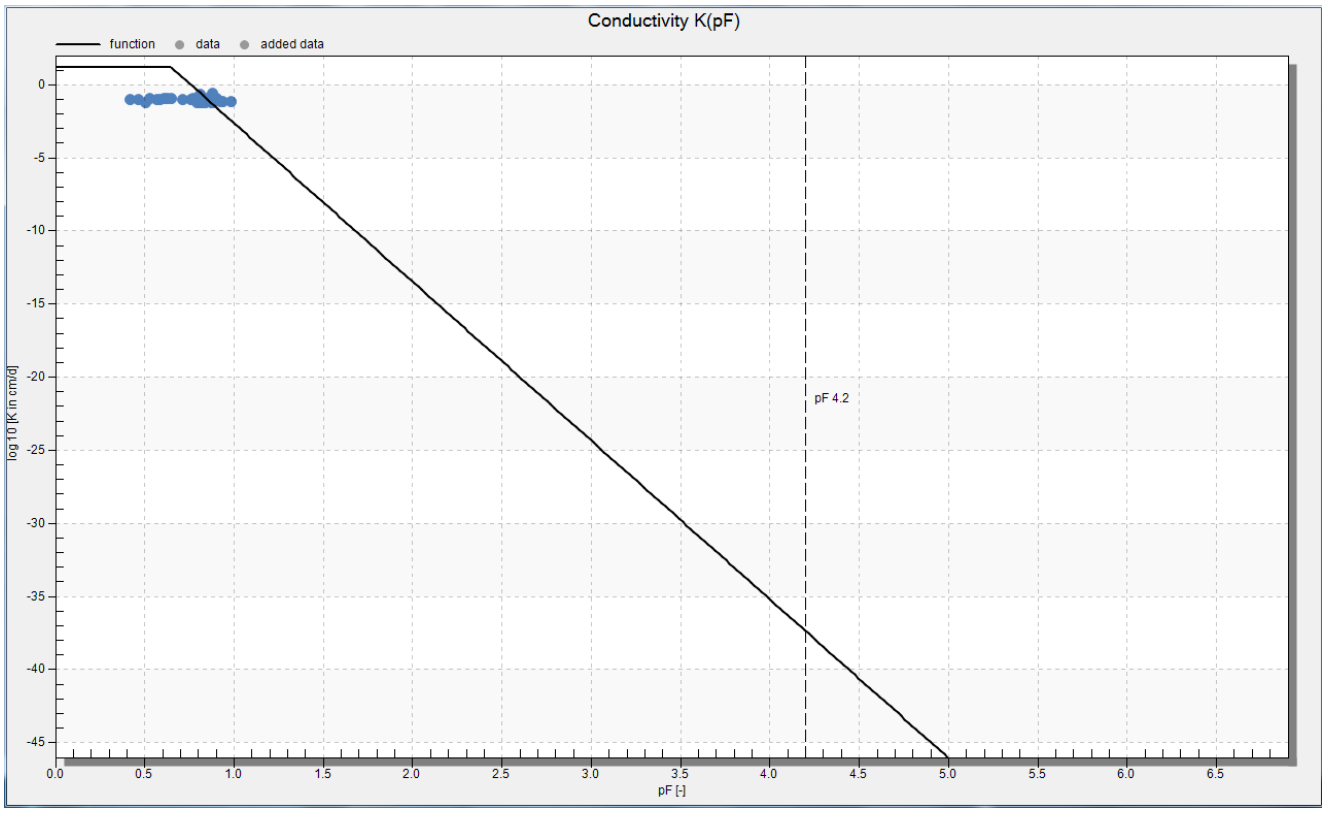
Top and bottom tentiometers reading

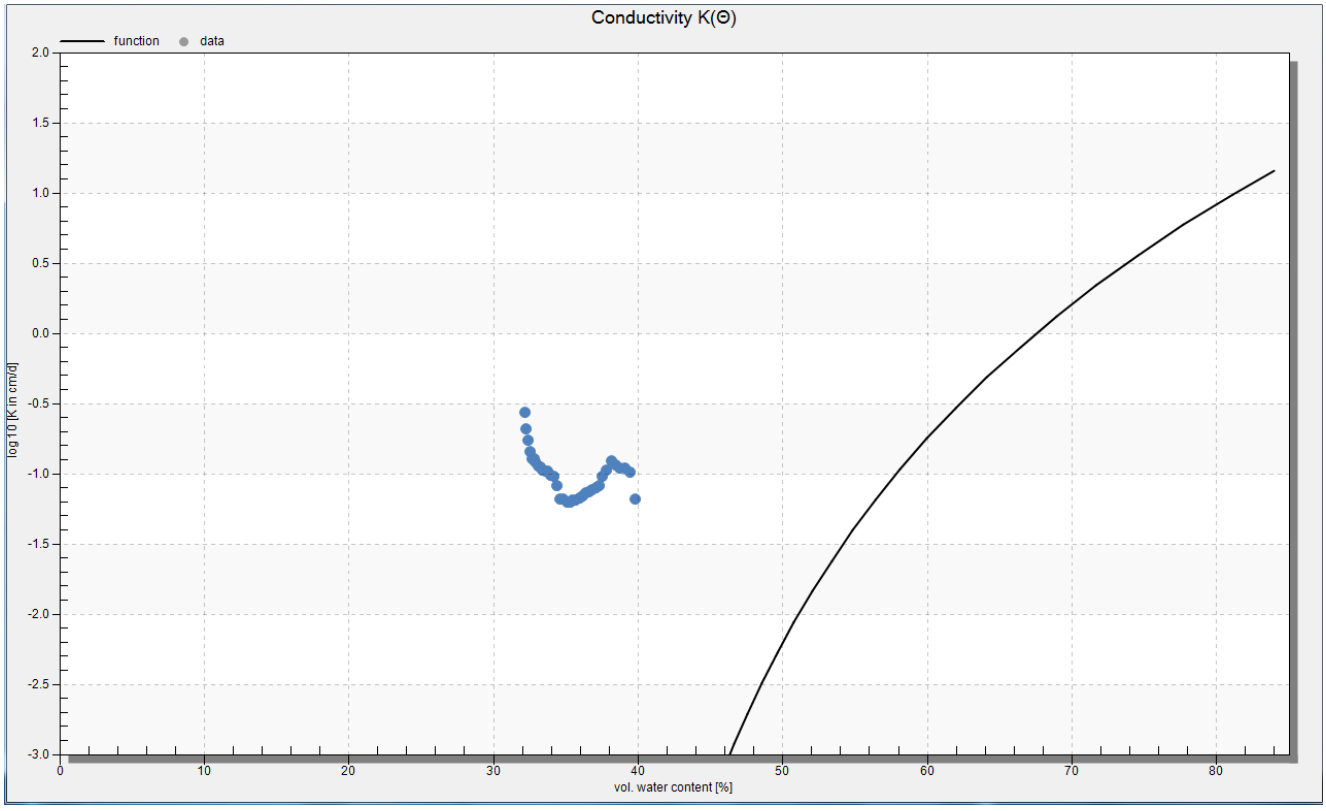


Retention results



Conductivity fitting graphs





Particle size distribution

Sample No.	**Matimba Coal Ash**	**Tutuka Coal Ash**	
Depth	-	-	
Sieve size	%Passing	% Passing	% Passing
75.00	100	100	
63.00	100	100	
53.00	100	100	
37.50	100	100	
26.50	100	100	
19.00	100	100	
13.20	100	100	
4.75	100	100	
2.00	100	100	
0.85	99	99	
0.425	98	98	
0.25	94	97	
0.15	82	91	
0.075	61	75	
0.04	45	56	
0.02	23	39	
0.006	7	12	
0.002	1	4	

Atterberg limits results

Sample No.	**Matimba Coal Ash**	**Tutuka Coal Ash**	
%Gravel	0	0	
%Sand	44	32	
%Silt	55	64	
%Clay	1	4	
NMC %	Not Tested	Not Tested	
Liquid Limit	NP	NP	
Plasticity Index	NP	NP	
Linear Shrink.	0.	0.	
Overall P.I.	NP	NP	
Grading Modulus	0.41	0.27	
H.R.B.	A-4 (5)	A-4 (8)	
Unified	ML	ML	
Weston swell (%) at 1 kPa			

Estimated Field capacity values

Field capacity	Brooks-Corey	Freduland-Xing	Kosugi	Van Genuchten m=1-1/n
WC@6kpa	35.7	33.2	38.9	38.1
WC@33kPa	35.1	28.5	38.9	38.1
WC@1500kPa	35.1	22.8	38.9	38.1

APENDIX 2: EQUATIONS USED FOR RETENTION MODELS

(SOURCE: PERTASSEK et al., 2015)

The unimodal constrained model of van Genuchten (1980)

$$S_e(h) = \left[\frac{1}{1+(\alpha|h|)^n}\right]^{1-\frac{1}{n}}$$

where α [cm^{-1}] indicates a shape parameter that is related to the inverse of the air-entry pressure, and *n* [-] is a shape parameter that controls both the bending of the retention curve at the air-entry region and the asymptotic curvature towards the residual water content.

With four free parameters, the constrained van Genuchten (1980) function is the most widely used expression to describe water retention data in vadose zone hydrology. It fits retention data with a unimodal shape, a gradual air entry, and an asymptotic approximation of a finite residual water content. Despite its wide use, the model has deficiencies if used for natural soils with structured pore systems, and for describing data that encompass a wide pressure head range and approximate smaller water contents towards dryness.

The model of Brooks and Corey (1964)

$$S_e(h) = \begin{cases} (\alpha\,|h|)^{-\lambda} & \text{for} \quad (\alpha\,|h|) > 1 \\ 1 & \text{for} \quad (\alpha\,|h|) \le 1 \end{cases}$$

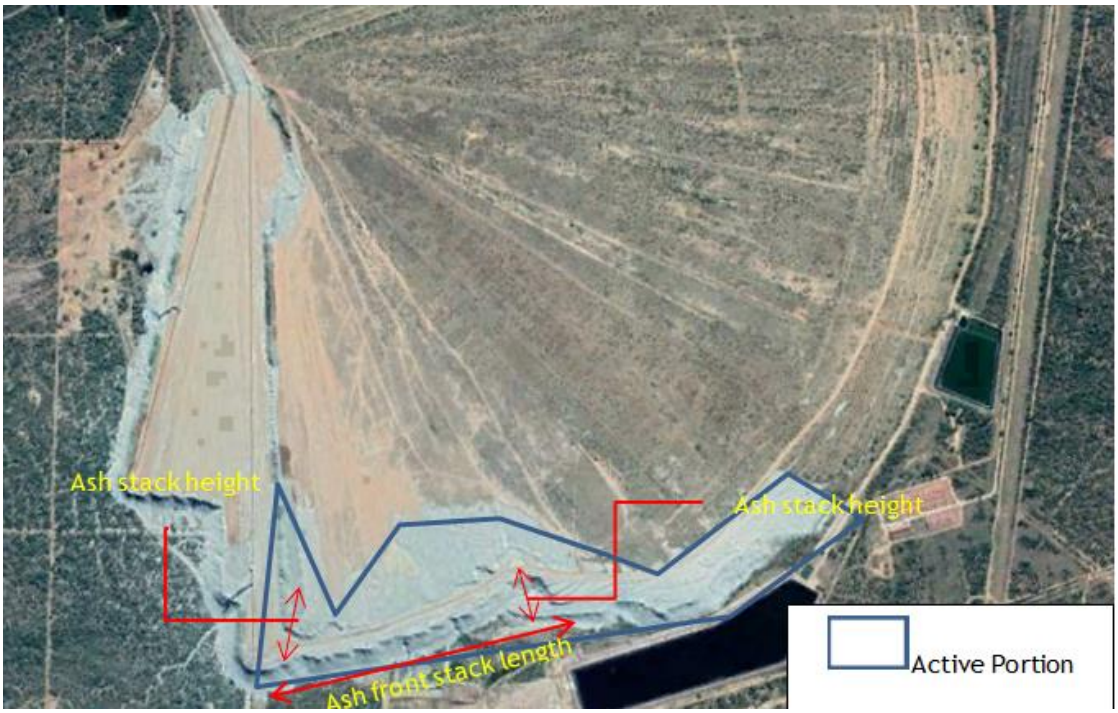
is a model that was traditionally widely used in the geosciences. Similar to the constrained van Genuchten model, it is a four-parameter model with λ expressing the width of the pore-size distribution. The model is particularly suitable for soils with a very sharp air-entry point. It is traditionally combined with the Burdine (1953) conductivity model, whereas the other six model in the HYPROP-DES suite are combined with the Mualem model.

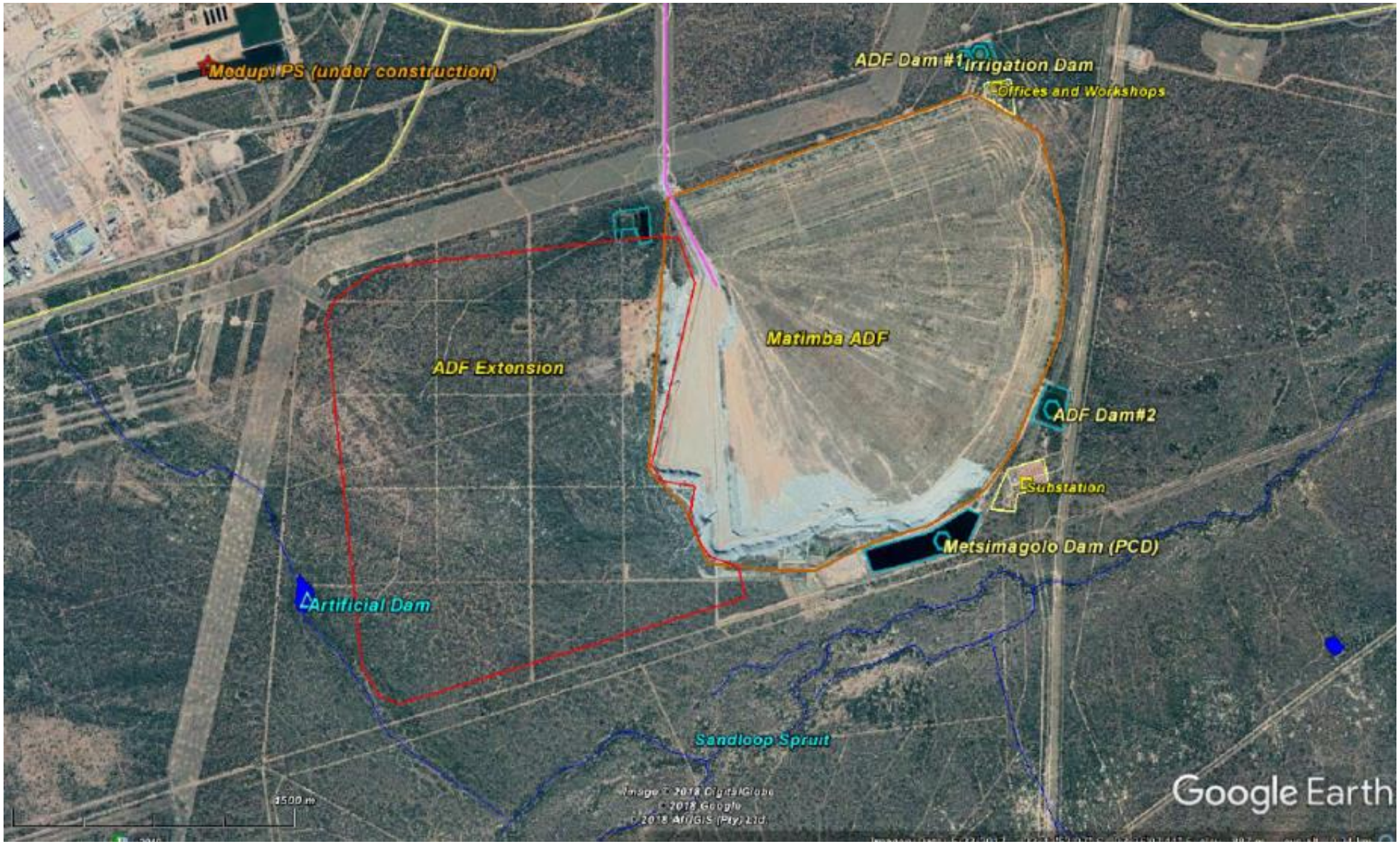
The model of Kosugi (1996) is given by

$$S_e = Q\left[\frac{\ln(h/h_m)}{\sigma}\right]$$

where *Q* indicates the integral of the Gaussian normal distribution, h_m [cm] is the pressure head at the pore-density maximum, and σ [-] indicates the standard deviation of the pore-size density distribution. The flexibility and overall shape of this four parameter model is very similar to the constrained van Genuchten model, but some users prefer it due to a more straightforward statistical interpretation of its parameters. A certain disadvantage is that the integral of the normal distribution is not a simple algebraic expression.

APENDIX 3: MATIMBA ASH DUMP




Modupi PS (under construction)
ADF Dam #1
Irrigation Dam
Offices and Workshops
Matimba ADF
ADF Extension
ADF Dam#2
Substation
Metsimagolo Dam (PCD)
Artificial Dam
Sandloop Spruit
Google Earth

APENDIX 4: LITERATURE RETENTION VALUE

Texture Class		Wilting Point WP %Vol			Residual wat. θ_r (%Vol)			Field Capacity FC %Vol		
		Min.	Avg.	Max.	Min.	Avg.	Max.	Min.	Avg.	Max.
Light textured soils	Sand	4.50	6.36	8.50	4.50	7.26	13.71	11.80	13.71	15.92
	Loamy Sand	4.85	7.32	10.90	4.85	8.07	15.58	13.20	15.58	18.10
	Sandy Loam	3.87	8.90	13.20	3.87	8.96	20.82	17.00	20.82	24.00
Medium textured soils	Loam	6.09	11.09	15.60	6.09	12.25	26.61	22.90	26.61	30.10
	Silt	3.40	7.92	9.50	3.40	11.57	30.64	30.10	30.64	31.20
	Silty Laom	6.45	11.36	19.69	6.45	13.74	30.76	23.40	30.76	40.19
	Sandy Clay Loam	6.33	14.20	17.50	6.33	12.46	26.76	25.30	26.76	28.50
Heavy textured soils	Clay Loam	7.92	16.13	20.00	7.92	15.44	32.99	30.50	32.99	34.94
	Silty Clay Loam	8.90	18.13	21.80	8.90	17.75	38.40	38.40	38.40	38.40
	Sandy Clay	10.00	20.36	29.40	10.00	16.85	32.83	27.40	32.83	38.80
	Silty Clay	7.00	22.01	32.60	7.00	17.60	42.34	37.80	42.34	47.80
	Clay	6.80	24.13	35.90	6.80	18.10	44.47	37.30	44.47	50.40

Texture Class		Saturation Wat. Cont. θ_S %Vol			Bulk Density BD g/cm^3			Hydraulic conductivity K Cond. cm/min		
		Min.	Avg.	Max.	Min.	Avg.	Max.	Min.	Avg.	Max.
Light textured soils	Sand	34.5	37.6	43.0	1.62	1.68	1.73	0.047000	0.214198	0.495000
	Loamy Sand	35.1	38.7	41.5	1.55	1.65	1.72	0.019667	0.105774	0.243194
	Sandy Loam	38.1	41.3	45.6	1.44	1.54	1.64	0.009500	0.047453	0.073680
Medium textured soils	Loam	39.9	44.3	48.9	1.35	1.44	1.56	0.005833	0.027508	0.047000
	Silt	40.5	42.9	48.9	1.55	1.57	1.58	0.004167	0.045821	0.057833
	Silty Laom	38.2	45.3	50.7	1.30	1.42	1.64	0.007500	0.034221	0.060667
	Sandy Clay Loam	38.4	45.0	48.3	1.37	1.39	1.41	0.002183	0.005001	0.009160
Heavy textured soils	Clay Loam	41.0	47.9	50.8	1.30	1.33	1.35	0.004000	0.004371	0.005681
	Silty Clay Loam	43.0	50.3	52.2	1.27	1.27	1.27	0.001167	0.004483	0.007715
	Sandy Clay	38.0	46.5	51.8	1.28	1.33	1.38	0.001500	0.002922	0.007882
	Silty Clay	36.0	50.0	54.7	1.20	1.24	1.28	0.000330	0.004334	0.006674
	Clay	38.0	50.3	55.2	1.19	1.24	1.29	0.001667	0.004213	0.010243

This Table is a part of the unpublished PhD Thesis of Dr. Mohammad Elnesr, Data in the table are collected from Keller and Karmeli (1975), Saxton et al. (1986), and van Genuchten et al (1991)

Keller, J., and D. Karmeli, 1975. *Trickle irrigation design*, Rain Bird Sprink. Manif. Corp. 133 pp.

Saxton, K. E., W.J. Rawls, J.S. Romberger, and R. I. Papendick et al. , 1986. *Estimating generalized soil-water characteristics from texture.* URL:http://www.bsyse.wsu.edu/saxton. Soil Sci. Soc. Amer. J. 50(4):1031-1036

van Genuchten M. Th, F. J. Leij, and S. R. Yates, 1991. *The RETC code for quantifying the hydraulic functions of unsaturated soils*, U.S. Salinity Lab., U.S. Dept. of Agric., Agric. Res. Service, Riverside, California. 93pp

APENDIX 5: TLCP LABOATRY ANALYSIS RESULTS

Parameter	Unit	Matimba #1	Matimba #2	Tutuka #1	Tutuka #2
Alkalinity M	mg/l CaCO3	1964	<1	1969	<1
Alkalinity P	mg/l CaCO3	<1	<1	<1	<1
Alkalinity Total	mg/l CaCO3	1964	<0	1969	<0
Aluminium as Al	mg/l	1.063	28.08	0.614	16.64
Ammonia as N	mg/l	<0.005	<0.005	<0.005	<0.005
Arsenic as As	µg/l	34	23	69	44
Anions	mg/l	2742.271	1040.484	2635.371	1203.189
Cations	mg/l	3050.522	1037.577	2987.933	1184.88
Cat/Anion Balance	%	5.321	-0.14	6.27	-0.767
Calcium as Ca	mg/l	304	334.4	296.4	87.38
Cadmium as Cd	mg/l	<0.005	<0.005	<0.005	<0.005
Chloride as Cl	mg/l	403	553	389	692
Chemical Oxygen Demand	mg/l	4500	4400	4200	4900
Conductivity	µS/cm	5072	1705	5008	1593
Chromium as Cr	mg/l	0.103	0.189	0.059	0.117
Copper as Cu	mg/l	0.024	0.049	0.022	0.061
Iron as Fe	mg/l	<0.005	0.336	<0.005	0.098
Flouride as F	mg/l	<0.030	<0.030	<0.030	<0.030
Mercury as Hg	µg/l	<1.000	<1.000	<1.000	<1.000
Potassium as K	mg/l	5.1	4.55	3.09	83.34
Antimony as Sb	mg/l	<0.005	<0.005	<0.005	0.009
Vanadium as V	mg/l	0.317	0.161	0.341	0.185
Magnesium as Mg	mg/l	33.2	46.23	32.21	37.84
Manganese as Mn	mg/l	0.633	1.432	0.605	1.147
Sodium as Na	mg/l	988	1.05	971	322
Nitrite as NO2	mg/l	0.08	<0.020	0.06	<0.020
Nitrate as N	mg/l	0.12	<0.02	0.85	0.88
Lead as Pb	mg/l	<0.010	<0.010	<0.010	<0.010
pH @ 25 °C		5.21	4.09	5.22	4.06
Ortho Phosphate as PO4	mg/l	0.4	0.9	0.9	1.2
Antimony as Sb	mg/l	<0.005	<0.005	<0.005	0.009
Selenium as Se	µg/l	17	8	22	12
Reactive Silica as SiO2	mg/l	6.56	160	5.65	130
Sulphate as SO4	mg/l	201	250	110	215
TDS	mg/l	2842	1232.3	2461.8	1137
High Level TOC TEKMAR TORCH	mg/l	2442	2388	2414	2398
Turbidity	NTU	0.131	0.17	0.093	0.134
Vanadium as V	mg/l	0.317	0.161	0.341	0.185
Zinc as Zn	mg/l	0.083	0.2	0.061	0.192